INVESTIGATION OF DIE WEAR BY MODELLING THE

EXTRUSION OF INCONEL 718

by

YU-PEI <u>LIN</u>

A thesis submitted to
The University of Birmingham
for the degree of
DOCTOR OF PHILOSOPHY

Mechanical Engineering
School of Engineering
The University of Birmingham
September 2009

ABSTRACT

Die wear is always an important issue in hot forming processes, such as in forging and extrusion. Die life affects the economics of process to product and in order to optimise die life, the mechanism of wear should be approached scientifically. The aim of this work is to provide a systematic method for predicting and quantifying wear occurring in the extrusion of INCONEL 718 (IN718), nickel superalloy.

To characterise wear, the process prediction which contributes to it must be identified and quantified. First, material characterisation was carried out using the Gleeble physical materials simulator. Then a set of unified viscoplastic constitutive equations was developed suitable for modelling microstructural evolution of IN718, i.e. evolution of average grain size, dislocation density and recrystallisation under hot forming conditions, which enabled resulting flow stress to be calculated and the microstructure of formed parts to be predicted.

Second, heat transfer and friction during the forming process were investigated, by upsetting cylinders and performing ring tests on IN718. The heat transfer experimental work centres rounded the development of a reliable method for the measurement of the sub-surface temperatures in the bottom die during upsetting. The experimental values of sub-surface temperatures under various lubrication and forging conditions were analysed. A theoretical approach was proposed for the determination of the values of effective heat transfer coefficient and effective friction factor, and comparisons of experimental results and those from FE simulations were made and satisfactory matchings were obtained.

Finally, integration of the material model and derived boundary conditions using subroutines for FEA are presented. Qualitative studies of abrasive die wear carrying out in a FE package, DEFORM, on the effect of various hot forming cases are shown. The numerical results are compared with the observations from mechanical measurements and metallurgical examinations for the studied die. Good correlations are found for most cases, which prove the presented methods can be used effectively in the prediction of die wear. Also, further work is suggested to enhance the modelling capabilities.

Dedicated to the memories of

Mr. Mike Williams and my grandfather

ACKNOWLEDGEMENTS

TABLE OF CONTENTS

LIST OF FIGURES

LIST OF TABLES

CHAPTER 1

INTRODUCTION

1.1 RESEARCH BACKGROUND

INCONEL 718 (IN718), nickel superalloy, was first developed in 1959. Since then various applications have been developed for it, which vary from rotating and static components in engines to high-strength bolts and fasteners, nuclear reactors and space vehicles, etc (Huang, 2001). The most used application of IN718 is in aircraft engines due to its favourable mechanical properties in an extreme working environment.

Figure 1.1 shows the different working conditions in the stages of a gas turbine engine. At the lower temperature stage, below approximately $400℃$, titanium is ideal for its strength and density, but at the higher temperature stages it is replaced by nickel-based superalloys. Further, IN718 has an inherently lower material cost than many other nickel-based superalloys due to its 20% iron content and lack of cobalt (Sims *et al.*, 1987). As a result, IN718 is the most widely used superalloy in the aerospace industry.

Creep resistance is an important property of aeroengine blades. It is greatly affected by the area of grain boundary of component parts. Nowadays, a casting technique is used to produce single-crystal blades. However, problems still exist with this casting technique, as recent evidence shows that cast single-crystal blades start to recrystallise due to the remaining residual stress after casting (Jo and Kim, 2003). In contrast, forged blades are cheaper to produce and are usable at slightly lower temperatures. The material property of forged parts could also be controlled by the forming procedure or heat treatment. Due to the high strength of IN718 at high temperatures, forging blades, which involves several operations, is difficult and incurs rapid tool wear.

In this research, the forming of IN718 for the compressor blade in an aircraft engine is studied. The operations of a typical forming procedure of a blade are shown in Figure 1.2. A glass coated slug, separated from the bar, is preheated to $1080℃$ for 900 seconds, then preformed by first extruding and then heading in separate dies with lubricant. After cooling to room

temperature, the preform is shot-blasted and coated in glass again and finish forged at $1010℃$, followed by ageing. The design of the several forming stages is to maximise material yield, which enhances die wear, and reduces the forming force of the final operation. The focus of this work is placed on preform extrusion, since extrusion die sustains significant die wear, compared with dies of other stages.
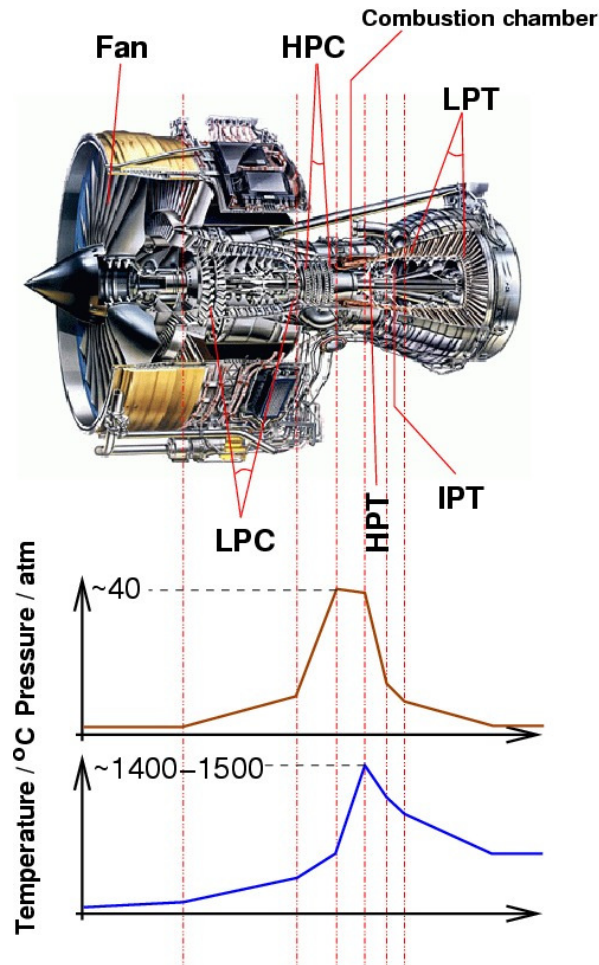
Figure 1.1 A jet engine (Rolls-Royce Trent 800), showing the different working stages: low pressure compressor (LPC), high pressure compressor (HPC), high pressure turbine (HPT), intermediate pressure turbine (IPT), low pressure turbine (LPT), and the pressure and temperature profiles along the engine (provided by Rolls-Royce).
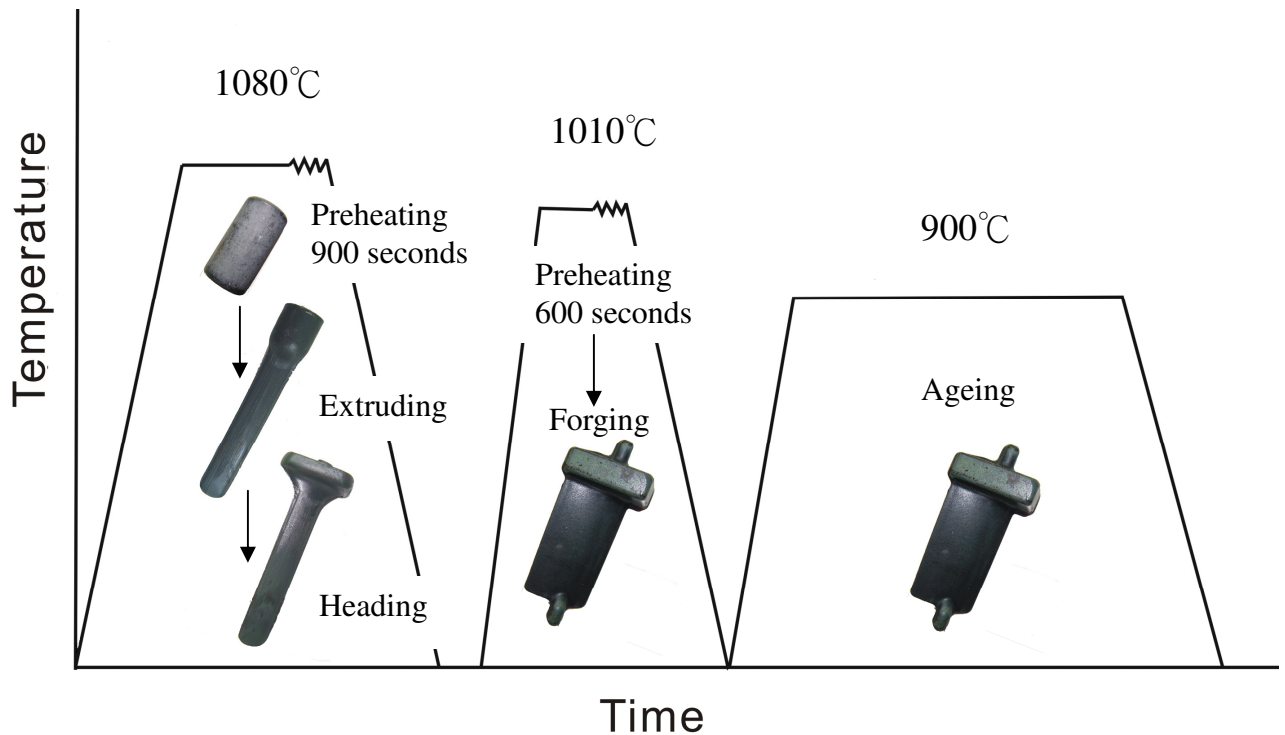
Figure 1.2 Forming procedure of the compressor blade (data provided by Mike Williams).

1.2 AIM OF THE WORK AND RESEARCH APPROACH

Under the effects of high temperature and large deformation, the die experiences complex conditions. Die costs have been reduced by the use of rapid, accurate manufacturing techniques, such as high-speed milling and EDM, but dies are still expensive items in the overall product cost and, therefore maximising tool life is essential for cost-effective production. Given that forging temperature, production rate and tool material are fixed, die life can be influenced by other process factors, such as lubrication affecting heat transfer and friction conditions, die geometry and forming speed.

The aim of this research is to examine the effect of these variables on metal flow and loads and by modelling the extrusion process deducing their effects on die wear. In order to achieve the goal, the project is designed in the following three stages:

1. The material properties of IN718 are characterised through experimentation and by constitutive modelling mathematically. Each key mechanism is represented by a

governing equation, which may be rate and temperature dependent, and is a function of all influencing mechanisms. Overall microstructural evolution is mapped by the interaction of these equations. Average grain size which affects blade property can be obtained by the model while interfacial pressure which affects die wear during forming can be predicted by considering microstructural mechanisms.

2. Compression tests are undertaken and by measuring the temperature profiles and incorporating FE method, heat transfer coefficients before, during and after forming are derived. Friction condition is examined by performing ring tests. In addition, the effect of process conditions on calibration curves is investigated.

3. The FE method is used to model the extrusion process. The constitutive equations and boundary conditions are integrated into an industrial standard FE simulation software, DEFORM. The affecting factors of die wear are identified and analysed.

The computational FE results derived from above three stages are also compared with the experimental results and observations for validation.

1.3 STRUCTURE OF THE THESIS

This thesis is organised as follows:
- Chapter1: Project background and aim and objectives of this research are introduced.
- Chapter2: Modelling techniques of material property considering microstructural evolution by other researchers are reviewed, followed by the experimental characterisation and the development of constitutive material model for IN718 by the author. Results and analyses are presented at the end of the chapter.
- Chapter3: Previous research of investigating heat transfer and friction conditions for metal forming are reviewed first. Then both conditions are investigated through experiments and FE simulations for forming of IN718 using H13 dies by the author. Results are analysed in the end.
- Chapter4: This chapter is dedicated to for the understanding of tribological work in metal forming. The die failure and die wear are discussed particularly, in addition, the wear

models are presented and analysed.

- Chapter5: Previous modelling work for examining die wear in forming is summarised. Then the method of integrating material model, boundary conditions and wear model to FE is presented. Computational results by comparing with the observations from the worn die are discussed in the end.

- Chapter6: The conclusions resulting from this research and recommendations for the future work are given.

CHAPTER 2
MATERIAL MODELLING OF IN718 DURING HOT FORMING

2.1 INTRODUCTION

IN718 is widely used for gas turbine parts in the aerospace industry, since it possesses good mechanical properties at high temperature in a high pressure working environment (Tien *et al.*, 1991; Yi, 2001; Cervenka, 2007). Hot forming processes are normally used to produce the parts of IN718 to take advantage of high formability and reasonably low forming forces. During hot forming, the microstructure of the metals changes dynamically (Luo *et al.*, 1991), which affects flow stress. The accuracy of prediction of flow stress is essential to enable not only forging load and therefore required machine capacity to be determined, but also to enable tool work-piece interface pressure to be calculated and thus tool wear to be predicted. Also, to be able to predict the microstructure of the formed part which is regarded as important in the blades, it is necessary to develop a model considering the microstructural evolution of the superalloy during deformation. State variables are normally introduced to represent the individual mechanisms of microstructural evolution (Luce *et al.*, 2001; Zhao *et al.*, 2004), such as dislocation density, recrystallisation, grain size, etc. State variables indicate softening mechanisms, i.e. recovery and recrystallisation, the hardening mechanism, accumulation of dislocations and increase in density.

In this chapter, a set of unified elastic-viscoplastic constitutive equations is introduced, incorporating mechanism-based state variables; this is calibrated for IN718 using results from thermal-mechanical experiments at a temperature range of between 950℃ and 1100℃ and a strain rate range of between 0.1/s and 10/s. Microstructural structure of the formed part can be modelled through state variables: dynamic recrystallisation, recovery, evolution of dislocation density and grain size, as predicted from the equations. The effect of the key material parameters on the elastic-viscoplastic flow of IN718 under hot forming conditions is analysed.

2.2 MATERIAL CHARACTERISATION

Hot uniaxial compression tests were carried out to characterise material behaviour of IN718 and test results were used to calibrate the constitutive equations described in later sections of this chapter.

A Gleeble 3500 material test station was used for all hot compression tests. The machine is a computer controlled, hydraulically activated linear test machine with resistive test-piece heating and a sealed test chamber. Features of the machine are highlighted in Figure 2.1.
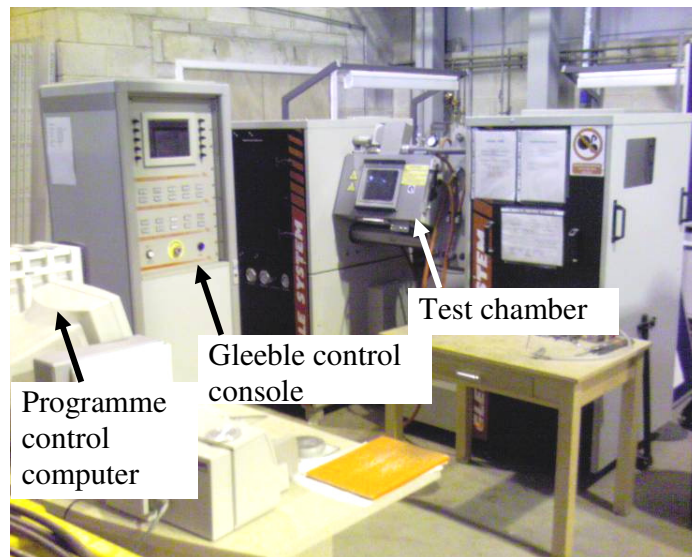
Figure 2.1 Gleeble 3500 material simulator.

2.2.1 Experimental design

The Gleeble test station has a load capacity of 100kN and a maximum stroke speed of 2m/s. However the time taken to accelerate the moving parts puts practical limits on the strain rate for the test-piece of approximately $10s^{-1}$. At this rate, adequate control is still available to keep the rate stable. A strain rate range of $0.1 \sim 10s^{-1}$, was selected. Table 2.1 outlines the test programme,

designed to obtain flow stress at typical forging temperature values for IN718 alloy.

Temperature (℃)	Strain Rate (1/s)
950	1
	5
	10
1000	0.1
	1
	5
	10
1050	0.1
	1
	5
	10
1100	0.1
	1
	5
	10

Table 2.1 Compression test programme.

2.2.2 Preparation and performing of the test

According to Measurement Good Practice Guide which was published by National Physical Laboratory (Roebuck *et al.,* 2002), a standard cylindrical compression specimen with height:diameter ratio = 1.5 was adopted. Also considering the Gleeble forming capability, the size of the test-pieces used was 8 mm in diameter and 12 mm in height. The test-pieces were machined from as-received slugs of 18 mm in diameter and 126 mm in height.

Mechanical displacement aimed to deform the test-pieces and electrical current used to heat them are transmitted via a static and a moving jaw, which moves along a horizontal axis. Tantalum foils were used to prevent the test-piece from sticking on the anvil during heating and graphite foils were inserted between tantalum foil and test-piece to stablise and enhance electric current flow to ensure uniform temperature within the entire volume of the specimen, as well as to act as a lubricant. Nickel high temperature lubricant gel was applied in two ends of specimen to reduce friction and stick the foils on the test-piece. A specially designed tong was used to place the test-piece at the centre of the anvil, as shown in Figure 2.2. Auxiliary pins were fit on the tong in order to ensure the test-piece is situated accurately on the position. A silicon C-gauge was mounted at the test-piece centre span to record increase in test-piece diameter and hence allow longitudinal strain to be calculated as:

$$\varepsilon = 2 \cdot \ln\left(\frac{d}{d_0}\right)$$

where d_0 is initial diameter and d is the instantaneous diameter. Figure 2.3 shows details of the test-piece mounted within the test chamber.

Figure 2.2 A tong was specially designed for placing the test-piece at the centre of the anvil.
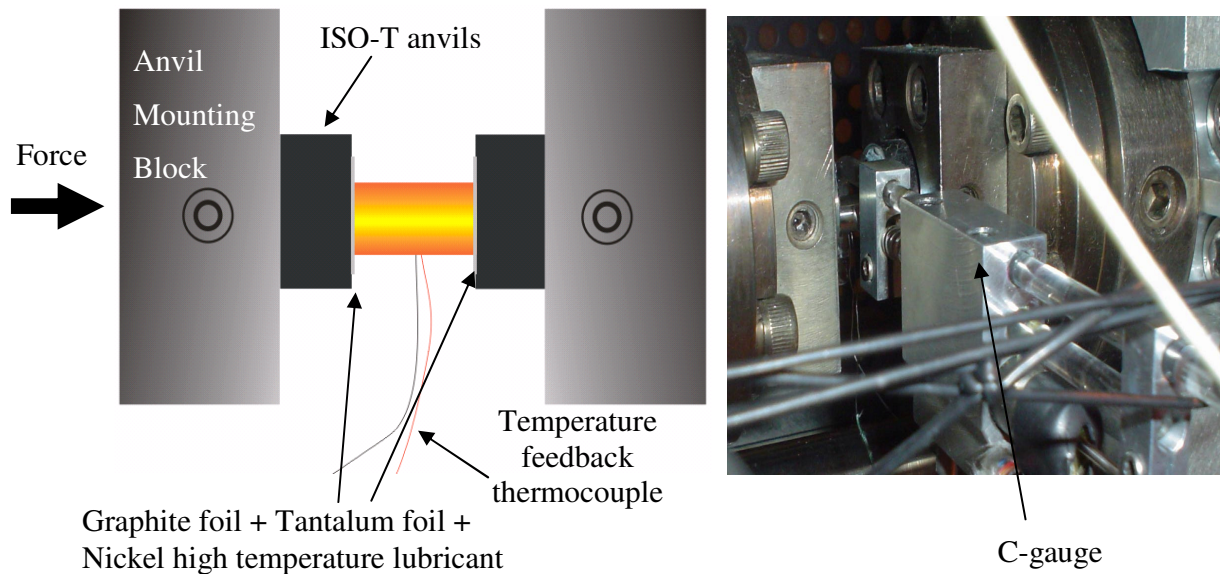
Figure 2.3 Detail of test-piece mounted in the Gleeble materials simulator.

Temperature feedback was via K-type thermocouples mounted at the test-piece centre, which offer accurate temperature measurement up to $1300°C$. Real-time strain rate control based on C-gauge diametric strain was not possible; therefore length control of the moving jaw was used to generate a near-constant strain rate.

To ensure the proper contact of foils and test-piece, a small force (<10N) was imposed to compact foils. An air ram, a special function using air pressure to hold the test-piece, was then used to hold it with a small gap between the moving anvil and the test-piece, without placing significant force on the test-piece. The judging of the gap is crucial since it should be big enough to accommodate the expansion of the specimen during heating; it also should be small enough to facilitate the air ram to hold the specimen to obtain stable resistance heating; besides the weight of the C-gauge also needs to take into account. By trial and error, a gap of 2 mm was found to be suitable for the tests.

A total of 27 tests, including repetitions, were conducted under isothermal conditions; the results are shown in Appendix A. Each specimen was heated at $20°C$/s to $100°C$ below deformation

temperature. Then the heating rate was changed to $10°C/s$ until the soaking temperature was reached, to prevent overheating. After a soaking time of 600 seconds, specimens were deformed at different strain rates. The compression test cycle is shown diagrammatically in Figure 2.4.

A: Heated $20°C/s$ to $100°C$ below deformation temperature.

B: Heated $10°C/s$ to deformation temperature.

C: Held for 600 seconds.

D: Deformed at different strain rates.

E: Cooled at room temperature.
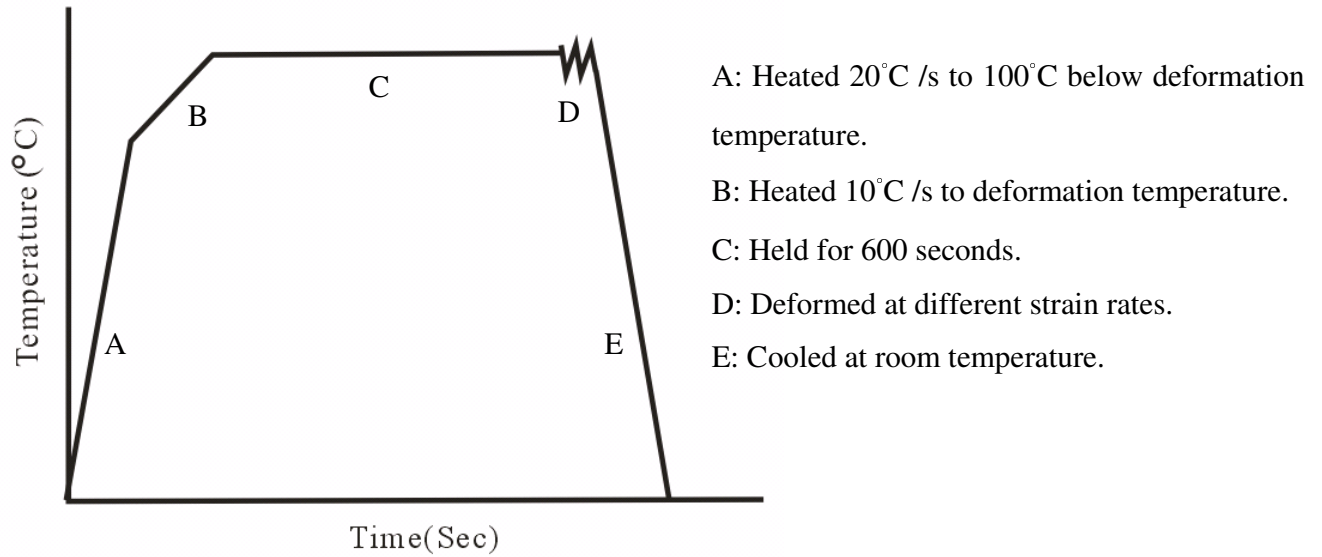
Figure 2.4 Programme for hot compression tests.

2.2.3 Barrelling coefficient (B)

A study conducted by the National Physical Laboratory (Roebuck *et al.,* 2002) recommends the use of a Barrelling Coefficient to verify the validity of a uniaxial compression test, and it is suggested that the Barrelling Coefficient, B, should be less than 1.1. If the value is greater than 1.1 the barrelling is too large and uniform deformation cannot be assumed. This approach was employed in the tests undertaken in this work, to discriminate the invalid data by judging the B value of the deformed test-piece which is defined as:

$$B = \frac{h_f d_f^{\,2}}{h_0 d_0^{\,2}}$$

where h_f is final height of specimen, and d_f is final diameter of specimen at mid-span which is shown in Figure 2.5.
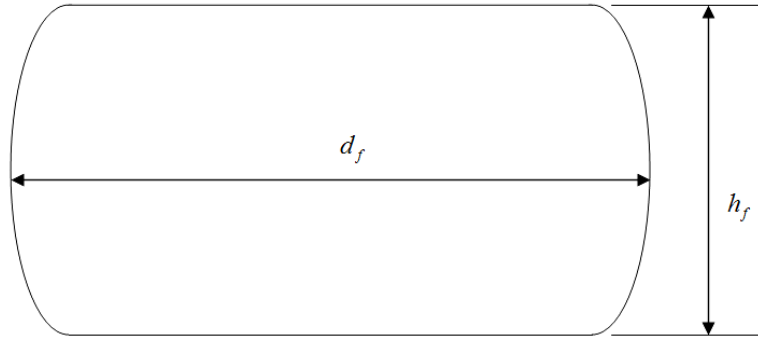
Figure 2.5 Definition of final dimension of deformed test-piece.

2.2.4 Test results

Figure 2.6 shows the typical elastic-viscoplastic material property of IN718 at different values of strain rate and elevated temperatures. At a temperature of 1050℃ higher the strain rate is seen to result in higher flow stress. Also, at a strain rate of 5/s, the higher the temperature, the lower the flow stress.
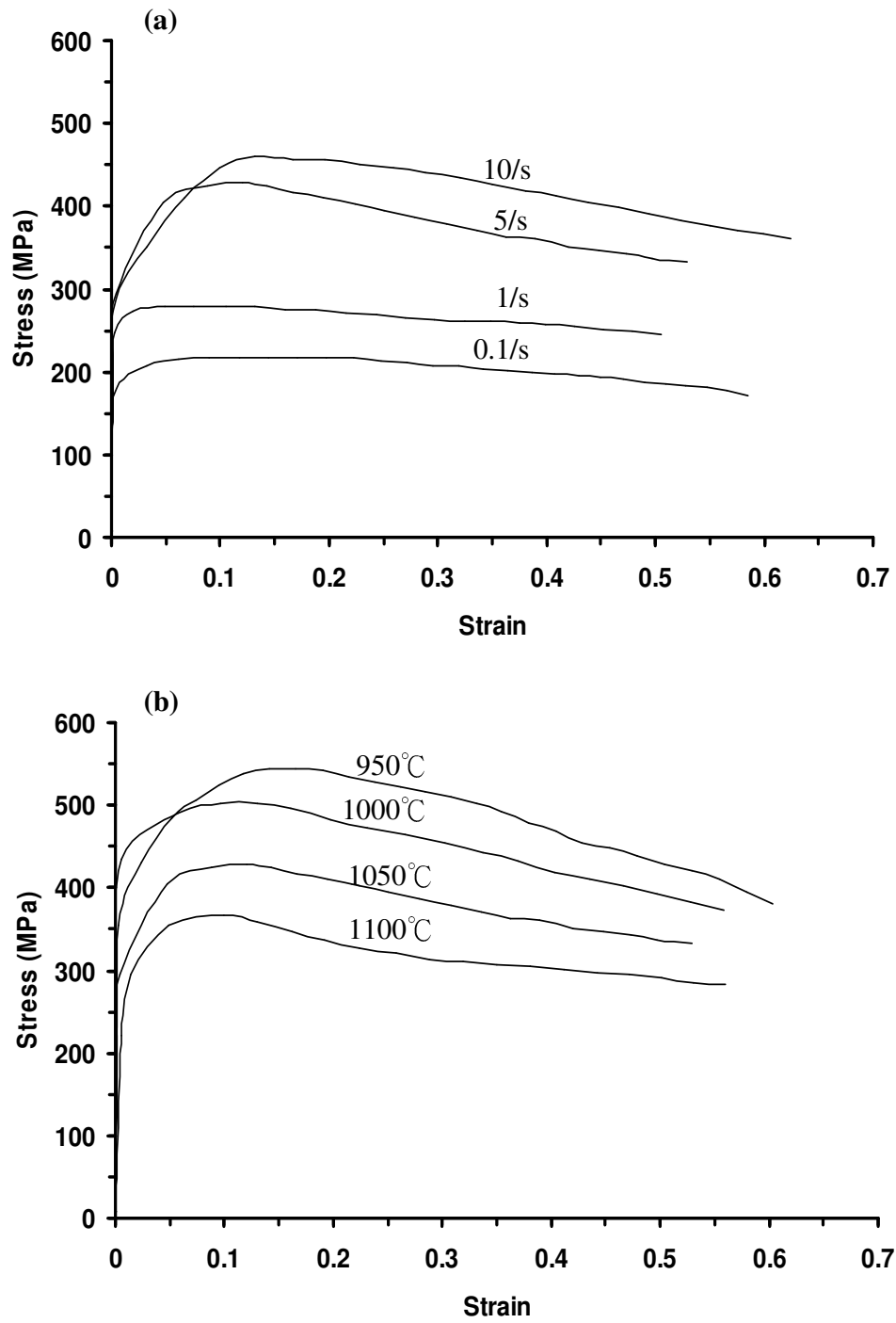
Figure 2.6 Elastic-viscoplastic material behaviour of IN718; (a) deformed at 1050℃ for different strain rates, (b) deformed at strain rate of 5/s for different temperatures.

The experimental data was then investigated for consistency and reliability. At low values of strain, little microstructural change occurs. Thus the temperature dependent elastic-viscoplastic flow of the material can be approximately described by $\dot{\varepsilon}_p \exp(Q/(RT)) \approx A_1 \sinh A_2 \sigma$ or $\ln \dot{\varepsilon}_p + (Q/(RT)) \approx \ln A_1 + A_2 \sigma$. Where $\dot{\varepsilon}_p$ is plastic strain rate. Q represents activation energy, R is gas constant. T stands for temperature in K. σ is stress. A_1 and A_2 are material parameters. First, an analysis was carried out to examine the effect of temperature on flow stresses. The symbols in Figure 2.7 (a) show flow stress against $1/T$. They were obtained from experimental data for $\dot{\varepsilon} = 10/s, 5/s$, $1/s$ and $0.1/s$ at a strain of 0.2. It can be seen that the data for a particular strain rate can be fitted approximately with a straight line. The lines are approximately parallel, which indicates that their activation energy is about consistent. The data plotted on scales of $\log \dot{\varepsilon}$ against σ for different temperatures, result in Figure 2.7 (b). Again, these experimental data can be approximated to parallel straight lines, the slopes of which are directly related to the A_2 value. According to Figures 2.7 (a) and (b), the experimental data are fairly consistent at low strains, which indicates that the tests were carried out with accuracy.
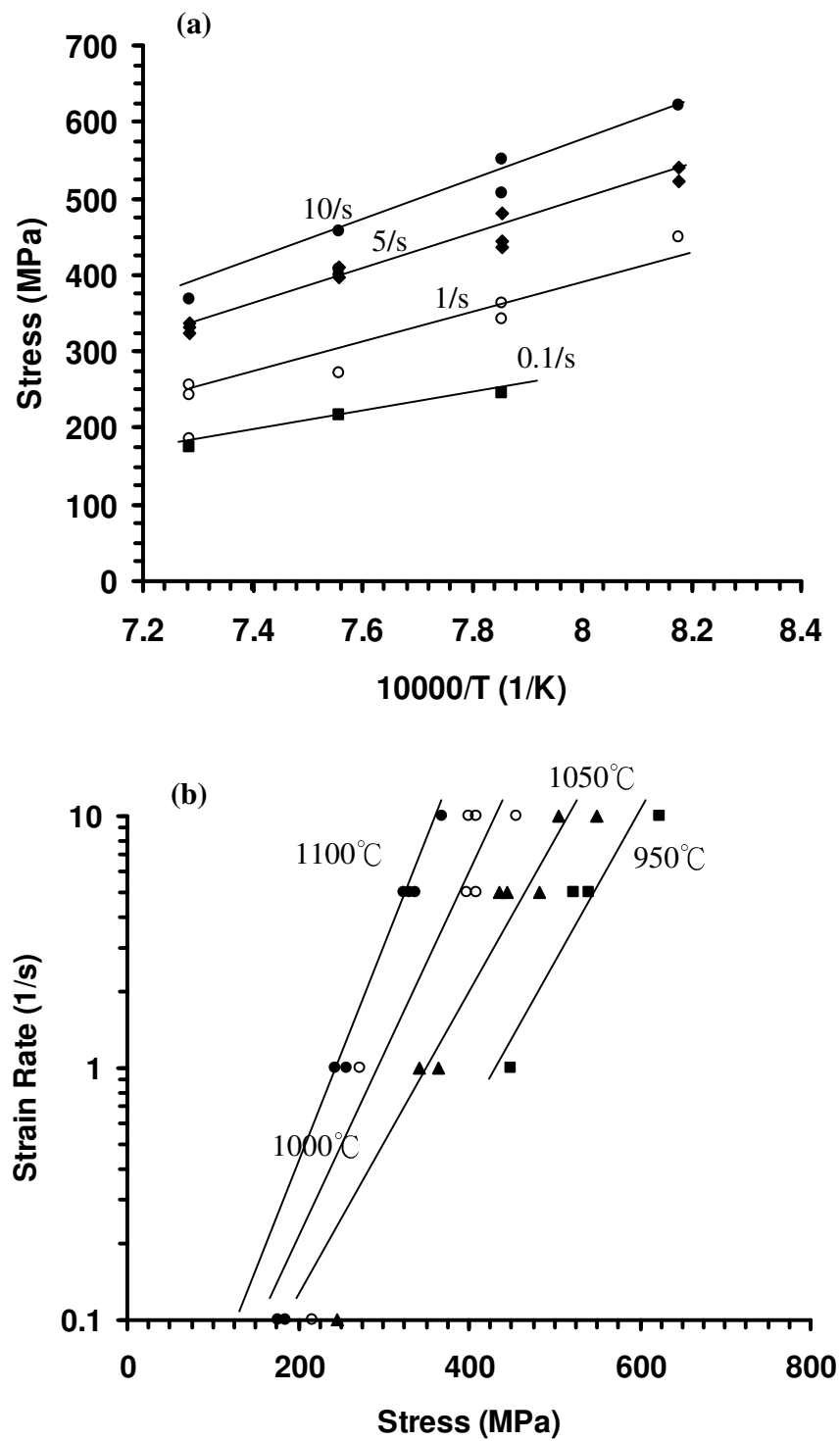
Figure 2.7 (a) Stress at $\varepsilon = 0.2$ against $1/T$ for different strain rates; (b) $\log \dot{\varepsilon}$ against stress at

ε = 0.2 for different temperatures. The solid lines are the fittings for the corresponding experimental data (symbols), which are obtained from uniaxial compression tests.

2.3   MODELLING   OF   MICROSTRUCTURAL   PHENOMENA   IN ELASTIC-VISCOPLASTIC THERMO-MECHANICAL DEFORMATION

Significant research has been performed to model the material flow under hot forming conditions, which is affected by microstructural evolution (Liu *et al.,*1997; Feng *et al.*, 2000; Medeiros *et al.*, 2000; Zhang *et al.*, 2000; Luce *et al*, 2001; Park *et al.*, 2001; Na *et al.*, 2003; Zhao *et al.*, 2004; Azadian *et al.,* 2004*;* Liu *et al.,* 2005; Thomas *et al.,* 2006). Early work was carried out on the modelling of recrystallisation and grain size for metals. In the modelling of recrystallisation, empirical equations are normally formulated by controlling a critical strain, ε_c. For example, Na *et al.* (2003) developed two separate equations for representing critical strains and one of these is applicable to their recrystallisation model, according to the strain rate value. For the modelling of the grain size evolution, Zhao (2004), Medeiros (2000) and Zhang *et al.* (2000) proposed that grain size variation is affected by temperature, strain rate and the evolution of recrystallisation. Park *et al.* (2001) also stated that the evolution of grain size was affected not only by strain rate but also by the initial grain size. Recently, Zhao *et al.* (2004) incorporated microstructural based state variables, such as dynamic recovery and recrystallisation, to the modelling of viscoplastic flow stress for IN718 in hot deformation. In their work, by considering the hardening of the material, due to the accumulation of dislocations and the softening mechanisms caused by dynamic recovery and recrystallisation, the elastic-viscoplastic flow of the material can be roughly modelled. Although many attempts have been made in the past, it is still difficult to accurately predict the whole elastic-viscoplastic material flow dynamics of IN718 under hot deformation.

2.3.1 Dynamic effects of microstructure on elastic-viscoplastic flow of IN718

For moderate to low stacking fault energy materials, such as nickel superalloys, high temperature

deformation is accompanied by thermally activated softening, indicated by a lowering of flow stress. This arises through change in strain and the evolution of microstructure (Honeycombe and Pethen, 1972). The main softening processes involved are recovery and recrystallisation. If the softening processes of recovery and recrystallisation occur during deformation at high temperature, the phenomena are called dynamic recovery and dynamic recrystallisation (Humphreys and Hatherly, 1994).

The evolution of dislocation density is essential in controlling these softening phenomena. The basic mechanisms of dynamic recovery are dislocation climb and glide (Dieter and Bacon, 1989), which result in the formation of low angle boundaries. The applied stress then provides a driving pressure for the movement of low angle boundaries and this leads to annihilation of dislocations.

Although recovery could annihilate some of dislocation, which leads to a slight decrease of stress, recrystallisaiton is the main reason for the large drop of stress, since it produces dislocation-free grains, as long as dislocation density exceeds a critical value. In Figure 2.8 at stage B, dynamic recrystallisation takes place when a critical deformation is reached as dislocation pile up. The average grain size of the material also undergoes a dramatic change at this stage. Dynamic recrystallisation generally starts at the old grain boundaries. The difference between original grains and the new grains nucleated at the boundaries of old grains forms a necklace microstructure of the material (Humphreys and Hatherly, 1994). New dislocation-free and small grains subsequently nucleated at the boundaries of the growing grains and eventually the material became fully recrystallised, as stage C shows. At this stage, the level of flow stress is much lower than that at the beginning of deformation and the dislocation density is sparser due to the newly formed grains.
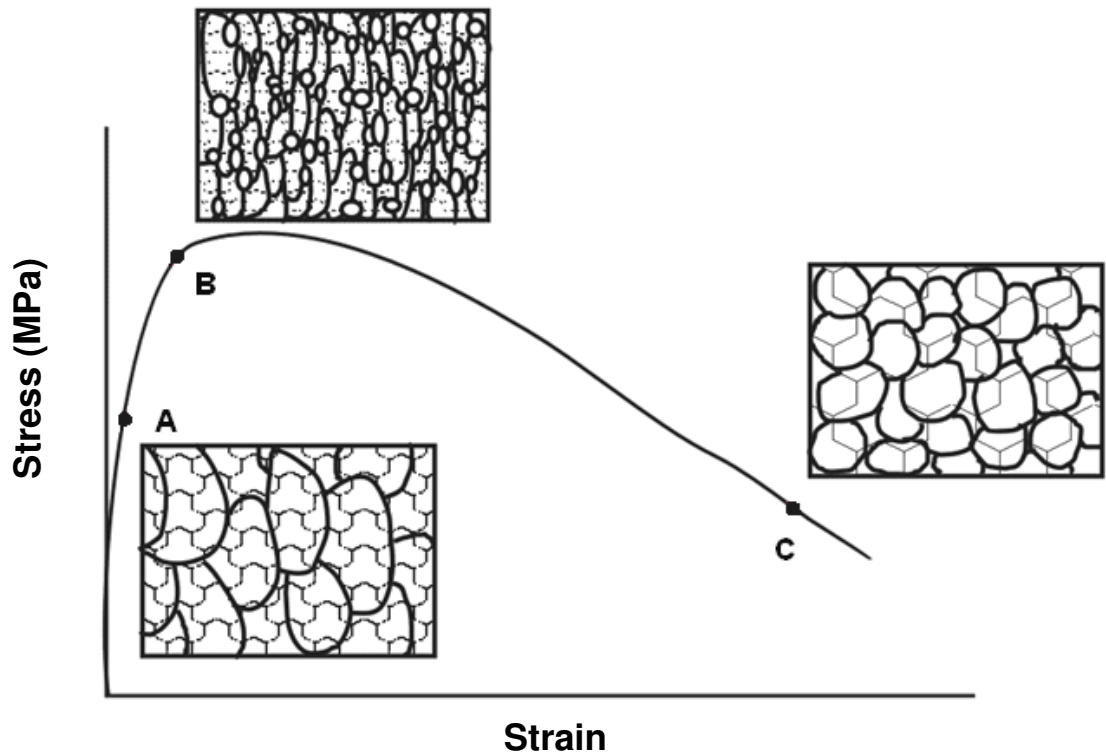
Figure 2.8 Microstructure evolution and material flow features during thermal mechanical processing of the material (adopted from Humphreys, 1995).

2.3.2 Modelling technique

Despite numerous attempts that have been made by researchers (Liu *et al.,*1997; Feng *et al.*, 2000; Medeiros *et al.*, 2000; Zhang *et al.*, 2000; Luce *et al*, 2001; Park *et al.*, 2001; Na *et al.*, 2003; Grass *et al.*, 2003; Zhao *et al.*, 2004; Azadian *et al.,* 2004*;* Liu *et al.,* 2005; Yuan and Liu, 2005; Thomas *et al.,* 2006; Lin *et al.*, 2008) in the modelling of microstructural evolution in materials during deformation, in terms of grain size evolution and recrystallisation, little has been mentioned of the interrelationship of these mechanisms and their effect on flow stress. Metal response to hot deformation conditions is affected not only by the deformation process parameters, i.e. strain rate, temperature etc., but also by thermal and mechanical cycles before and after the current deformation step. (Bariani *et al.*, 2004).

Material behaviour is usually modelled through constitutive equations, taking into account dependence on only the instantaneous values of process parameters. The definition of correct analytical relationships involves a clear understanding of all phenomena occurring during deformation, such as strain hardening, dynamic recovery, and dynamic recrystallisation at hot deformation. These are complex and difficult to model. Therefore most models are empirical and specific and only can be used in limited conditions (Lissel, 2007).

2.3.2.1 Dislocation and grain boundary sliding

The dislocation structure developed during plastic deformation constitutes a driving force for microstructural evolution, such as recrystallisation and grain growth, during and after deformation at high temperature. Dislocations mainly concentrate on sub-grain boundaries, where the average dislocation density is expressed as ρ.

Taking the strain hardening and the recovery of dislocations into account, in the same way as is frequently used in connection with creep type processes, but neglecting recrystallisation, the dislocation density rate has been described by (Sandstrom and Lagneborg, 1975a; Sandstrom and Lagneborg, 1975b) as:

$$\dot{\rho} = \dot{\varepsilon}^p / (bl) - 2M\tau\rho^2 \tag{2-1}$$

where $\dot{\varepsilon}^p$ is the true plastic strain rate, b Burger's vector, l the dislocation mean free path, M the mobility of grain boundaries and τ the average energy per unit length of a dislocation. The first term in Equation (2-1) describes the development of a dislocation and the second represents the static recovery due to annealing at high temperature. Once dislocation density increases to a critical value ρ_c at high temperature, recrystallisation may take place (Djaic and Jonas, 1972). A dislocation density evolution model considering dynamic recovery is expressed as

$$d\rho / d\varepsilon^p = K_1\sqrt{\rho} - K_2\rho \tag{2-2}$$

where the coefficients K_1 and K_2 characterise the processes of dislocation storage and concurrent dislocation annihilation by recovery, respectively. Particularly the coefficient K_2 represents a thermally activated process of dynamic recovery by dislocation cross-slip (at low temperature) or dislocation climb (at high temperature). Adding another term in Equation (2-2), enables recovery to be taken into account. Thus, the evolution equation for dislocation density is given as (Estrin, 1998):

$$\dot{\rho} = (K_1 \sqrt{\rho} - K_2 \rho)\left|\dot{\varepsilon}^p\right| - r \qquad (2\text{-}3)$$

where

$$r = r_0 \exp[-U_0 /(K_B T)]\sinh[\beta\sqrt{\rho}/(K_B T)] \qquad (2\text{-}4)$$

and K_B denotes the Boltzmann constant, U_0 the activation energy, β and r_0 are constants and T is temperature. This constitutive equation enables the dislocation density evolution to be well modelled for a microstructure before dynamic/static recrystallisation takes place. According to high temperature deformation mechanisms, grain size and strain rate play important roles in dislocation density evolution. The dominant deformation mechanism for fine equiaxial grain structures under low strain rate deformation is grain boundary sliding. At a grain boundary, which defines the interface between two neighbouring grains having different crystallographic orientations, not all the atoms are properly bonded, giving rise to the increased boundary energy. In addition, impurity atoms often preferentially segregate along boundaries, because of the higher energy state. It is therefore easy for deformation to occur through grain boundary sliding. In this case, the dislocation density does not increase proportionally with plastic strain. For example, the dislocation density does not reach the critical value ρ_c for many cases of superplastic deformation, thus dynamic recrystallisation does not occur. However, for large grain structures (for example, 200 μm) under high strain rates, for example, 10/s, (much greater than that in metal creep), there is little time for grain boundary diffusion to take place and large grains are difficult

to rotate during deformation. The dominant deformation mechanism under this condition is dislocation slip. Thus, dislocation density increases quickly with plastic strain, which may result in dynamic recrystallisation, depending on the processing conditions. The recrystallisation process refines grains, which may facilitate grain boundary sliding taking place.

2.3.2.2 Recrystallisation

When crystalline materials are deformed at high temperatures, the accumulated dislocations are destroyed by two separate processes. The one discussed above is dynamic recovery, which leads to the annihilation of pairs of dislocations, as well as to the formation of sub-grains. In high stacking fault energy materials (such as aluminum alloys), such recovery processes completely balance the effects of strain- and work-hardening, leading to a steady state flow stress. In materials of moderate to low stacking fault energy, dislocation density increases to appreciably high levels; eventually the local differences in density are high enough to permit the nucleation of recrystallisation during deformation. Such dynamic recrystallisation leads to the elimination of a large number of dislocations, and creates dislocation-free grains. The critical value of dislocations for recrystallisation is expressed as

$$\rho_c = 4\sigma_{surf} / (\tau d^*)$$ (2-5)

where σ_{surf} is the grain boundary energy per unit area, and d^* is the diameter of the recrystallised nucleus.

During recrystallisation, a fraction of a grain boundary area is mobile. This fraction varies slightly during the process. It has been shown (Sandstrom and Lagneborg, 1975a; Sandstrom and Lagneborg, 1975b) that for static recrystallisation this fraction increases with time in the beginning and decreases towards the end of the recrystallisation. The velocity $v(\rho)$ of a moving grain boundary is approximately given by the following expression:

$$v(\rho) = M\tau\rho \tag{2-6}$$

During dynamic recrystallisation, it is likely that the time variation is smaller since some boundaries may be mobile over several cycles of recrystallisation. Although many models have been proposed for grain boundary movement and the growth of recrystallised grains (Sandstrom and Lagneborg, 1975a; Sakai and Jonas, 1984; Li *et al.*, 1999; Humphreys, 1999), the modelling of recrystallised volume fraction, S, has been undertaken normally using empirical expressions, such as (Sakai and Jonas, 1984):

$$S = 1 - \exp[-(K/D_0)t^n] \tag{2-7}$$

where K and n are constants, D_0 is the initial grain size.

2.3.2.3 Grain size evolution

During recrystallisation, new grains are nucleated and the total number increases. Consequently, the average grain diameter, d, decreases. At the same time, normal grain growth takes place working in to increase grain size. Taking only recrystallisation into account, the evolution of the average grain diameter, d, can be written as

$$\dot{d} = -d(df/dt)\ln N \tag{2-8}$$

where N is the number of new grains per old grain after one cycle of recrystallisation, which may be grain size dependent; f is the number of recrystallisation cycles, which can be a non-integer number.

The grain growth rate can be expressed as:

$$\dot{d} = M\sigma_{surf}d^{-r_0} + \alpha\dot{\varepsilon}^P d^{-r_1} \tag{2-9}$$

where γ_0, γ_1 and α are constants. The first term of the equation represents the static grain growth, which is directly related to grain boundary mobility, *M* and grain boundary energy density, σ_{surf}. The second term describes plastic strain induced grain growth, which has been discussed by Cheong *et al.* (2000). Compared with grain refinement due to recrystallisation, dynamic grain growth plays a less important role during deformation because of dynamic recrystallisation, which takes place at an early stage of hot deformation and reduces the average grain size. However, between operations of hot forming processes, static grain growth becomes more important than recrystallisation.

2.4 DEVELOPMENT OF UNIFIED ELASTIC-VISCOPLASTIC CONSTITUTIVE EQUATIONS

A set of unified elastic-viscoplastic constitutive equations has been proposed by Lin *et al.* (2005) and has been successfully used to model recrystallisation, grain size and dislocation density evolution in hot rolling of steels. In hot deformation of IN718, similar phenomena of elastic-viscoplastic flow and microstructural evolution exist. The constitutive equations developed by Lin *et al.* have been employed in this work, by considering the particular features of IN718 during thermal-mechanical processing and are discussed as follows:

Elastic-viscoplastic flow of the material is modelled using a hyperbolic sine law which is considered to accommodate a wide range of temperature and strain rate (Honeycombe and Pethen, 1972; Lin *et al.*, 2005) and is expressed as:

$$\dot{\varepsilon}_p = A_1 \sinh\left[A_2\left(\sigma - R - \sigma_y\right)\right] \tag{2-10}$$

where *R* is an isotropic hardening variable. Recrystallisation takes place during hot deformation

and new microstructure is formed, thus, hardening of the material could be assumed as isotropic which is directly related to dislocation density, ρ. A_1 is a temperature dependant variable. σ_y is yield stress which varies with temperatures and A_2 is a material constant.

2.4.1 Modelling dislocation density

In the model, a normalised dislocation density ($\bar{\rho}$) concept is introduced by defining, $\bar{\rho} = 1 - \rho_i / \rho$, where ρ_i is the initial dislocation density and ρ is the dislocation density after deformation. The normalised dislocation density varies from 0 (the initial state) to 1 (the saturated state).

The dislocation density accumulated during deformation provides a driving force for microstructural evolution, such as recrystallisation and grain growth at high temperatures. Taking strain hardening and recovery into account, the dislocation density rate can be described as:

$$\dot{\bar{\rho}} = C_0 \left(d / d_0\right)^{\delta_1} \left(1 - \bar{\rho}\right) \left|\dot{\varepsilon}_p\right|^{\delta_2} - C_r \bar{\rho}^{\delta_3} - \left(C_s \bar{\rho}\right)/\left(1 - S\right)^{\delta_4} \dot{S} \tag{2-11}$$

where d is the average grain size, d_0 is the initial average grain size, δ_1, δ_2 and C_0 are material constants. The first term of the equation symbolises the increase in dislocation density due to deformation and the dynamic recovery. The term d / d_0 indicates that if the average grain size increases, the dislocation density increases more rapidly, since less grain sliding occurs. In the model, dynamic recovery enables normalised dislocation density to be constrained to a maximum value of the saturated state of 1. The second term of the equation models the static recovery where C_r is a temperature dependant variable and δ_3 is a material constant. Finally, the third term expresses the effect of recrystallisation, S, for the evolution of dislocation density. The terms C_s and δ_4 are material constants.

2.4.2 Modelling recrystallisation

In this research, it is assumed that once the normalised dislocation density increases to a critical value, $\bar{\rho}_c$, given sufficient time, which is controlled by introducing the recrystallised onset parameter, x, recrystallisation takes place. Recrystallisation can be dynamic, which occurs during deformation, or static and meta-dynamic, which happens after forming or between forming operations. The microstructural features, i.e. grain size and dislocation density, affected by recrystallization, change and this affects the mechanical properties of the material. Thus unified elastic-viscoplastic constitutive equations should be able to capture these features and their interactive effects. The modelling of the fraction of recrystallisation, S, takes the form:

$$\dot{S} = H_1 \left[x\bar{\rho} - \bar{\rho}_c (1 - S) \right] (1 - S)^{\lambda_1} \qquad (2\text{-}12)$$

where H_1 and λ_1 are material constants and $\bar{\rho}_c$ is used here as a critical value of normalised dislocation density, below which recrystallisation will not take place. Also it is evident from practical experiments that there is a need for an incubation time for the onset of recrystallisation and this time varies with the value of dislocation density, while the dislocation density must exceed $\bar{\rho}_c$. The parameter x as incubation fraction is given below:

$$\dot{x} = X_1 (1 - x) \bar{\rho} \qquad (2\text{-}13)$$

where X_1 is a temperature-dependent parameter. The recrystallised volume fraction varies from 0 to 1, depending on the evolution of dislocation density.

2.4.3 Modelling of average grain size evolution

In considering static grain growth and new grains nucleated during recrystallisation, the total number of grains may increase and the average grain size, d, may decrease. The evolution of the average grain size can be written as:

$$\dot{d} = G_1(d_0/d)^{\psi_1} - G_2\dot{S}(d/d_0)^{\psi_2}$$

<div align="right">(2-14)</div>

where G_1 is a temperature dependant variable and ψ_1 is a material constant. The first term of the equation describes static grain growth. The second term of the equation models grain refinement due to recrystallisation which reduces the average grain size, where G_2 and ψ_2 are material constants.

2.4.4 Unified elastic-viscoplastic constitutive equations

Considering each feature of microstructural evolution such as recovery, recrystallisation and evolution of grain size, the physically-based unified elastic-viscoplastic equations for IN718 during hot forming take the form:

$$\dot{\varepsilon}_p = A_1\sinh\left[A_2\left(\sigma - R - \sigma_y\right)\right]$$

<div align="right">(2-15)</div>

$$\dot{S} = H_1\left[x\bar{\rho} - \bar{\rho}_c(1-S)\right](1-S)^{\lambda_1}$$

<div align="right">(2-16)</div>

$$\dot{x} = X_1(1-x)\bar{\rho}$$

<div align="right">(2-17)</div>

$$\dot{\bar{\rho}} = C_0(d/d_0)^{\delta_1}(1-\bar{\rho})\left|\dot{\varepsilon}_p\right|^{\delta_2} - C_r\bar{\rho}^{\delta_3} - (C_s\bar{\rho})/(1-S)^{\delta_4}\dot{S}$$

<div align="right">(2-18)</div>

$$\dot{R} = 0.6B\bar{\rho}^{-0.4}\dot{\bar{\rho}}$$

<div align="right">(2-19)</div>

$$\dot{d} = G_1(d_0/d)^{\psi_1} - G_2\dot{S}(d/d_0)^{\psi_2}$$

<div align="right">(2-20)</div>

$$\sigma = E(\varepsilon_T - \varepsilon_p)$$

<div align="right">(2-21)</div>

where E is Young's modulus (142,000MPa for IN718 within the hot deformation temperature range). Softening mechanisms, dynamic recovery, static recovery (annealing) and recrystallisation are included in the equations and the interrelationship of the physical variables and elastic-viscoplastic flow of the material can be fully described. The factors, A_1, X_1, σ_y, C_r, $\bar{\rho}_c$, G_1 and B, arising within the constitutive equations (2-15) to (2-20), have been assumed to

be temperature-dependent parameters, which are defined using the classic temperature-compensated parameters in Arrhenius relations and are listed in Table 2.2.

$\sigma_y = \sigma_0 \exp(Q_p /(\kappa T))$	$C_r = C_{r0} \exp(-Q_r /(\kappa T))$
$\overline{\rho}_c = \overline{\rho}_{c0} \exp(Q_c /(\kappa T))$	$G_1 = G_{10} \exp(-Q_{gg} /(\kappa T))$
$A_1 = A_{10} \exp(-Q_a /(\kappa T))$	$X_1 = X_{10} \exp(-Q_x /(\kappa T))$
$B = B_0 \exp(Q_b /(\kappa T))$	

Table 2.2 List of temperature dependent parameters. $\kappa = 8.31$ $J \cdot mol^{-1} \cdot K^{-1}$ (Universal gas constant); T is absolute temperature in K.

2.5 PROCEDURE FOR CALIBRATING THE EQUATIONS

The procedure for determining the values of constants within the constitutive equations is divided into two steps. The first step is to determine the constants relating to static grain growth, which is modelled using the first term of Equation (2-20). Experimental data of static grain growth reported by Zhang *et al.* (2000) are shown using symbols in Figure 2.9 (a) and were used for this work. The data were obtained for aging temperatures of 980℃ and 1020℃ for IN718 deformed at $\dot{\varepsilon} = 0.01/s$ to a strain of 0.4. The constants, G_1 and ψ_1 within the static grain growth term were determined from the experimental data using an Evolutionary Programming (EP) based optimisation method, which has been developed for this purpose by Li, Lin and Cao *et al.* and detailed elsewhere in (Lin and Yang, 1999; Li *et al.*, 2002; Cao and Lin, 2008). The solid lines shown in Figure 2.9 (a) are the fitted results. Normally, the temperature window for hot forming is within the range of 950℃ to 1050℃. The dashed curves are the predicted results from the equation for the two extreme temperatures considered in the work, from which reasonable results were derived.

The second step is to determine the other constants within Equations (2-15) to (2-20) and their corresponding temperature dependant variables. Five selected experimental stress-strain curves

from the Gleeble compression tests, representing different strain rates and temperatures, were used for the work and are shown with symbols in Figure 2.9 (b) for a temperature varying from 1000℃ to 1100℃ and a strain rate from 1/s to 10/s. The temperature and strain rate values selected are those most appropriate for hot forming IN718 components in industry. The same technique of determining constants using EP was used for this work. The determined values of the constants are listed in Table 2.3 and their fit with experimental values, by solid lines in Figure 2.9 (b). In addition, the determined unified elastic-viscoplastic constitutive equations are validated using other experimental data obtained from the Gleeble compression tests shown by symbols in Figure 2.9 (c), where good agreement (the error of predicted stress is under 10%) between calculated and experimental results are evident.

The metallurgical investigations was also undertaken to compare the microstructures of the extrudate and the FE simulations of employing the constitutive equations. The extrusion FE model will be detailed in Chapter 5. Two sections of the extrudate were compared, i.e. width and depth sections, and good correlation was derived. The comparison is shown in Appendix B.

Q_p (J/mol)	Q_c (J/mol)	σ_0 (MPa)	C_{r0} (1/s)	ρ_{c0} (-)	A_{10} (1/s)	A_2 (1/MPa)
174996.050	149720.400	3.380×10^{-6}	56941.400	2.000×10^{-9}	1.990×10^{-2}	0.027
δ_4 (-)	H_1 (1/s)	λ_1 (-)	Q_{gg} (J/mol)	G_{10} (μm /s)	C_0 (-)	d_0 (μm)
10.000	7600.000	0.500	1187815.55	1.094×10^{51}	1.900	20.00
δ_1 (-)	δ_2 (-)	δ_3 (-)	C_s (-)	B_0 (MPa)	X_{10} (1/s)	ψ_1 (-)
0.100	2.000	2.500	3.000	0.077	0.840	4.905
ψ_2 (-)	Q_a (J/mol)	Q_r (J/mol)	Q_b (J/mol)	Q_x (J/mol)	G_2 (μm)	
0.010	7455.000	64481.100	87461.077	5273.550	200.000	

Table 2.3 The determined constants within the unified elastic-viscoplastic model for IN718.

(a)

(b)
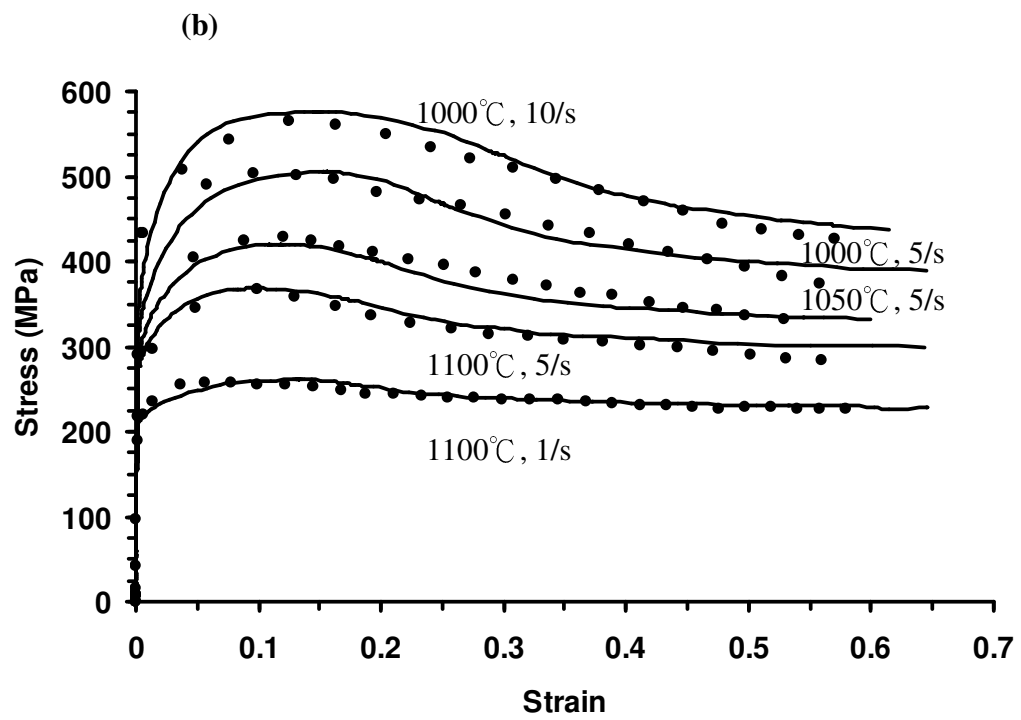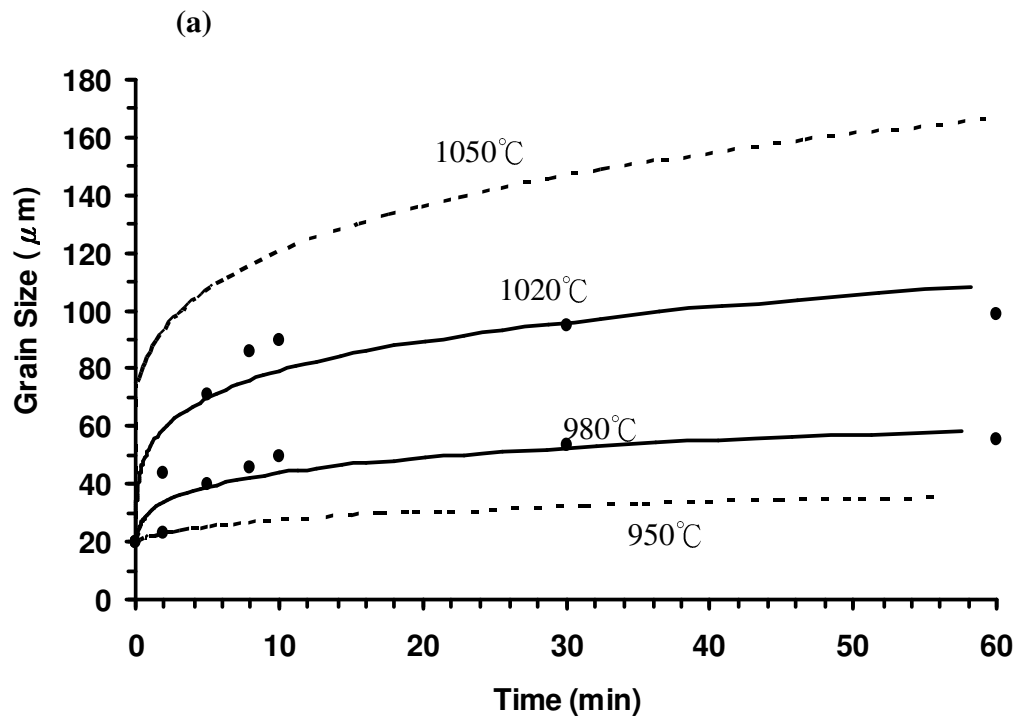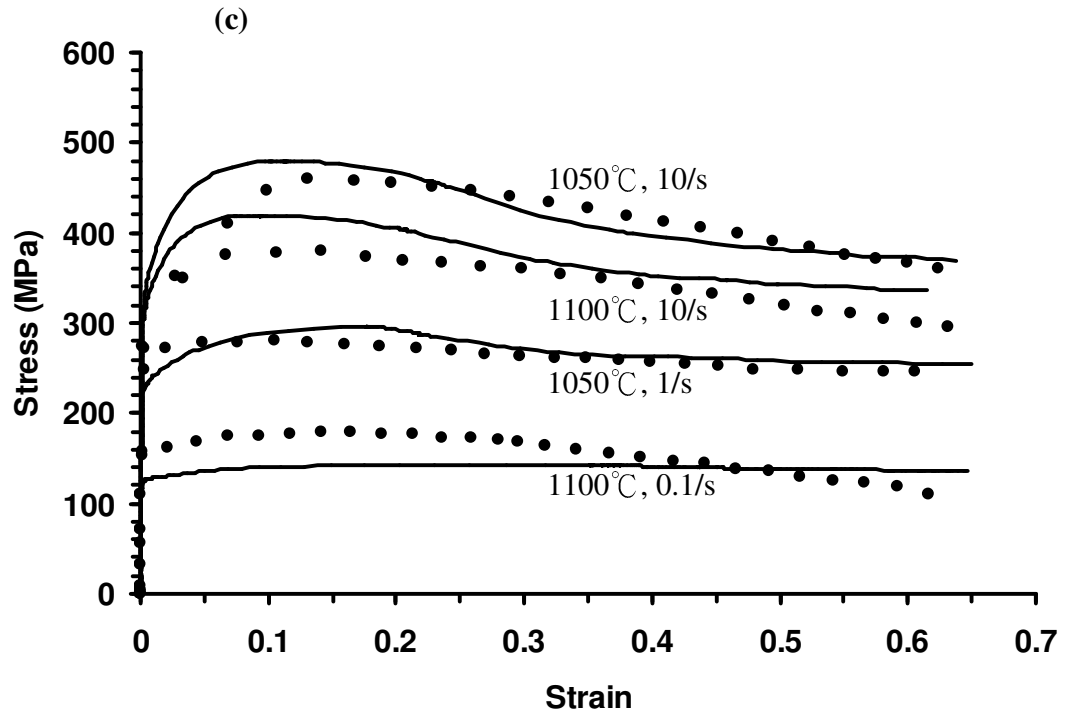
Figure 2.9 Comparison of experimental (symbols) and computed (solid curves) results for (a) static grain growth (the dashed curves are predicted results) and (b) stress-strain relationships for IN718 deforming at different temperatures and strain rates, (c) validation of the model by comparing the predicted (curves) and experimental (symbols) results.

2.6 ANALYSES OF MICROSTRUCTURAL PARAMETERS

For different materials, softening mechanisms can be attributed to a combination of microstructural changes, i.e. dislocation evolution, recovery and recrystallisation. But for a given situation, one mechanism might be dominant. To investigate the effect of individual softening mechanisms on material flow, a comparison between experimental flow curves, calculated curves and amended calculated curves (with no consideration of softening mechanisms) has been made. A stress-strain curve for 1050℃ and strain rate of 5/s has been used for the investigation and the results presented as symbols in Figures 2.10 and 2.11.

2.6.1 Effect of recovery and recrystallisation on the material flow

In Equation (2-18), dislocation accumulation is controlled by the first term through strain increase, followed by a reduction in number of dislocations due to static recovery and recrystallisation in the second and third terms. For investigating the effect of static recovery for the whole material flow, the term is eliminated, (shown as a dashed line), by setting C_r to 0 in Figure 2.10. It can be seen that the stress level becomes higher at low strain. The following decrease of stress is ascribed to recrystallisation term (the third term) in Equation (2-18). For further investigation, both C_r and C_s have been set to 0 in the equation and the resulting curve is shown as a thick solid line in Figure 2.10. It is obvious that recrystallisation is a vital factor in controlling the softening trend at higher values of strain, while recovery occurs at the beginning of deformation, as shown by comparing dashed and thick solid curves. It is also demonstrated that much energy is needed for recrystallisation to take place, as it occurs only after considerable deformation has taken place. From the analysis, it is clear that if the softening mechanisms are not considered, the flow stress of the material cannot be properly modelled.
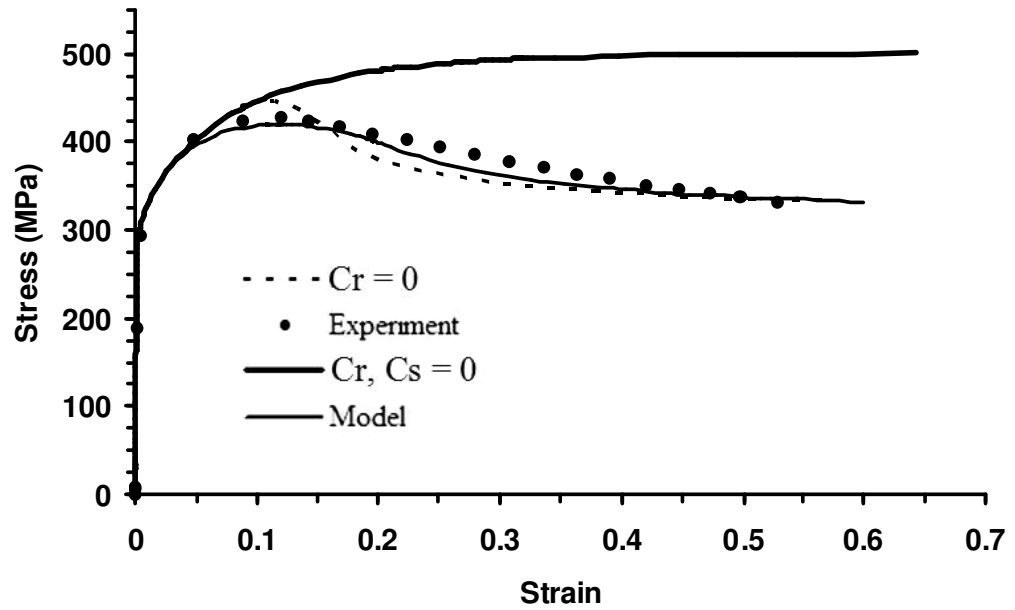
Figure 2.10 Comparison of predicted and experimental result in considering the effect of recovery and recrystallisation. Symbols are the experimental data, thin solid line is fitting result.

2.6.2 Effect of average grain size evolution on the material flow

The assumption used in formulating the model is that the effect of average grain size evolution on flow stress of IN718 is small, which can be seen in Figure 2.11. This is reasonable for many forging operations that are of short duration. Change of flow stress, due to grain movement, may be ignored for short forming times (say, within three seconds) whereas the effect of grain size evolution might be important in a longer duration forming processes, such as creep forming and ring rolling. Computation has been carried out with both G_1 and G_2 set to 0 in Equation (2.20), thus the factor of grain size evolution is eliminated. In addition, with H_1 set to 0, the diamond symbols in Figure 2.11 represent results from the model, ignoring both recrystallisation and grain size evolution. The thick solid line represents the prediction of material flow, omitting recrystallisation only. The two lines overlap, which demonstrates that grain size evolution is not

32

significant, regarding metal flow.
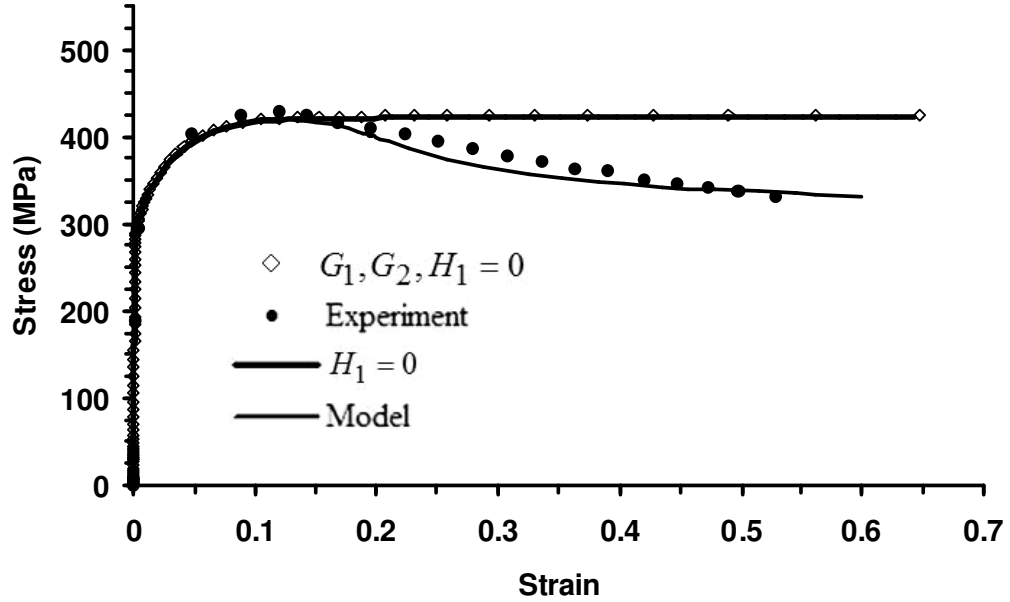
Figure 2.11 Comparison of predicted and experimental results in considering the effect of grain size evolution. Symbols are the experimental data, thin solid line is fitting result.

2.6.3 Prediction of critical strain for recrystallisation

In this research, the definition of critical strain for recrystallisation is the strain when $x\rho - \rho_c = 0$ in Equation (2-16), which means once dislocation density reaches a critical value and given sufficient time, recrystallisation will happen. In Figure 2.12, the predicted values of critical strain for recrystallisation, for different values of strain rate and temperature, are computed from the model and shown as dots. It can be seen that at different strain rate values, the critical strain for recrystallisation varies. Accumulation of dislocations, incubation time and energy are three important factors for initiating recrystallisation. At slow strain rates, there is more time for recovery to take place, which reduces the number of dislocations. Thus, the critical strain for recrystallisation will be higher. On the other hand, there is less incubation time for

recrystallisation, during fast strain rate deformation; hence the critical strain for recrystallisation will also be higher. At a higher temperature, the critical strain for recrystallisation is lower, compared with that at lower temperature, as the higher temperature provides higher energy for promoting its onset. Therefore, the strain rate at which critical strain is the lowest, varies with temperature for this deformation process.
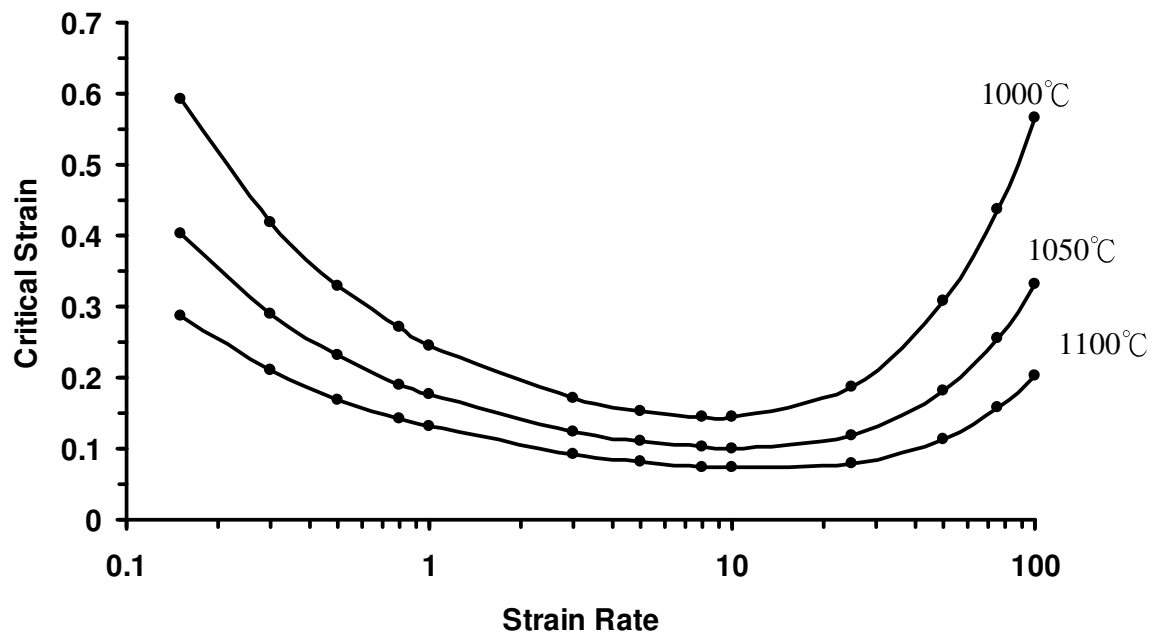
Figure 2.12 The relationship between critical strain and strain rate at different temperatures.

CHAPTER 3

INVESTIGATION OF INTERFACIAL HEAT TRANSFER AND FRICTION DURING FORMING THROUGH EXPERIMENTS AND MODELLING

3.1 INTRODUCTION

The heat transfer and frictional conditions between work-piece and tools, are two difficult factors to analyse during forming. For the heat transfer conditions in the preform extrusion process, die temperatures are much lower than those of the work-piece, which leads to the chilling of work-piece near the die surface. Thus the flow stress of the work-piece increases as does the contact pressure at the die/work-piece interface. This could result in a break down of the lubricant layer, increasing both flow of heat to the die and die temperature. Consequently, die strength is reduced and wear is increased. The mechanism of heat loss to the die is complex in nature and is mainly dependent on the physical properties of the work-piece, the die material and the characteristics of the interface (Jain, 1990). Also, heat transfer can influence work-piece attributes such as; microstructure, mechanical and physical properties. (Wanheim, 1973; Malinowski *et al*., 1994).

The frictional conditions prevailing at the tool/work-piece material interface, in general, increase the redundant work in all metal forming operations by increasing the load and energy requirements. Friction also plays a significant role in determining the life of the tools and the formability of the work-piece material. Therefore, in order to obtain a scientific understanding of thermo-mechanical processes, the nature of interfacial heat transfer and frictional conditions, arising during hot forming, has to be quantified and understood.

In this chapter, following the review of previous research, the methods employed for investigating interfacial heat transfer and frictional conditions will be presented. These include experimental work and FE modelling and discussion of results.

3.2 INVESTIGATION OF HEAT TRANSFER CONDITIONS

The first recorded measurement of die surface temperature during forming is from the research of Vigor and Hornaday (1961). They designed a high-response thermocouple device to measure the surface and near-surface temperature during non-isothermal upsetting of medium carbon steel cylinders. The concept is derived from Hackemann (cited in Kellow *et al.*, 1969) who developed this type of device for the measurement of gun barrel temperatures during WWII. The principles of construction of the thermocouple used by Vigor and Hornaday are shown in Figure 3.1. The hot junction was formed between a constantan wire and a thin steel shim. Temperatures thus recorded were those occurring 0.002 in. below the die surface. In their research, they studied the effects of process parameters such as lubrication, speed and reduction on die heating but did not attempt to estimate heat transfer coefficient from their data, since the influences of deformation heating, heat distribution within work-pieces and interfacial friction heating are difficult to quantify.

Earlier, Beck (1958) gave extensive consideration to heat transfer and thermodynamics in simple upsetting and die forging operations. Steel and an aluminium alloy were used as work-piece materials with operations being carried out on a hydraulic press, crank press and drop hammer. Die temperatures beneath the surface of the die were measured with thermocouples from which the die surface temperatures were predicted. This semi-empirical analysis resulted in an intercept chart which can be used for calculating the temperature drop in forgings during and before deformation. From his research, he concluded that the heat transfer coefficient under nominally zero load was an order of magnitude less than that under high pressure. In addition, above a certain threshold pressure, its value was relatively constant.

Kellow *et al.* (1969) applied the concept of thermal conductance to the study of distribution of temperature in forging dies and, based on their analysis, calibration curves were generated to determine heat transfer coefficient. A robust and responsive device to measure the temperature from the surface and sub-surface of the die was also developed. Jeswiet and Zou (1992) developed a similar device to measure the die temperature during cold rolling approximately 20 years later. In Kellow's study, the internal heat generation within the work-piece, high

speed frictional heating at the surface of the die and oxidation of the work-piece, were shown to have significant effects on the die temperature. The construction of the thermocouple is shown in Figures 3.1 and 3.2 respectively, for surface and sub-surface die temperature measurements.
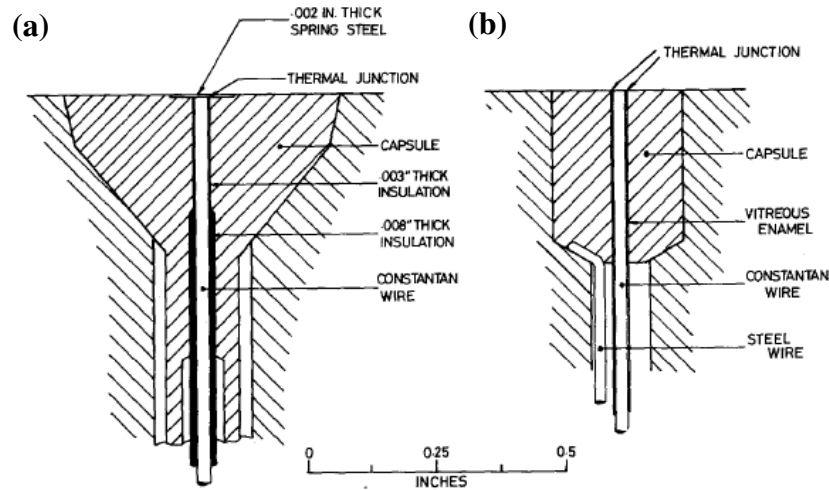
Figure 3.1 (a) Thermocouple construction used by Vigor and Hornaday; (b) thermocouple construction used by Kellow *et al*. to measure surface temperatures (Kellow *et al*., 1969).
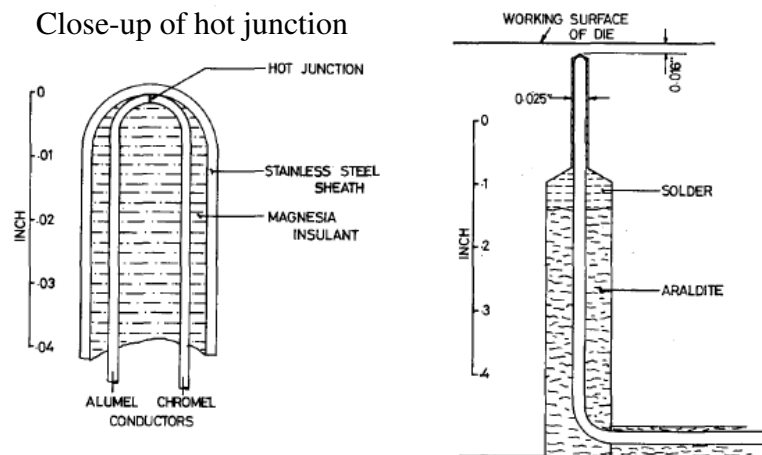
Figure 3.2 The thermocouple construction designed by Kellow *et al*. to measure the sub-surface temperature of the die (Kellow *et al*., 1969).

Later, Semiatin *et al*. (1987), Im (1989) and Burte *et al*. (1990) determined the coefficient of

heat transfer for various forming conditions. Semiatin *et al.* also first used the FE method to produce results for comparison with curves generated from an analytical method using Kellow's equation, but they neglected the generation of heat during deformation. Based on the investigation, they drew the following conclusions:

1. In the absence of deformation, the heat transfer coefficient increases with applied interface pressure up to a point and then maintains a constant value.
2. The heat transfer coefficient increases by approximately an order of magnitude as the pressure level increases from nominally zero to that typical of bulk forming processes.
3. Under conditions involving both deformation of a work-piece and heat transfer, the latter increases with deformation rate.
4. The effect of heat transfer could be ignored in developing calibration curves for the shear friction factor in non-isothermal forging operations.

Recent research (Malinowski *et al.*, 1994; Hu *et al.*, 1998; Li and Sellars, 1998; Chang and Bramley, 2002; Rosochowska *et al.*, 2003), has been focused on the development of a technique for determining the heat transfer coefficient for the contact between die and work-piece, using both the FE method and reverse algorithm.

In published research, values of heat transfer coefficient vary substantially, perhaps due to different experimental methods, material properties, lubricant and forming conditions. Therefore it is essential to derive the values according to a specific forming condition.

3.3 INVESTIGATION OF FRICTIONAL CONDITIONS

The difficulty faced for quantitative evaluation of frictional conditions during actual forming operations has led to the evolution of various tests, which may be divided into two groups.

One group of tests is quantitative tests in which the friction conditions are examined by monitoring force, pressure or topographic variations of the specimens. This type of tests is difficult to perform, because it is sometimes restricted in specific conditions and requires intricate instruments and elaborated work in the laboratory. The examples in this catalogue of

tests are: strip drawing test (Lancaster and Rowe, 1958); surface stress measurement using pins (Van Rooyen and Backofen, 1960; Tuncer and Dean, 1987); total force measurement in upsetting (cited in Schey, 1983); pin-on-disk test (Kluge *et al.*, 1989). Two tests only suitable for small deformation are: hard ball on ring test (Shaw *et al.*, 1960) and ridge plough test (Bay and Hansen, 1985).

The other group comprises intuitive tests in which the friction condition is basically determined by observing the geometric change of the test-pieces. These tests rely on a comparison of geometric changes or flow patterns of the work-pieces. The test methods for these tests are simple. With the aid of theories the results can be quantified, but with uncertainties (Schey, 1983). The measurements are usually made subsequent to the tests, thus, the results relate to the final stage of the deformation while possible different intermediate values of friction are not accounted for. This type of test is also suitable for ranking or comparing various frictional conditions and lubricants. Examples are upsetting test, a.k.a cigar test (Hill, 1950; Schey and Wallace, 1968); combined-forward-backward cup extrusion, a.k.a double-cup test (Frederiksen and Wanheim, 1985; Ghobrial *et al.*, 1993; Fereshteh-Saniee *et al.*, 2004); extrusion forging, a.k.a. spike forging test (Isogawa *et al.*, 1992) and ring test, which will be further discussed later. A comparison of the suitability of each test, for different conditions, and the diagrams to describe these tests (except ring test which will be detailed in section 3.3.1) are listed in Appendix C.

3.3.1 Review of ring test

Currently, the most popular method of determining frictional conditions during bulk plastic deformation of metals is the ring test. The technique, first proposed by Kunogi (1954) and later developed by Male and Cockcroft (1964), allows a friction factor or a coefficient of friction to be determined by comparing the change in the inner diameter of a ring with its reduction in height.

As the ring deforms, at any instant there exists a neutral radius. Inside this radius, metal flows towards the centre of the ring and outside it flows to the external perimeter. If the tool/work-piece interface is frictionless, the radius will be zero since all material flows outwards and the ring will deform as though it was a solid body. The higher the value of friction, the larger is the neutral radius and for very high friction, most metal flows inwards then closes the bore of the ring. As a generality, for a given reduction in height, the smaller is the bore of the ring, the greater is the friction. The changing shape of the deformed rings subjected to friction is shown in Figure 3.3.
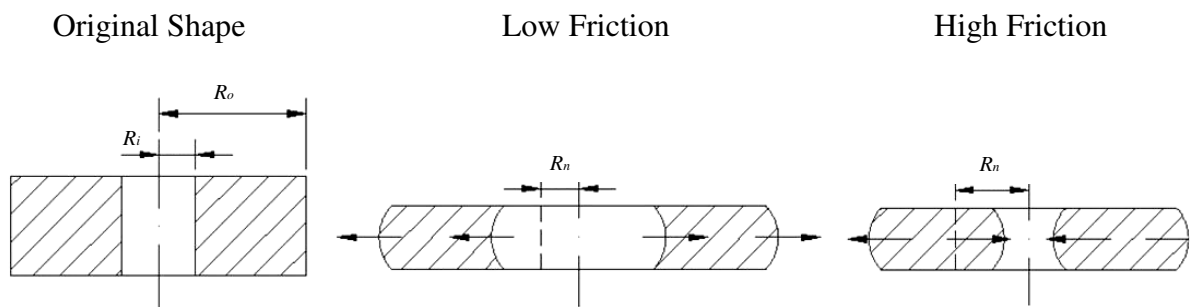
Figure 3.3 The changing shape of the ring before and after deformation; R_o = outer radius, R_i = inner radius, R_n = neutral radius.

Many theoretical and experimental analyses (Male, 1962; Male, 1964; Male and Cockcroft, 1964; Hawkyard and Johnson, 1967; Avitzur, 1968; Male and DePierre, 1970; Lee and Altan, 1972; Liu, 1972; DePierre and Gurney, 1974) have been undertaken that account for the effect of various parameters such as bulging, strain hardening, specimen geometry, strain rate, lubricating conditions, temperature, etc. The results of the analyses are presented in the form of calibration curves, plotted as reduction of inner diameter against deformation in height. Several researchers have attempted to produce an ever improving set of calibration curves.

The first study of the influence of process parameters on friction was completed by Male and Cockcroft (Male, 1962; Male and Cockcroft, 1964) using purely an experimental analysis for investigating sticking friction, intermediate friction and zero friction conditions. Most of the calibration curves produced were based on the assumption of an isothermal condition and a coefficient of friction at the contacting surface, constant and uniform.

Subsequent mathematical analysis (Avitzur, 1964; Male and DePierre, 1970; Male *et al*., 1972; Liu, 1972) provided a possible mean for a more accurate calibration for friction evaluation. The analysis by Avitzure (1964) using upper bound methods assumed a constant shear factor, m, and a material which followed the von Mises flow rule. Hawkyard and Johnson (1967) presented a set of calibration curves for the 6:3:2 ring geometry derived from a stress analysis approach and compared these with the experimental curves of Male and Cockcroft (1964). It was found that the general form of their curves corresponds well with the experimental curves. They have also alleged that their theoretical curves developed for the geometric ratio of 6:3:2 could be used for any other sizes of specimen, as long as the ratio remained unchanged.

Later Male *et al*. (1970; 1972) established a set of calibration curves for five different sizes of

rings. Theoretical results obtained for the ratio of 6:3:2 of the rings were compared with the experimental results from previous Male and Cockcroft's work (1964). It was found that the experimentally derived curve for $m=1$ was higher than the theoretical maximum curve. At $m=0$, their theoretical conditions were not achieved during the experiments. They also suggested an approximate empirical relationship between coefficient of friction μ and friction factor m of $\mu = m_{ring} / 2\sqrt{3}$. This equation is derived by comparing their theoretical curves with the previous experimental curves at 50% deformation.

Some work was targeted at narrowing the discrepancy between the theoretical and experimental results by incorporating a greater number of parameters in the mathematical model, by introducing barrelling. Liu (1972) and Lee and Altan (1972) adopted the upper bound method to analyse the ring compression test. In their analysis a set of calibration curves for 6:3:2 ring specimens were derived for $m=0.2$ and $m=1$. Experiments were conducted to verify the analytical solutions and it was found that at $m=1$, there was discrepancy, while at $m=0.2$ the curves were identical. The difference at $m=1$ was due to the errors in the analytical technique. Also, comparison was made from their results with those developed by Male *et al*. (1970; 1972) and it was found that the curves developed by Lee and Altan were closer to the experimental results.

More recently, Rao and Sivaram (1993) pointed out that great care should be taken in applying these theoretically derived calibration curves from various research due to the fact that assumptions were different with respect to the bulging and the velocity field made in the computations, when the upper bound theory was adopted. They compared calibration curves obtained by several researchers for friction factors equal 0 and 0.05, as shown in Figure 3.4.

The calibration curves varied according to the frictional theory on which they are based for friction factor = 0.05. More recently still, Sofuogou and Rasty (1999) observed, from their experimental studies using plasticine together with FE analyses, that the available calibration curves were not applicable to all types of materials and conditions. They suggested that the results of ring compression tests should be used in conjunction with calibration curves generated specifically for the material under investigation.

For extrusion, in addition to feasibility and convenience, there are some aspects that a test method should fulfill for the accurate analysis of frictional behaviour. Bulk plastic deformation, surface enlargement, and high forming rates are the most important features of extrusion which should be present in a test for the investigation of friction. Friction tests involving little or no plastic deformation, do not match extrusion conditions.

As was stated above that the ring test is assessed by physical measurement of shape change, unlike quantitative tests which require the information of mechanical properties of the material and the forming loads where the measurement of these parameters present major difficulties under high temperature forming conditions. Although the ring test does have its limitations, a well-known one is its relatively small surface expansion ratio (Hironaka *et al*., 2009). Compared with spike or double-cup tests, the results are reproducible after long periods of time using specimens produced in the same batch, as the experimental conditions are easy to control. Also it is easy to carry out and is applicable over wide variations with respect to temperature, amount of deformation, lubrication, etc. Therefore, it was chosen in this research to examine frictional conditions, as described in section 3.4.
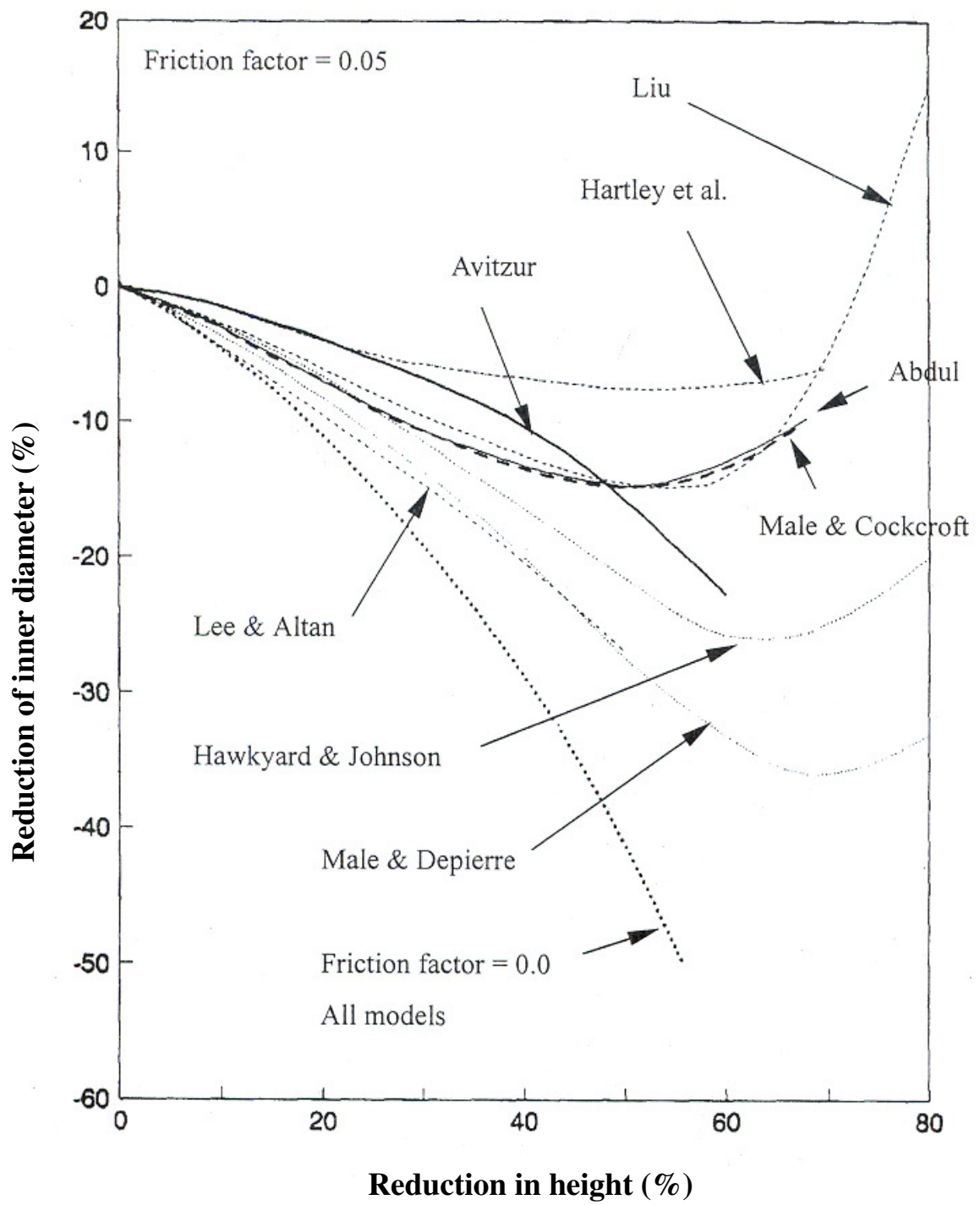
Figure 3.4 Comparison of the calibration curves derived by several researchers for effective friction factors of zero and 0.05 (Rao and Sivaram, 1993).

3.4 SETTING AND PERFORMING OF THE TESTS

3.4.1 Tooling set-up

Compression tests were performed to examine heat transfer condition during hot forming while ring tests were carried out to investigate the frictional conditions. Both tests were undertaken on a Wilkins & Mitchell 200-tonne crank press (similar to the one in industrial use) using the same dies. The mechanism of the press and the displacement-time characteristic for the slide, are shown in Figure 3.5 (a) and (b), respectively. A pair of flat dies made of AISI-H13 hot work tool steel, were mounted in a two-column die-set which was fixed to the press. Heater bands were fitted to both top and bottom dies, to enable their temperature to be raised to predetermined values. In order to reduce heat loss from the dies, they were supported by light springs which separated them by approximately 3 mm from the tool set, in the unloaded situation. The whole set-up is shown in Figure 3.6.

For measuring temperature fields during forming, the bottom die was instrumented with six K-type thermocouples at various radii and depths, as shown in Figure 3.7. Thermocouples A1, A2 and A3 were located 2 mm whereas B1, B2 and B3 were located 1 mm, under the die surface. The thermocouples were attached securely to the die by removing the tips of the sheaths of standard 2-mm diameter thermocouples and by welding the hot junctions to the bottom of the pre-drilled holes.
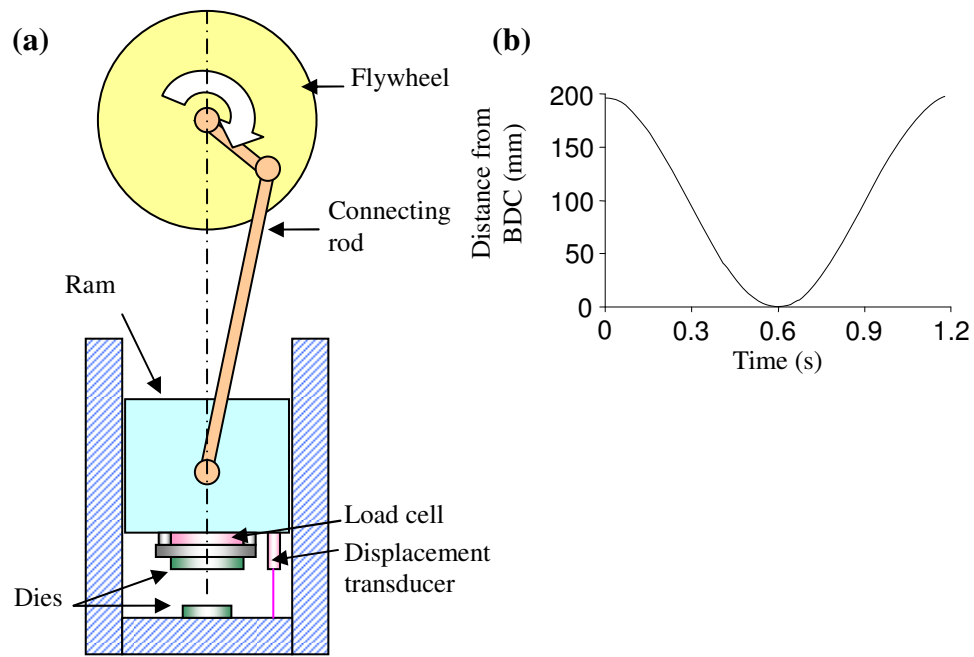
Figure 3.5 (a) Direct crank drive mechanical press (adapted from Lange, 1976); (b) displacement-time profile of the slide.
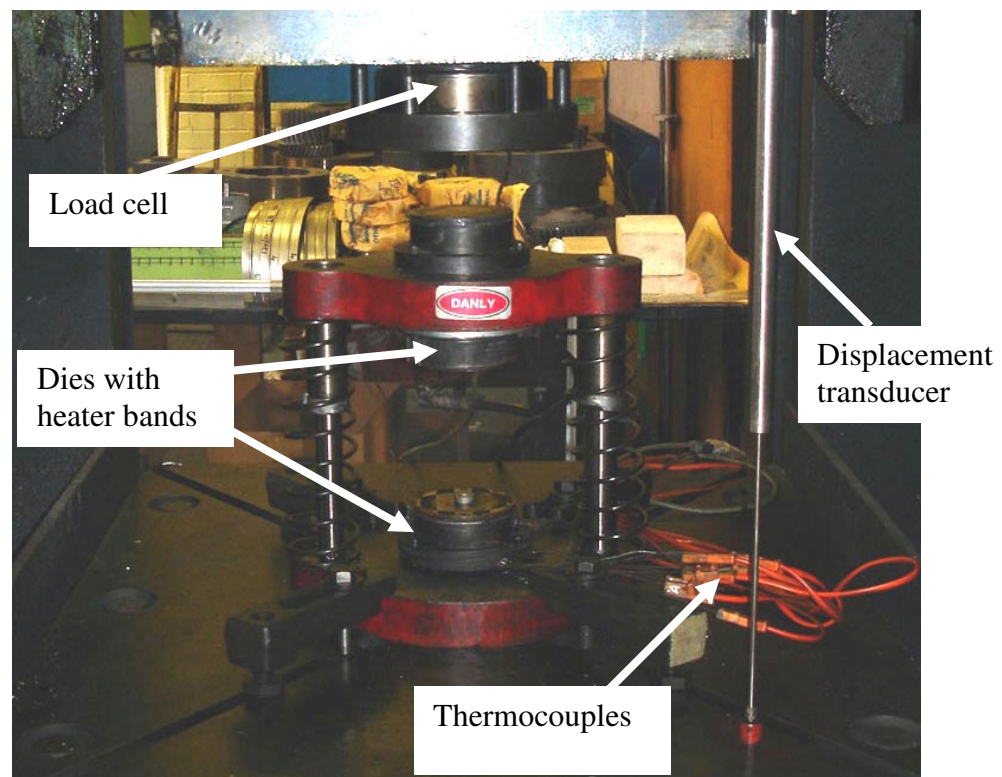
Figure 3.6 The set-up of the experiments.
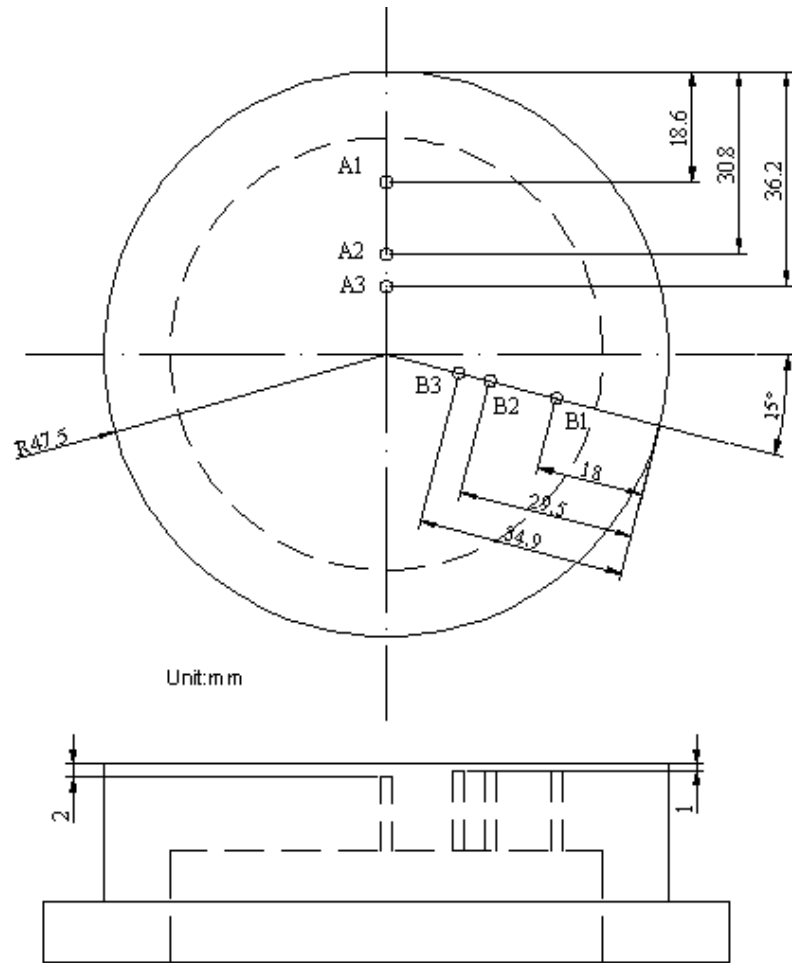
Figure 3.7 The positions of six thermocouples on the bottom die.

3.4.2 Test-piece and die preparations

Solid billets of 41 mm diameter and 13 mm height were machined from IN718, nickel superalloy for compression tests and rings for the friction tests were machined into the following geometric ratio: outside diameter 6: bore diameter 3: height 2. The external and inner diameters of rings are 18 mm and 9 mm, and the height is 6 mm.

Prior to the testing, billets and rings were first shot blasted and cleaned by acetone, to facilitate the coating process and then glazed. Glaze was applied by dipping the test-piece into the glass liquid at room temperature. The desired thickness of glaze was built up by applying layer upon previously dried layer. The final thickness was measured using a micrometer. Prior to forging, glazed test-pieces were placed on supports in a muffle furnace to prevent the

coating from sticking to the hearth, and were heated for ten minutes (billet) and five minutes (ring) to ensure a uniform temperature distribution. Supports used for both tests are shown in Figure 3.8 (a) and (b).
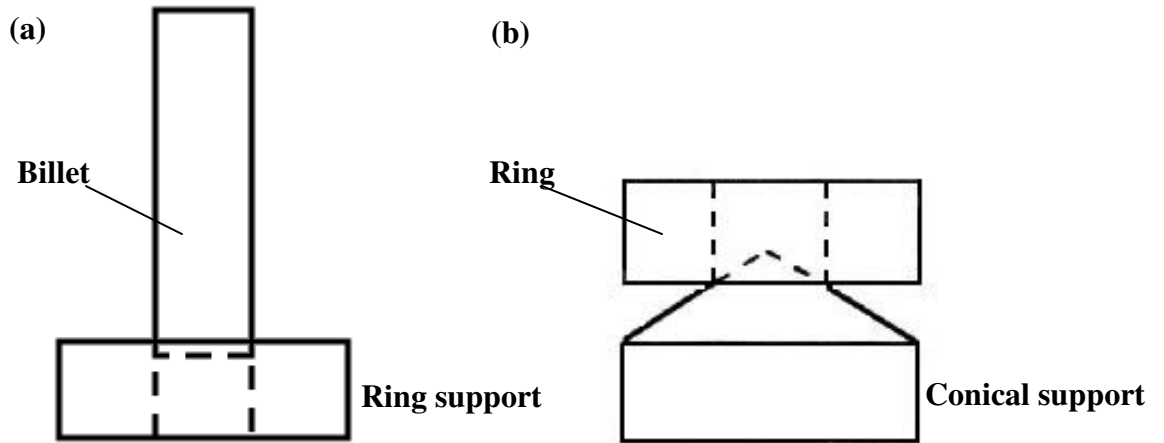
Figure 3.8 (a) Ring support for billets and (b) conical support for rings in order to prevent the coating sticking on other surfaces.

3.4.3 Test methodology

The flat surfaces of the heated top and bottom dies were cleaned and a water-based colloidal graphite lubricant was applied to them by hand spray before each test. Calibration of the number of sprays and quantity of deposited lubricant was undertaken prior to the forging tests. The amount of lubricant deposited on the dies was determined by spraying it on an aluminum foil which was the same size with the die. The foil with coated dry lubricant was weighed. After deducting the weight of the foil, the quantity of the lubricant per unit of area was determined. Different amounts of glass glaze and graphite lubricant were applied for investigating their effects on the heat transfer and frictional conditions. The quantity will be listed in sections 3.5.1 and 3.5.2.

Test-pieces, hand held in tongs, were transferred from the furnace to the centre of the bottom die and forged within three seconds, to the preset height reductions. The tong, shown in Figure 3.9, was designed to ensure all specimens were placed concentrically on the bottom die. The rod and auxiliary pins were adjustable in order to accommodate test-pieces for different

sizes. Then the dies were cleaned with abrasive and lubricated for the next test. Load, temperature and displacement of the press slide were recorded against time for both tests. The signals were recorded and processed firstly by a signal amplifier and then by a data-logging system. For the ring tests, after forging, the rings were cleaned with abrasive and acetone. Plasticine was used to fill the deformed bores, to derive a representative value of the inner diameter of rings, due to barrelling of the inner holes after deformation.
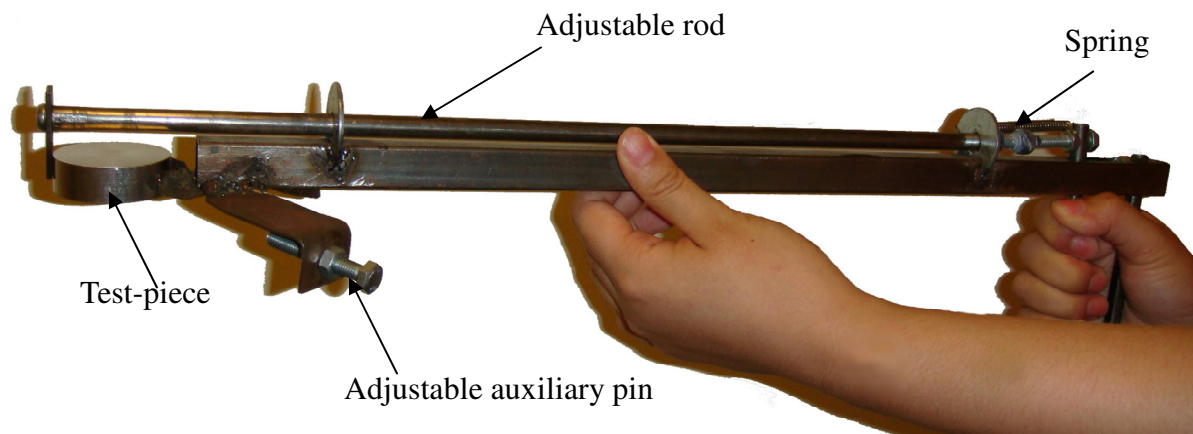
Figure 3.9 Designed tong for placing test-pieces on the die centre.

3.5 EXPERIMENTAL PROGRAMMING

3.5.1 Compression Test

Nine tests were performed, according to the L9 factorial experimental design, for evaluating the effect of each variable on the value of effective heat transfer coefficient. In addition, tests for die temperature $= 100℃$ and work-piece temperatures $= 1100℃$ were undertaken for validating the determined heat transfer coefficients. The L9 experimental matrix is shown in Table 3.1.

Test No.	Test-piece Temp. (℃)	Die Temp. (℃)	Thickness of Coating (µm)	Lubricant Quantity (g/mm^2)	Reduction of Test-piece (mm)
1	1050	200	30	2.82×10^{-5}	0.5
2	1050	200	30	7.05×10^{-5}	1
3	1050	200	30	12.70×10^{-5}	1.5
4	1050	200	60	2.82×10^{-5}	1
5	1050	200	60	7.05×10^{-5}	1.5
6	1050	200	60	12.70×10^{-5}	0.5
7	1050	200	90	2.82×10^{-5}	1.5
8	1050	200	90	7.05×10^{-5}	0.5
9	1050	200	90	12.70×10^{-5}	1

Table 3.1 Control values for each factor in heat transfer tests according to L9 factorial experimental design.

3.5.2 Ring test

Ring tests were performed using two different thicknesses and amounts of coating and lubricant under different die/work-piece temperatures. Glass coating thicknesses were, 40 µm and 60 µm and lubricant amounts were, 2.82×10^{-5} **g/mm** ^{2} and 7.05×10^{-5} **g/mm** ^{2} . Reductions were 1 mm, 2 mm, 3 mm and 4 mm for each test condition, in order to compare the calibration curves generated from FE simulations. The programming matrix is outlined in Table 3.2.

Work-piece Temperature (℃)	Die Temperature (℃)	Thickness of Coating (μm)	Lubricant Quantity (g/mm^2)
1050	100	40	2.82×10^{-5}
		40	7.05×10^{-5}
		60	2.82×10^{-5}
		60	7.05×10^{-5}
	150	40	7.05×10^{-5}
		60	
	200	40	7.05×10^{-5}
		60	2.82×10^{-5}
		60	7.05×10^{-5}
1080	200	60	7.05×10^{-5}
1100	100	40	7.05×10^{-5}
		60	2.82×10^{-5}
		60	7.05×10^{-5}
	200	40	2.82×10^{-5}
		60	

Table 3.2 Ring test programme.

3.6 FE MODELLINGS OF COMPRESSION AND RING TESTS

The simulations for compression tests were performed first. The values of effective heat transfer coefficient were amended in the FE simulations, in order to fit experimental temperature curves derived from the tests. Then, the determined effective heat transfer coefficient was used to obtain friction calibration curves from FE simulations. In conjunction with experiments, the effective friction factors for various forming conditions, such as different coating/lubricant, forming temperatures etc. were obtained.

Two models were built for simulating compression and ring tests. For modelling heat transfer, DEFORM-Multiple Operation was the software used. The whole forming simulation was divided into three stages: before forging (sitting for one second), during forging and after forging.

For modelling the ring tests, DEFORM-2D V9.1.1 software was used. The modelling of ring test was divided into two stages: before forging (with a ring sitting on the bottom die for one second) and, during forging. The derived heat transfer relation was input in the model. The friction calibration curves were generated by amending the value of effective friction factor at the die/work-piece interface and measuring the dimensional changes of the internal diameter corresponding to the reduction of height.

The heat generated by friction and deformation was also included in the simulations. The top and bottom dies for both models were meshed for the fully coupled thermo-mechanical analyses. Due to the axisymmetrical nature of the problem only a half of the cross-section of the specimens was modelled and both top and bottom dies were assumed to be semi-infinite in the 2D simulations. The justifications of the choice of mesh sizes for both tests are presented in Appendix D. In addition, because of the small amount of deformation, imposed in the heat transfer tests, the amount of frictional heating was assumed to be sufficiently small to be ignored, in the simulations of compression tests. For the simulations of ring tests, the forging stroke was 4 mm, giving a deformation of 67% for each ring.

For both simulations, assumptions were made as following:
- No heat lost from the work-piece during the transport from furnace to the die.
- Friction remained constant throughout deformation (friction factor = 0 in the simulations of compression tests).
- Friction is uniform over the die/work-piece interface.

The deformation kinematics in the simulations was set identical to those of the real tests. The total stroke is 200 mm and the movement is 0.83 strokes per second. The models of compression tests and ring tests are shown in Figure 3.10 (a) and (b). The constitutive relations to describe mechanical material properties of IN718 used in both models, defined in

Chapter 2 as an elastic-viscoplastic material, were input using subroutines which will be detailed in Chapter 5. Thermal material data, i.e. thermal conductivity and heat capacity of IN718 were provided from the DEFORM material library as functions of temperature, are listed in Appendix E. The thermal material property for AISI-H13 die defined as a rigid body was obtained from the DEFORM database and is also listed in Appendix E.
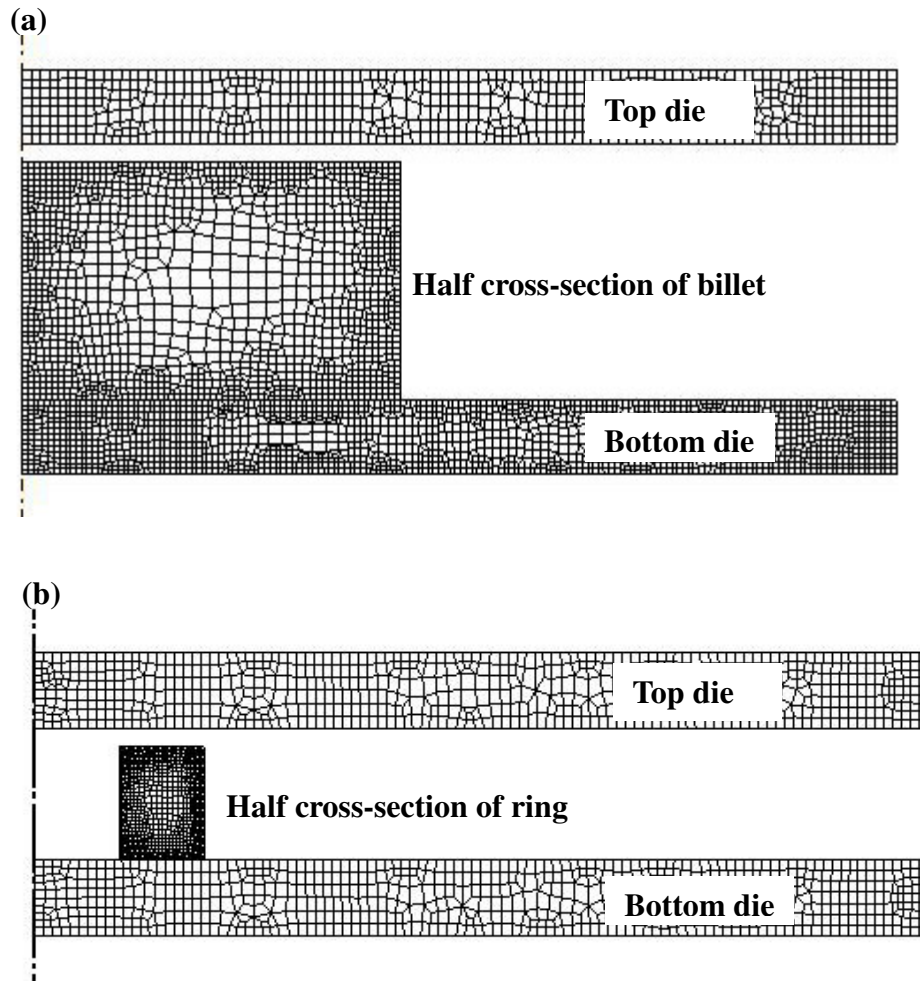
Figure 3.10 Axisymmetrical FE models for simulating (a) compression and (b) ring tests.

3.7 RESULTS AND ANALYSES OF HEAT TRANSFER COMPRESSION TESTS

The deformed and original test-pieces for compression tests are shown in Figure 3.11, while typical experimental temperature curves are compared with those derived from the FE analyses, in Figure 3.12. Lines are the experimental data obtained at different thermocouple positions and symbols represent the simulation results. Temperatures recorded by thermocouples A1 and B1 have changed little, because at no stage were they underneath the hot billet.
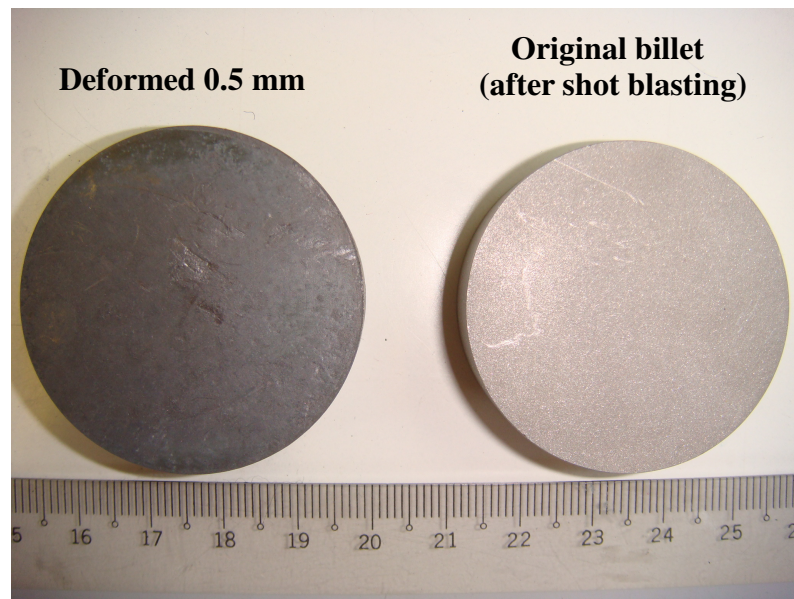
Figure 3.11 Deformed and original billets.
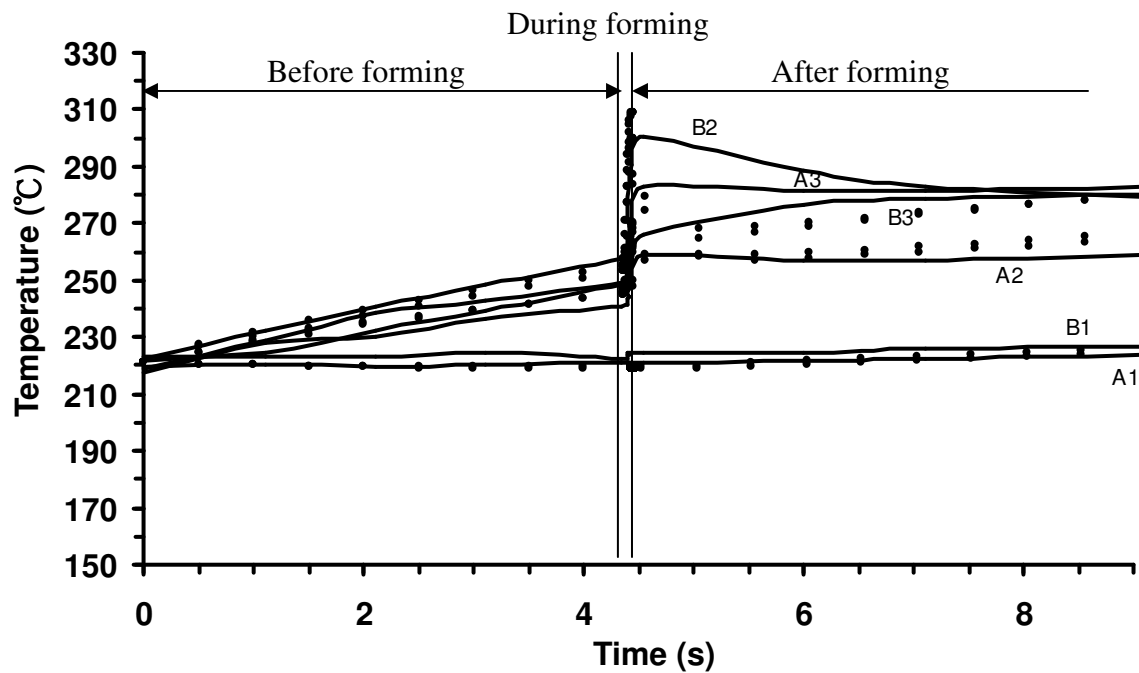
Figure 3.12 A comparison of computed (symbols) and experimental (lines) temperature histories under different positions of the bottom die.

It can be observed that die temperatures increased slowly when the work-piece was placed on it. As the pressure was very low before forming, the area of interfacial contact would have been low and the uncompressed glass/lubricant layers would have acted as heat transfer barriers. The effective heat transfer coefficient would have been low, resulting in a low rate of heat transfer to the die.

During forming, the pressure increased at the interface and intimate die/interface/work-piece contact would have become more widespread, enabling heat to be transferred more easily. It can be seen that a sudden jump of die temperatures occurred when forging started, because of the sharp increase in the value of effective heat transfer coefficient corresponding to the increase in pressure at the interface.

After deformation, the temperatures dropped due to the heat lost as well as to relatively poor die/work-piece surface contact, compared with that observed during the forging process.

Lubricant and coating were two important factors to affect heat transfer between die and

work-piece, before forming. As may be seen in Figure 3.13, the effective heat transfer coefficient is influenced by lubricant quantity, particularly in the presence of thin glass coating, but lubricant quantity has little effect on effective heat transfer coefficient for a glass thickness above 60 μm. The calculated effective heat transfer coefficients before forging varied from 143 W/m^2 ℃ to 200 W/m^2 ℃ for different coating and lubricant thicknesses.
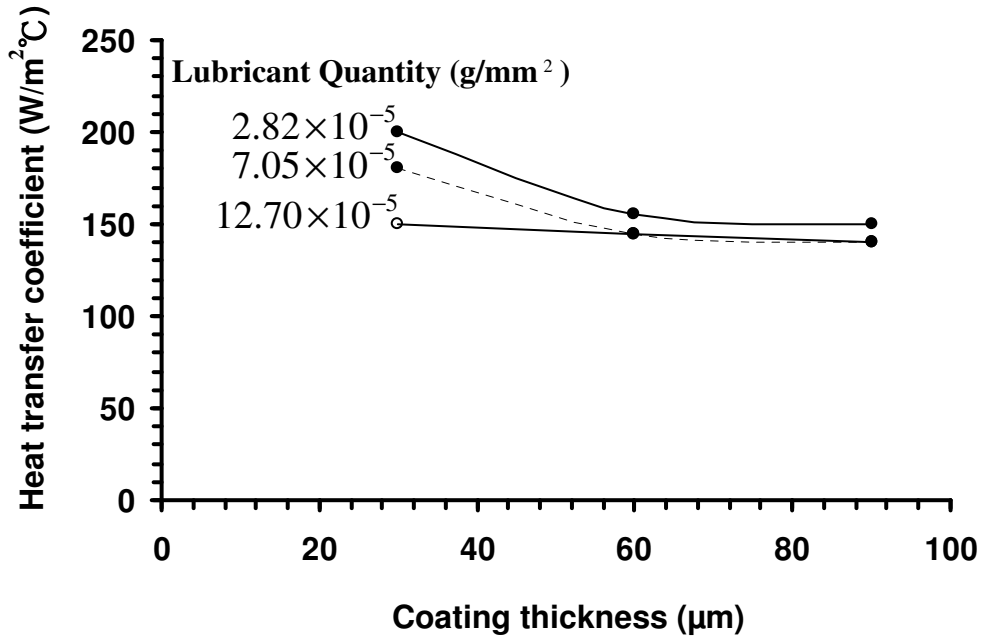
Figure 3.13 Variation of effective heat transfer coefficients before upsetting with glass coating thickness, for different amounts of graphite lubricant.

In contrast to the condition before deformation, the reduction of work-piece became the most influential factor affecting heat transfer during forging. The relations between effective heat transfer coefficient and forming pressure is plotted in Figure 3.14 (a) and (b). Due to the small deformation, the barrelling effect was ignored and the final cross-sectional areas for three reductions could be calculated. The pressures were derived by measuring maximum loads divided by the final cross-sectional areas for three different reductions of the billets. The maximum loads for three reductions are 25 tonne (0.5 mm), 30 tonne (1 mm) and 40 tonne (1.5 mm) respectively, regardless of coating/lubricant. The heat transfer coefficients are increased by approximately two orders of magnitude by the high forging pressure. The effect of the lubricant and coating thickness on heat transfer was reduced during forging, compared

with that in the zero pressure pre-forging stage. This might be due to the initially different thicknesses of the interface layers, being reduced to a common value, by pressure and increased surface contact.

The mechanics of the interrelationship of lubricant and coating to heat transfer during forging is a subject yet to be investigated scientifically, but it can be seen from Figure 3.14, that, although it does appear that thinner glass coating and thicker lubricant layer tend to promote a higher heat transfer coefficient, there is no obvious trend in change of values for different coating thicknesses and lubricant quantity that can be accepted with confidence. In addition, the values of effective heat transfer coefficient varied from 18000 W/m^2℃ to 27000 W/m^2℃. A definite trend shown in the figures is the increased effective heat transfer coefficient at higher pressures. In Figure 3.15, the average values of effective heat transfer coefficient against pressure are: 19170 W/m^2℃ (179 MPa); 20500 W/m^2℃ (206 MPa) and 24000 W/m^2℃ (263 MPa), for three reductions only, regardless of lubricant and coating conditions. This pressure dependent relation will also be used for generating friction calibration curves later.

The values of effective heat transfer coefficient after deformation were approximately similar to those before forging but it was difficult to investigate the effects of lubricant and coating because both lubricant and coating were dramatically changed after forming.
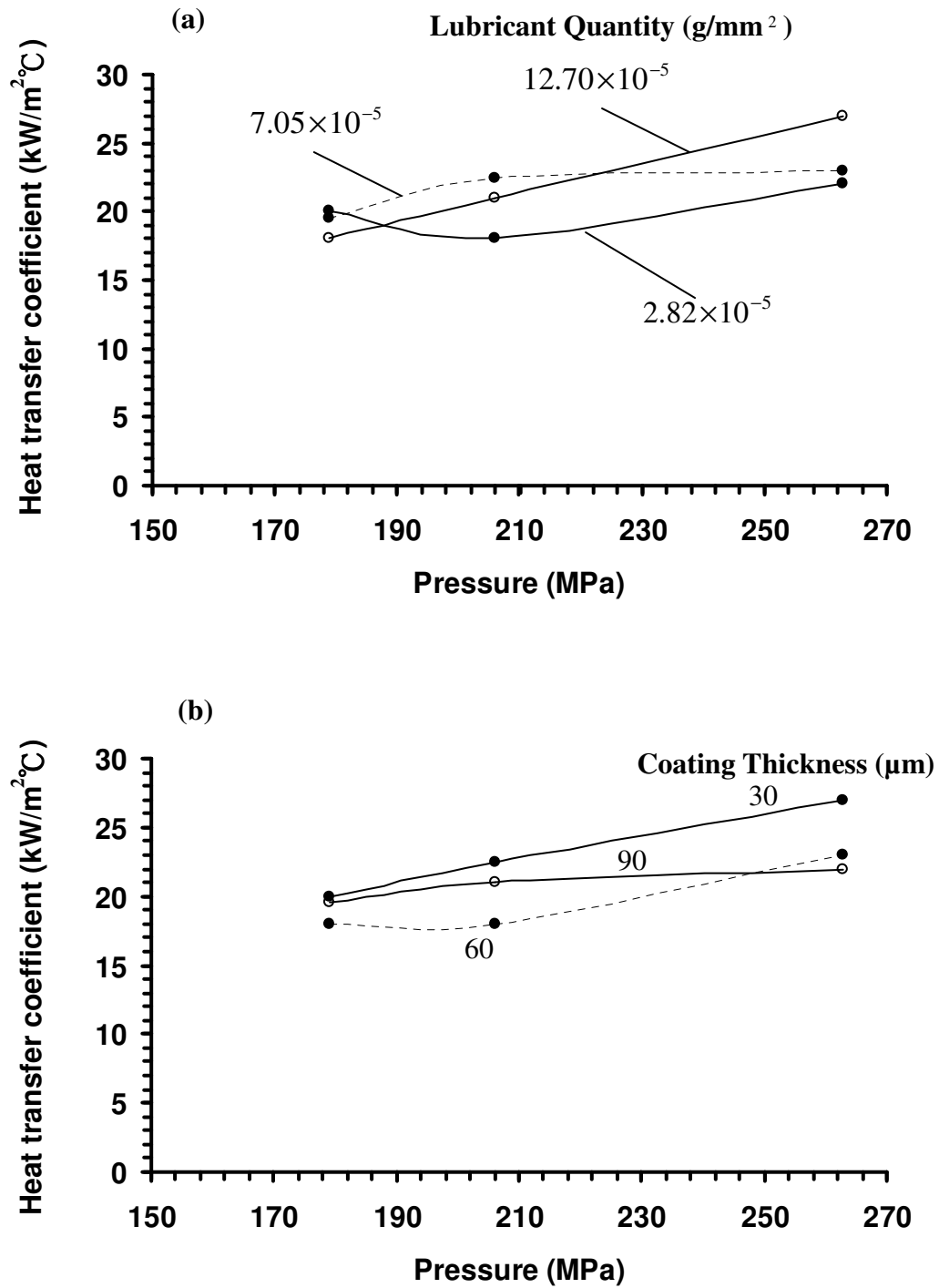
Figure 3.14 Variation of effective heat transfer coefficients during upsetting under different pressures (a) for different lubricant conditions; (b) for different coating thickness.
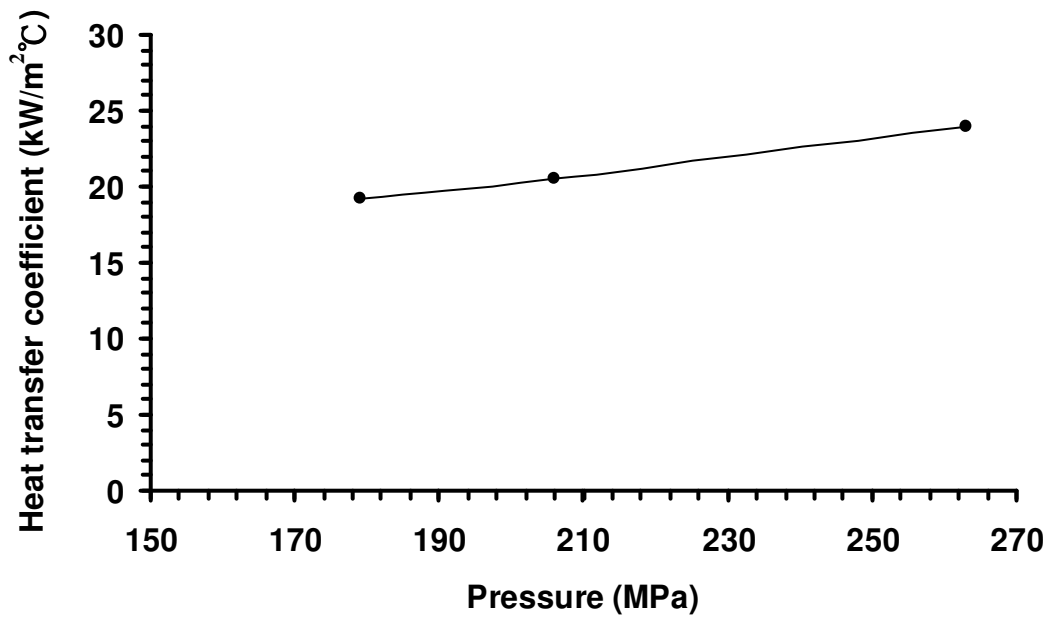
Figure 3.15 Trend of variation of effective heat transfer coefficients with pressure, regardless of coating/lubricant conditions.

3.7.1 Prediction of temperature curves

The determined effective heat transfer coefficients from the nine tests were used to predict temperature curves for three different combinations of die/work-piece forging temperatures under three forming stages (heat transfer coefficients set as pressure dependent during forming and 172 $W/m^2\,^\circ C$ for before and after forming). The results are shown in Figure 3.16 (a)~(c). Since thermocouples A1 and B1 have little changes, they are not included in the figures. The figures show that the determined effective heat transfer coefficient could be used for forging simulations with different die/work-piece temperatures within the practical forging window, with acceptable accuracy in which the errors were within 16% for before forming stage and within 6% for during forming stage.
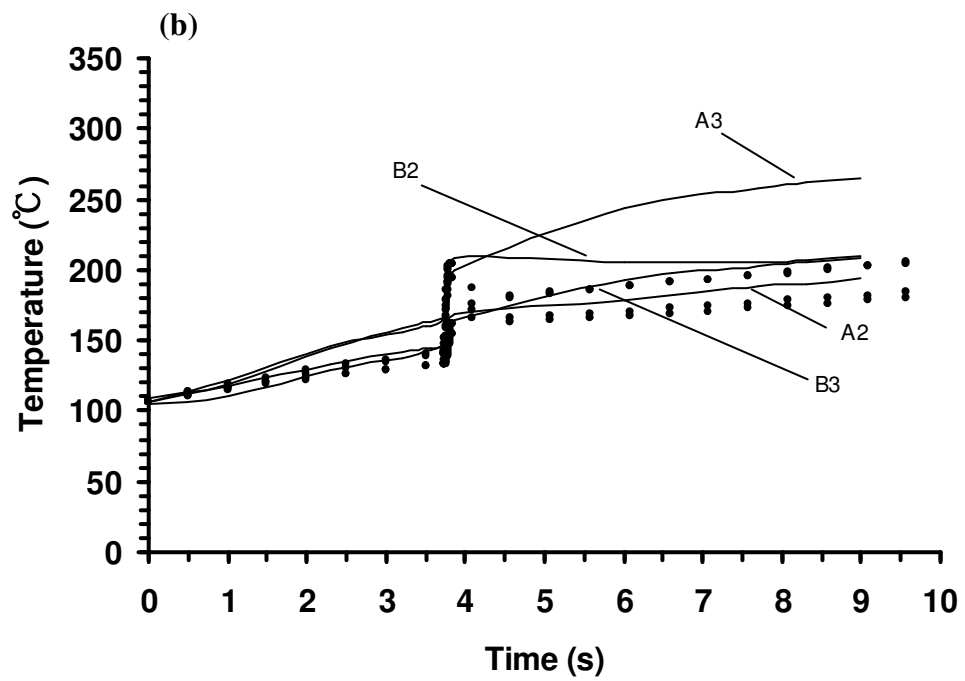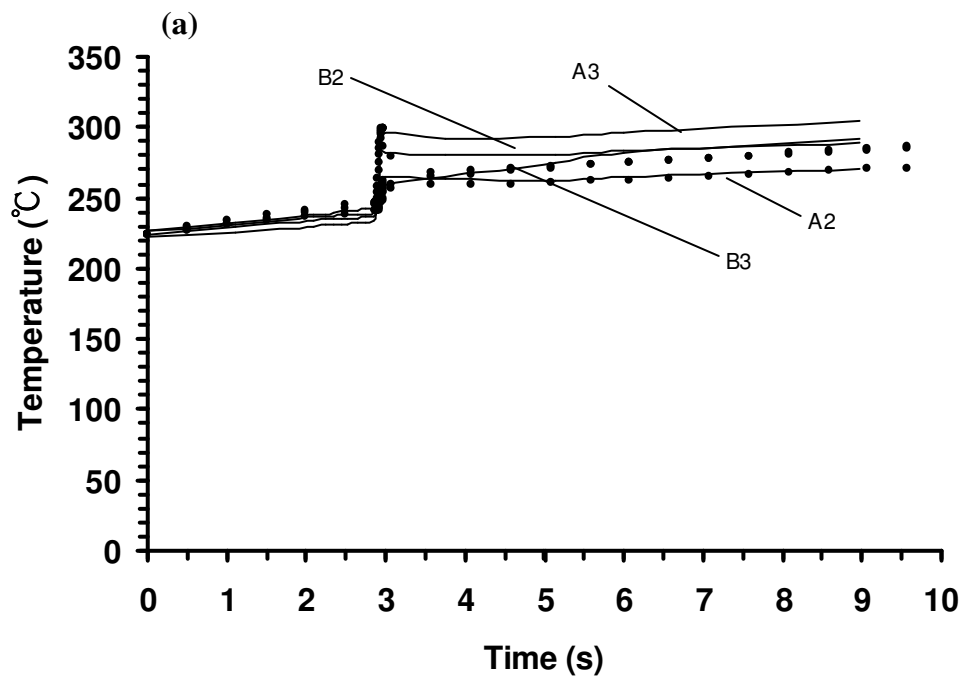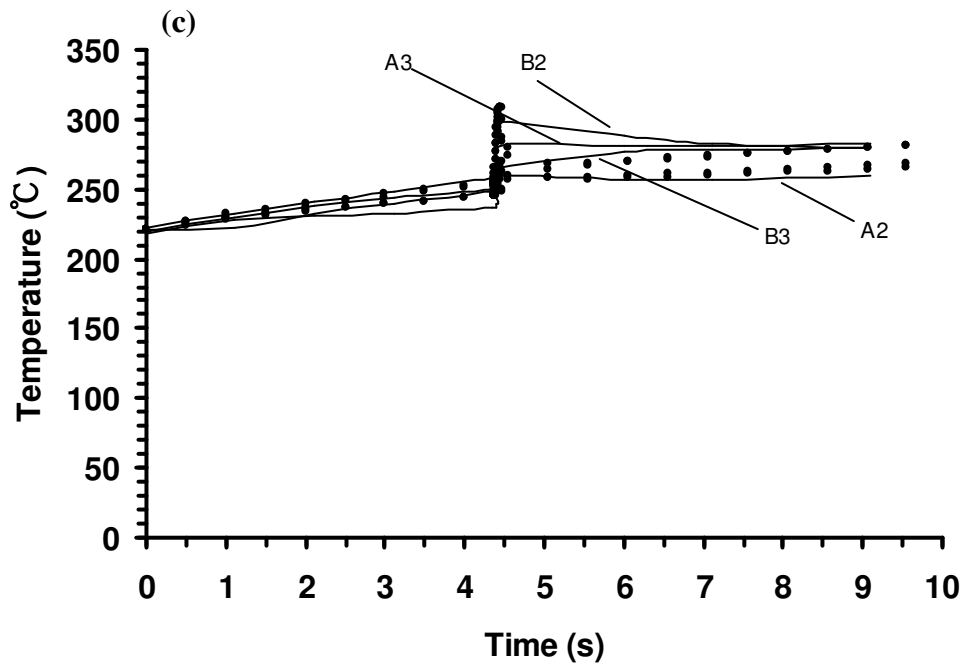
Figure 3.16 Predictions of temperature curves for deforming billets 1 mm at different die/work-piece temperatures within forging window, using the derived set of effective heat transfer coefficients: (a) die temperature is 200℃; work-piece temperature is 1050℃; (b) die temperature is 100℃; work-piece temperature is 1050℃; (c) die temperature is 200℃; work-piece temperature is 1100℃.

3.8 FRICTION CALIBRATION CURVES FOR RING TEST

The determined effective heat transfer coefficients from the compression tests and FE analyses were used for generating friction calibration curves in two forming stages.

3.8.1 Generation of calibration curves

3.8.1.1 Choosing theoretical friction model for the simulation of ring tests

Choosing the most appropriate friction model for FE is still a matter of discussion. Therefore compromises and assumptions must be made in choosing a suitable model currently. Friction

models normally applied in finite element analyses for bulk metal forming are listed as following:

1. Coulomb friction model

   $\tau = \mu p$

   where τ is friction stress, μ the coefficient of friction ($0 \leq \mu \leq 1/\sqrt{3}$), p the normal pressure.

2. Shear friction model

   $\tau = mk$

   where m is friction factor ($0 \leq m \leq 1$), k the shear flow stress.

3. General friction model

   $\tau = f\alpha k$

   where f is the friction factor expressing the friction in the real contact area ($0 \leq f \leq 1$), α is the ratio of the real to the apparent contact area.

A recent study published by Tan (2002) examined the above friction models and their variations. The research found that it was very hard to identify which friction model in FE simulations is of higher accuracy since the agreement of shape of calibration curves and experimental data can always be obtained by adjusting the value of friction coefficient, or friction factor, so that they can become what is often termed colloquially, "fudge factors." It is meaningless if the validity of a friction model is judged only according to FE analysis. Nevertheless the use of calibration curves and friction models can provide indications of relative difference in friction values under various forming circumstances.

In this research, the shear friction model was adopted to construct the calibration curves of ring tests using FE simulation, for comparing with the experimental results.

3.8.1.2 Calculation of inner diameter for the ring

In Figure 3.17, the solid lines were generated by measuring the mid-height value of the inner diameter of rings to calculate the change of the diameter. The points represented by symbols were obtained by measuring the volume change of ring bores using CAD software to calculate

the average inner diameter. Both methods were used to generate curves for the ring size of outside diameter 18 mm; bore diameter 9 mm; height 6 mm under same heat transfer conditions. The curves obtained from measuring mid-height of bores are slightly higher, but there is little difference for the curves generated by these two methods.

In Figure 3.18, two sets of calibration curves calculated from mid-height inner diameter and average inner diameter are compared at three reductions.

The relative difference of inner diameter reduction was calculated as:

$$\frac{\left|D_a - D_m\right|}{D_o}$$

where D_a is average inner diameter, D_m is mid-height inner diameter, and D_o is the original bore diameter before deformation.

For the lowest reduction in height of 20%, the difference between the curves generated from two methods is less than 1.5%. For the higher reductions, of 40% and 60%, the difference between average diameter and mid-height diameter increases a bit, but it is always under 4%. The figure also shows that as friction increases, the largest difference occurs at the deformation of 40% between mid-height diameter and average diameter comparing it at deformation of 60%. This is because at the highest deformation of 60%, the bore of the ring is almost closed under high friction and the free surface of the ring has been folded into contact with the dies.

Considering the consistency with which hot forging processes may be carried out, the difference for two methods is small enough to be ignored and the simpler approach of measuring the mid-height (smallest) inner diameter provides sufficiently accurate data and was adopted for the work of generating friction calibration curves.
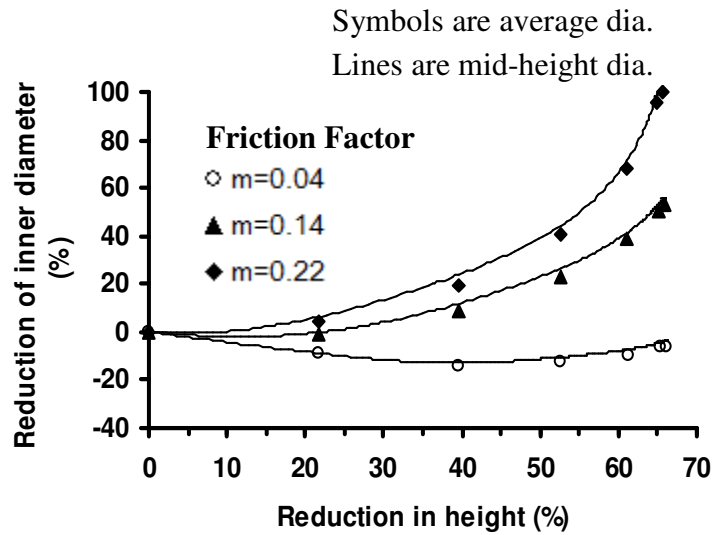
Figure 3.17 Friction calibration curves generated by calculating variations of average and mid-height inner diameters of rings at m = 0.04, 0.14 and 0.22.
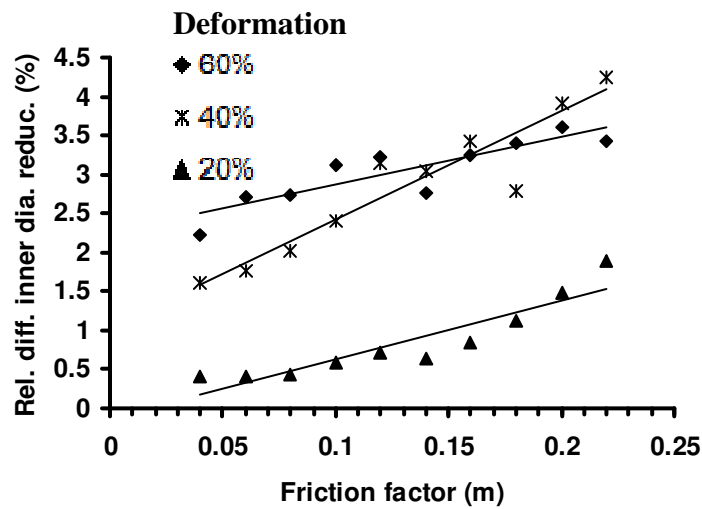
Figure 3.18 Difference between calibration curves generated using two methods. Deformation in height 20%, 40% and 60% respectively.

3.8.2 Factors affecting the calibration curves

Some researchers (Schey, 1983; Rao and Sivaram, 1993; Sofuoglu and Rasty, 1999) have pointed out that friction calibration curves may not be used generally. To establish the effects

of process variables, other than interfacial ones, on calibration curves, a sensitivity study has been carried out with FE analyses to investigate the discrepancy of the curves generated under various forming conditions.

In an attempt to examine the sensitivity of ring deformation to process variables other than friction, ring compression was simulated assuming three different thermal conditions: 1. isothermal; 2. adiabatic, and 3. heat transfer, through interfaces with having experimentally determined values of coefficients. Also, the effect of different constitutive relations of test-piece metal was examined.

3.8.2.1 Definition of relative difference of inner diameter reduction

The relative difference of inner diameter reduction defined here differs from the one defined in section 3.8.1.2 which is under the same heat transfer conditions. Figure 3.19 shows a geometric comparison of two deformed rings (outer diameter 18 mm: inner diameter 9 mm: height 6 mm) for zero friction under isothermal and heat transfer conditions, respectively. By subtracting the mid-height point of the inner diameter of each ring, after deformation, the difference of inner diameters can be determined. This value, divided by the original inner diameter before deformation, gives the relative difference in diameter reduction. This definition will be used in the following analyses.
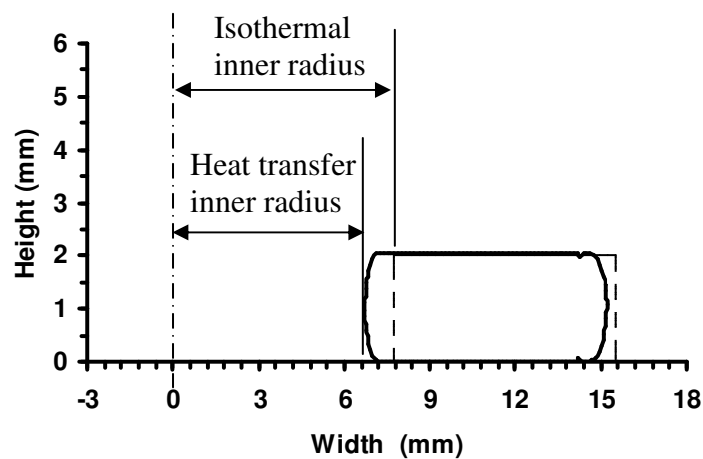
Figure 3.19 Comparison of geometry of half cross-section of rings after deformation compressed from 6 mm to 2 mm for isothermal and heat transfer conditions.

3.8.2.2 Effect of interfacial heat transfer

Calibration curves were generated for an effective friction factor ranging from 0 to 0.22 which covered the frictional circumstances during hot upsetting from the experiments, for three thermal conditions. In Figure 3.20, thirty-three calibration curves (presented as symbols) generated from three conditions are compared for a deformation of 50% for different effective friction factors. The figure shows that in the results of adiabatic and isothermal assumptions at high friction values, the curve rises above zero. This may be due to the temperature increased internally for the adiabatic condition, i.e. a temperature gradient arises within the adiabatic rings. The comparisons of deformed inner diameters are plotted as the ratios given in the key. Even for zero friction, barrelling arises when heat transfer is considered while the difference of inner diameter is 10%. As friction increases, the material flow is hindered by the effect of both heat loss and friction, which leads to a difference as high as 30%.
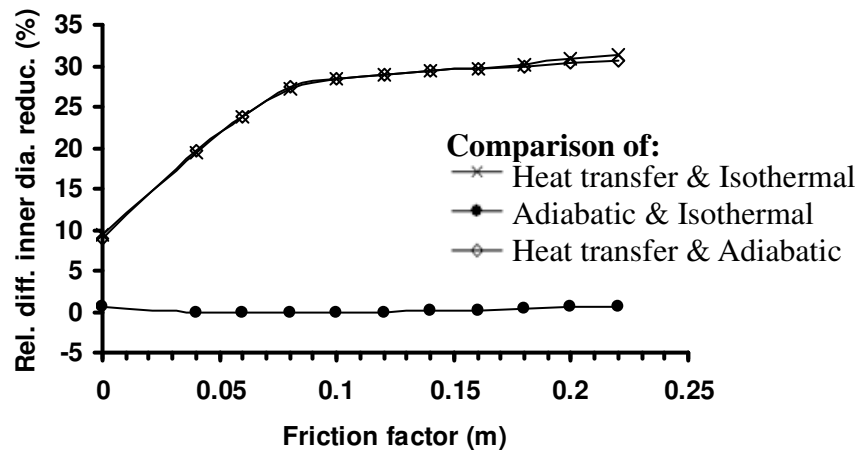
Figure 3.20 Comparisons of inner diameters of rings under interfacial heat transfer, isothermal and adiabatic conditions for different effective friction factors.

Both isothermal and adiabatic rings deformed as though they were a solid body without barrelling for zero friction and, as friction increases, barrelling starts to take place. It is apparent that both interfacial heat transfer and interfacial friction contribute to barrelling.

The effect of effective heat transfer coefficient on calibration curves was also studied. By

altering the effective interfacial heat transfer coefficient (three different heat transfer coefficients were used here: pressure dependent (values are shown in the key); 11 kW/m^2℃ and 5 kW/m^2℃, plus an isothermal condition. The calibration curves for zero friction are presented in Figure 3.21.
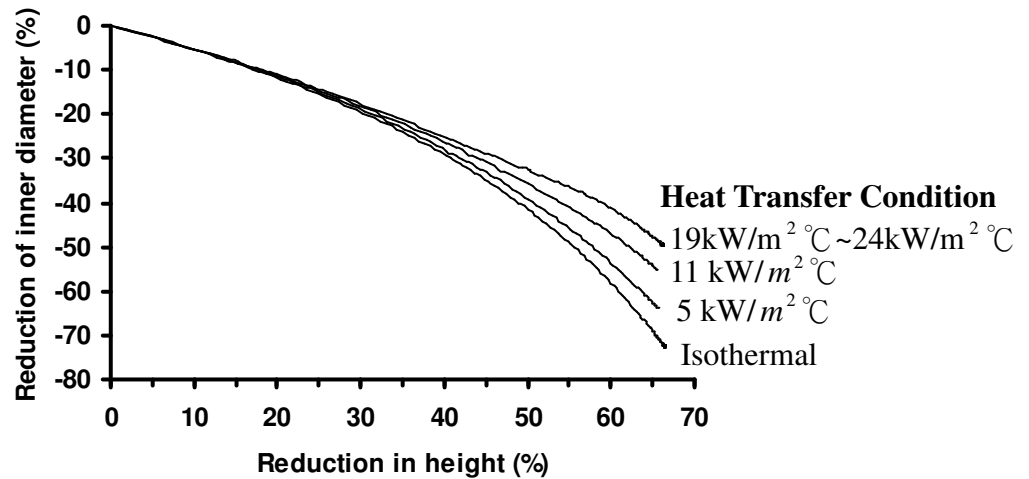
Figure 3.21 Calibration curves of four heat transfer conditions for ring size as 18:9:6 mm at zero friction.

The result shows that calibration curves are also affected by the value of effective heat transfer coefficient. As the value increases, the heat loss from the work-piece surface increases, leading to a greater difference in surface/internal material flow, thus reduction in inner diameter is formed.

3.8.2.3 Effect of forming speed

The effect of forming speed is examined; Figure 3.22 shows, the relative difference in inner diameter reduction between interfacial heat transfer and isothermal conditions for three typical forging speeds, for zero friction and for a deformation of 50%. As the forming speed increases, the difference between isothermal and interfacial heat transfer conditions becomes smaller. This is because the shorter forging time reduces heat loss at the interfaces, thus bringing the deformation closer to adiabatic conditions.
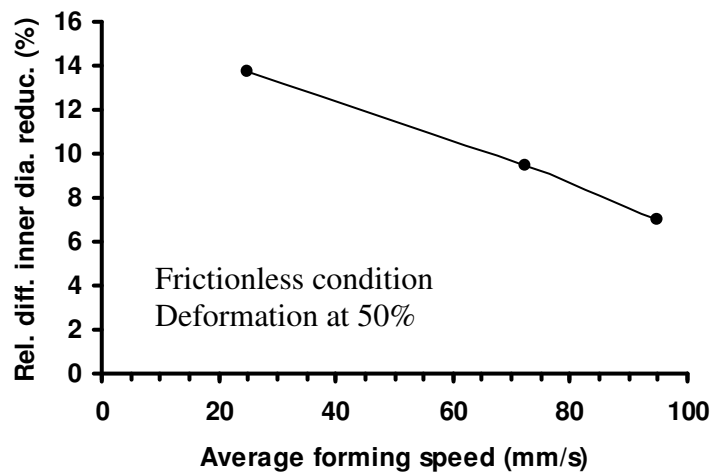
Figure 3.22 Comparison of inner diameters of rings for interfacial heat transfer and isothermal conditions for three forming speeds.

3.8.2.4 Effect of die/work-piece temperatures

Figure 3.23 shows, calibration curves generated from three different combinations of die/work-piece temperature relevant to forging practice compared for the same material and conditions of interfacial heat transfer and friction. There is little difference between these curves. This shows that for a normal forging temperature window, the effect of die and work-piece temperature on the calibration curves is not significant for the friction value used.
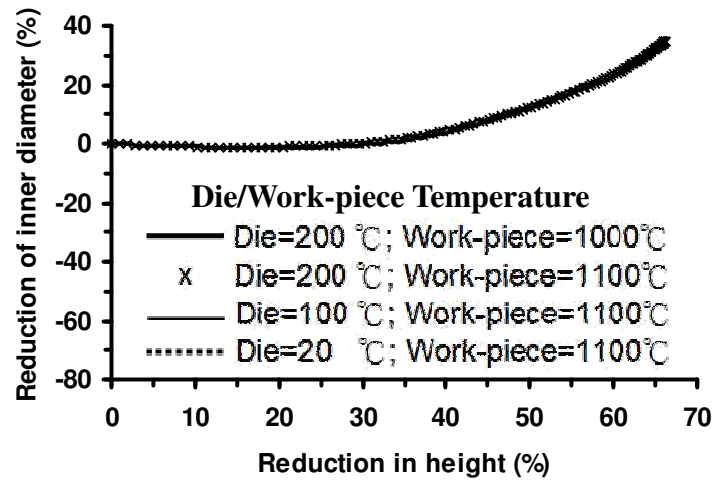
Figure 3.23 Friction calibration curves generated from different die/work-piece temperatures under same material and process conditions (m=0.2).

3.8.2.5 Effect of ring size

In order to examine the effect of the size of rings on values of calibration curves, three different ring sizes: big: 36:18:12 mm; medium: 24:12:8 mm; small: 18:9:6 mm are used, with all other parameters remaining identical. Figure 3.24 shows the relative difference of inner diameter reduction for interfacial heat transfer rings compared with those for the isothermal condition. It can be seen that ring size affects inner diameter deformation. The small rings might lose more heat during the compression, which results in greater inner diameter reduction compared with isothermal ones. Inner diameter reduction for big rings is about 8% less than that for small ones. This might be due to the fact that big rings retain more heat inside the work-piece, leading to more uniform temperature distribution than the small ones.

In order to support the above statements, Figures 3.25, where the normalised height is calculated by dividing the final height of deformed rings for both sizes, is generated. The figure shows the small ring with greater temperature gradient and lower temperature than the big ring.
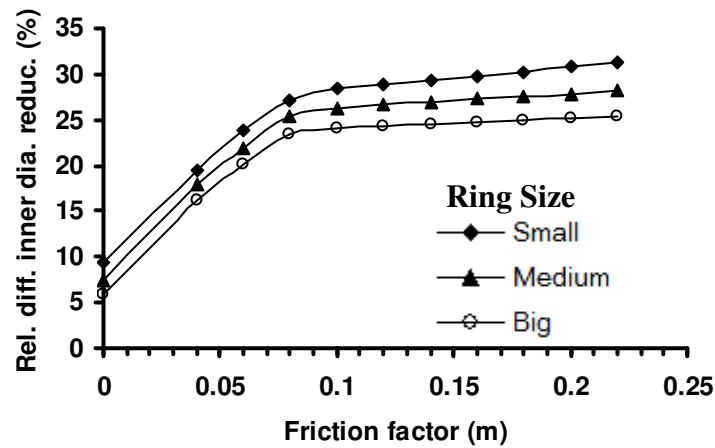
Figure 3.24 Comparisons of inner diameters of rings under interfacial heat transfer and isothermal conditions for three sizes of rings at die = 200℃ and work-piece = 1050℃.
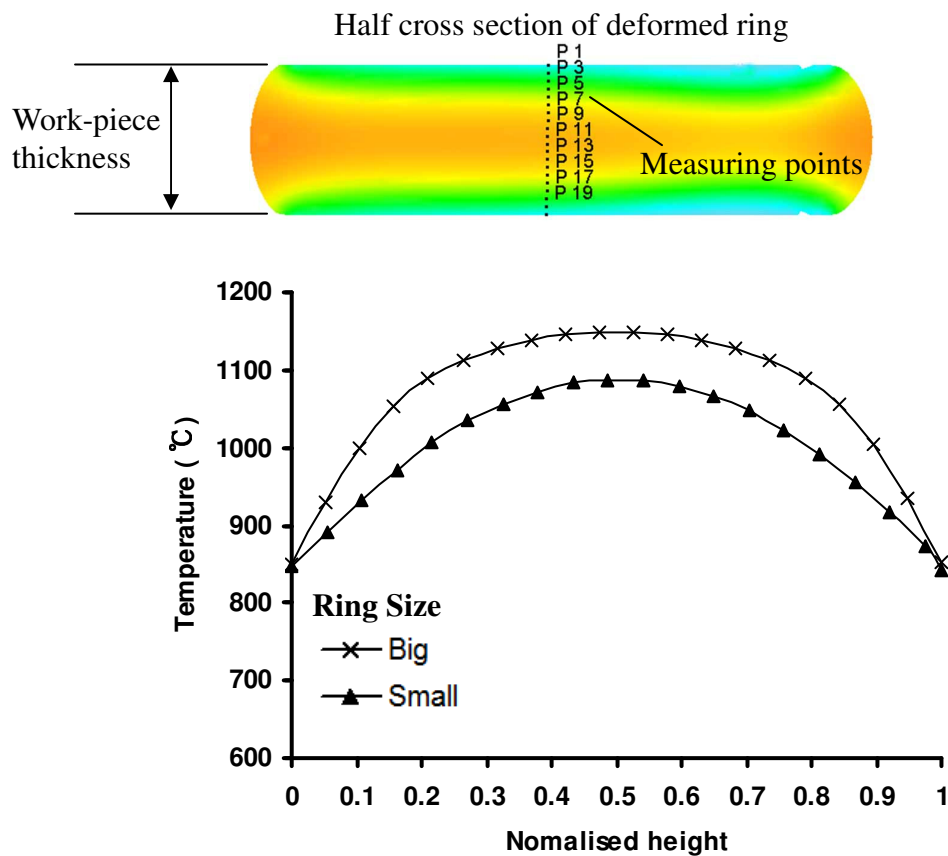
Figure 3.25 A comparison of temperature gradient for big and small rings measured at the middle of half cross-section of the rings after deformation (66%) at friction factor = 0.2.

70

For investigating the barrelling conditions existing in both rings, a barrelling factor is introduced, which is defined as:

$$\frac{R_o - R_d}{R_o}$$

where R_o is original bore radius before deformation, R_d is bore radius after deformation at different position of height.

Figure 3.26 is generated by plotting barrelling factor against normalised height of deformed rings. The result shows that the small ring possesses higher barrelling factor. These results demonstrate that the small ring with greater temperature gradient and lower temperature has the same effect as friction in causing barrelling.
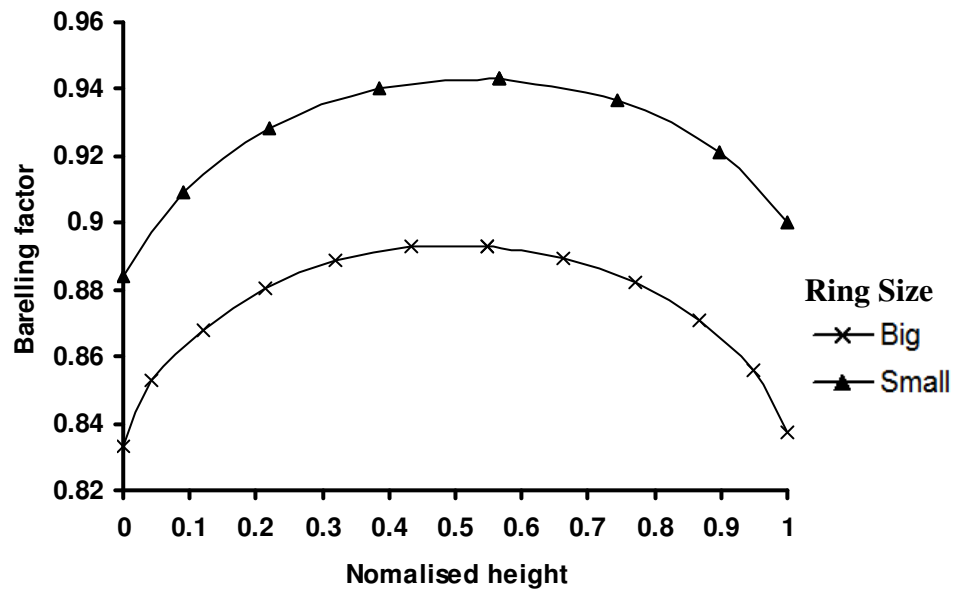
Figure 3.26 A comparison of barrelling condition for big and small rings measured at the middle of half cross-section of the rings after deformation (66%) at friction factor = 0.2.

3.8.2.6 Effect of material property

An elastic-viscoplastic material and an elastic-plastic hardening material were used to study the effect of material property on calibration curves under isothermal condition. In Figure

3.27, the pink lines represent the elastic-viscoplastic material, while blue lines stands for the elastic-plastic hardening material, for isothermal deformation. There is almost no difference between the curves for low friction (m = 0 and 0.1) as the curves are overlapping, but when friction factor = 0.5, a difference arises.

Also, the calibration curves obtained for the elastic-viscoplastic material are lower than those for the elastic-plastic hardening material for the high friction value. This is possibly due to the strain sensitivity of the materials. At the same strain rate, the strain hardening exponent (n) for the elastic-viscoplastic material is approximately 0.15 whereas for the elastic-plastic hardening one, n is approximately 0.09 deformed at the same forging temperature. The bigger the n value, the higher is the increase in strength with deformation (Kalpakjian, 1997), which will also affect material flow. For material with higher strength, the less the change of bore diameter at high friction when compared with those with lower strength deformed at the same forming condition, affects the calibration curves. Therefore, this fact might explain why the curve of the elastic-viscoplastic material is lower. The results show that different material constitutive relations do produce different calibration curves at high friction but the effect at low friction conditions could be ignored.
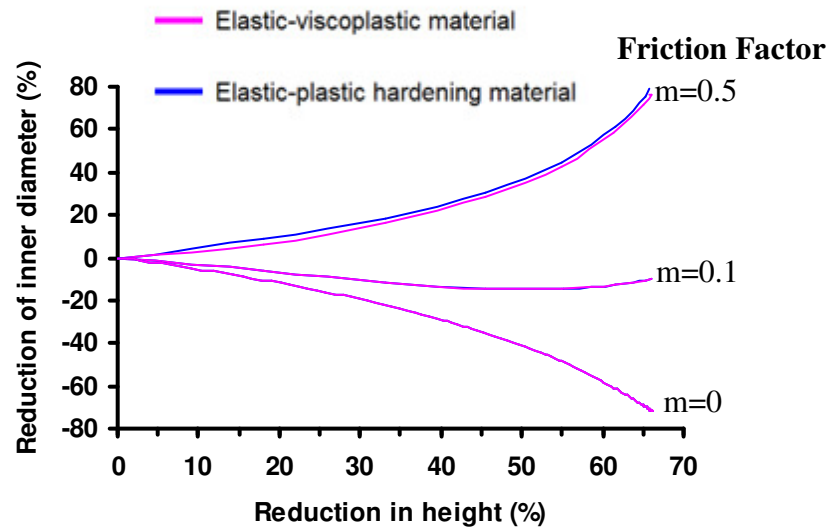
Figure 3.27 Friction calibration curves generated from two materials and compared at m = 0.5; m = 0.1 and m = 0 for isothermal condition.

3.9 RESULTS AND ANALYSES OF RING TESTS

Figure 3.28 shows deformed rings for upsetting with a die temperature of 100℃ and work-piece temperature of 1050℃ at the same initial coating/lubricant conditions. In all cases the inner diameter decreased as the deformation increased; all the determined friction factors for different forming conditions are listed in Appendix F.
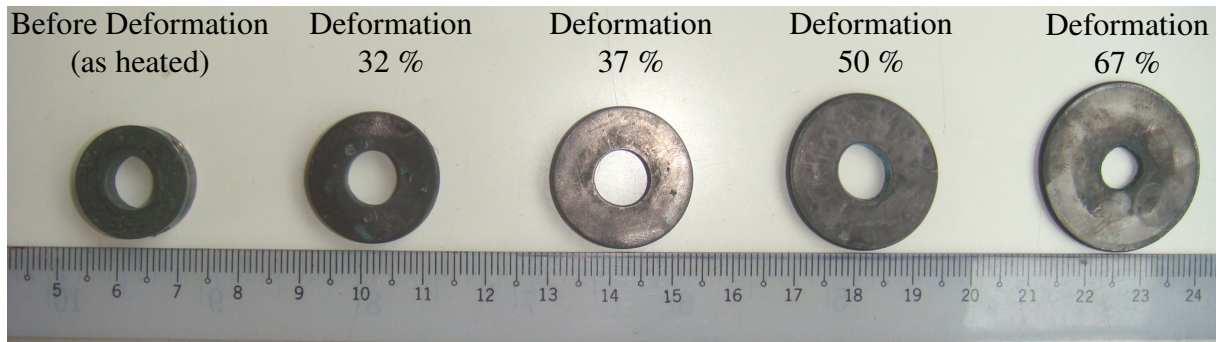
Figure 3.28 Rings deformed at different deformations at same die, work-piece temperatures and initial coating/lubricant conditions.

3.9.1 Effect of lubricant quantity

Friction calibration curves generated from FE simulations according to the experimental conditions from friction factor (m) = 0.04~0.22 were compared with the experimental data for two different amounts of lubricant, as shown in Figure 3.29. It is obvious that under the same process conditions, as the amount of lubricant increases, the friction decreases (m = 0.10 for most lubricant; m = 0.16 for least lubricant).
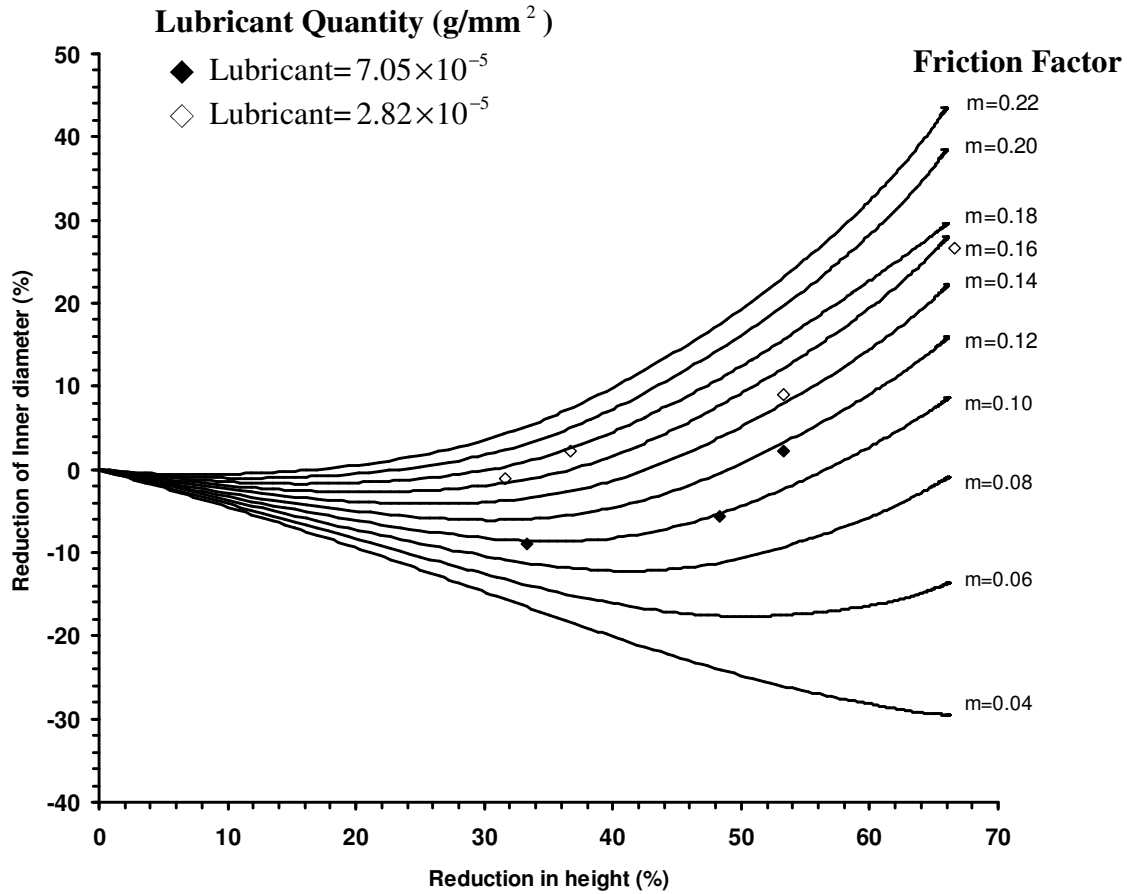
Figure 3.29 Variation of friction under two different amounts of lubricant for die $= 100℃$, work-piece $= 1050℃$ and coating thickness $= 60$ μm.

3.9.2 Effect of coating thickness

Figure 3.30 shows the effect of coating. As seen from the figure, for a lubricant quantity of 2.82×10^{-5} g/mm^2, friction values for two different glass coatings are similar. For a larger lubricant quantity of 7.05×10^{-5} g/mm^2, again, coating thickness has little effect on friction, as the value for a coating thickness of 60 μm is 0.10, which is only slightly lower than that for a 40 μm thick coating, at 0.12. Compared with the effect of lubricant quantity, friction is less affected by coating thickness, although friction with rings with thickest coating and lubricant had the lowest values.
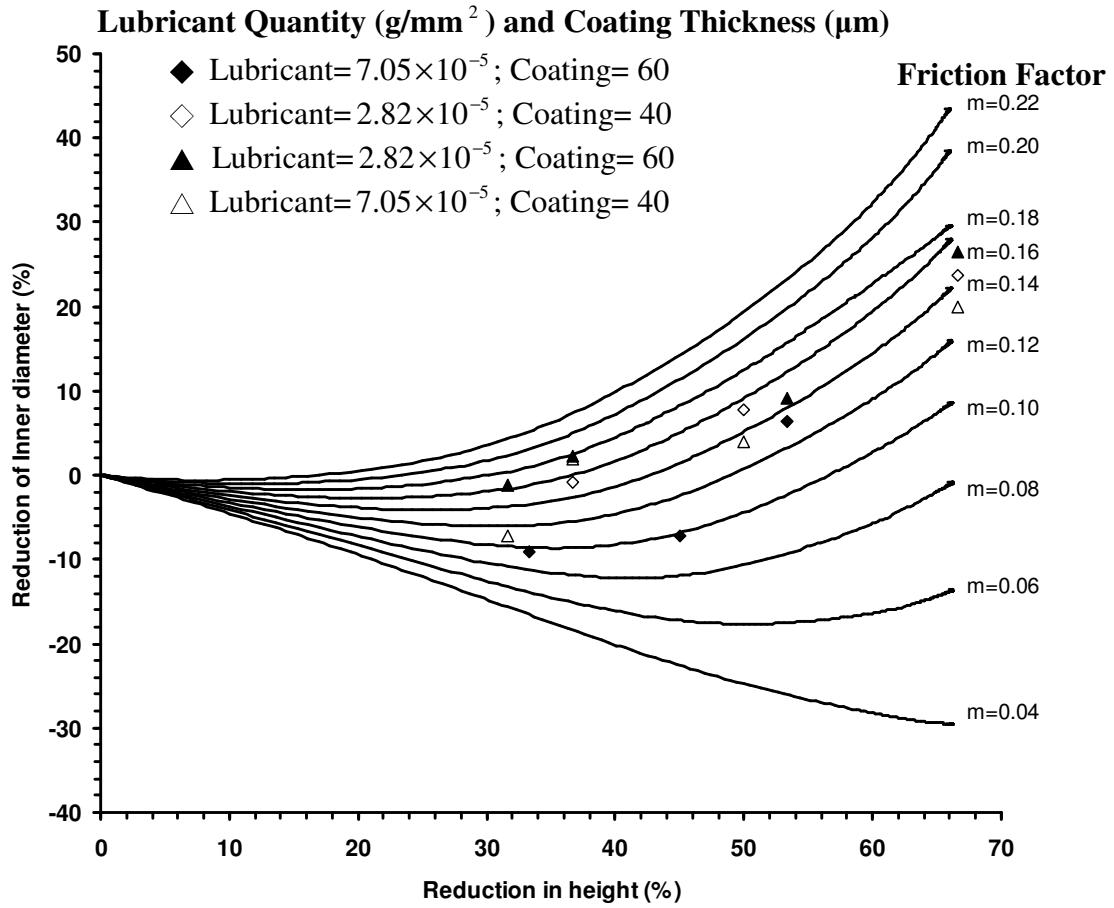
Figure 3.30 Variation of friction under two different amounts of lubricant/coating for die = 100℃, work-piece = 1050℃.

3.9.3 Effect of die temperatures

The effect of die temperatures on friction is presented in Figure 3.31 (a) and (b). In Figure 3.31 (a), the value of effective friction factor is higher at 0.14, for rings deformed at the lowest die temperate of 100℃. The reason might be due to the fact that the viscosity of glass coatings increases as temperature is reduced and a low die temperature will result in lower interfacial temperatures, because of a higher rate of heat transfer, a fact which corroborates that of Hu and Dean's research (2001). Thus a higher friction value will result.

In Figure 3.31 (b), the rings deformed at a die temperature of 100℃ still with higher value of friction factor (m = 0.12), but overall, the value of effective friction factor tends to be lower

than that in Figure 3.31 (a), deformed at die = 100 ℃. This might because the coating/lubricant combination is thick enough for no great difference in heat transfer to arise. In addition, it should also be noted that as deformation increases, friction values tend to converge to the same value. This might be because lubricant thinning caused by the increasing pressure and by surface expansion change conditions from thick film to boundary contact with a similar characteristic, regardless of the different starting conditions. Different types of lubricating contact in forming will be detailed in Chapter 4.

The results show that the die temperatures did affect friction conditions and ring geometry, probably due to changing viscosity of the glaze and also, possibly, to the heat transfer at and close to the interface.

(a)

(b)
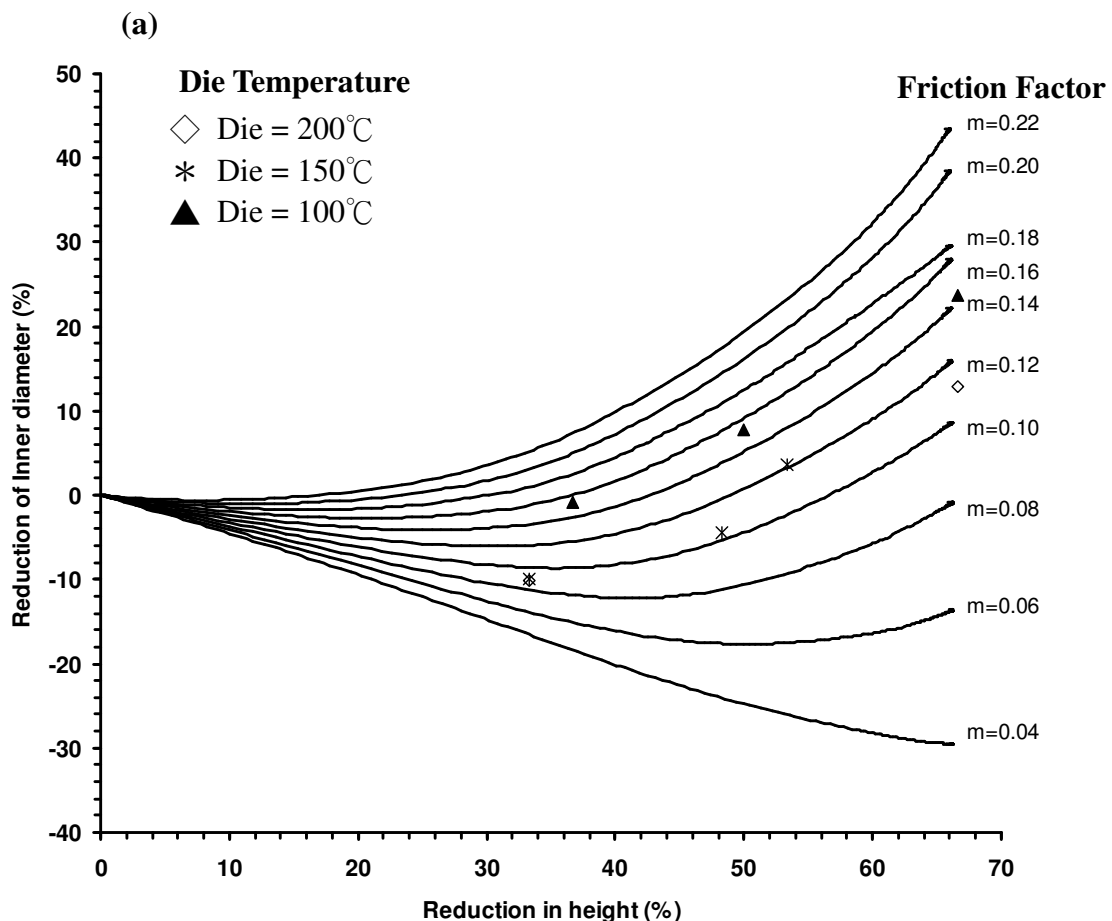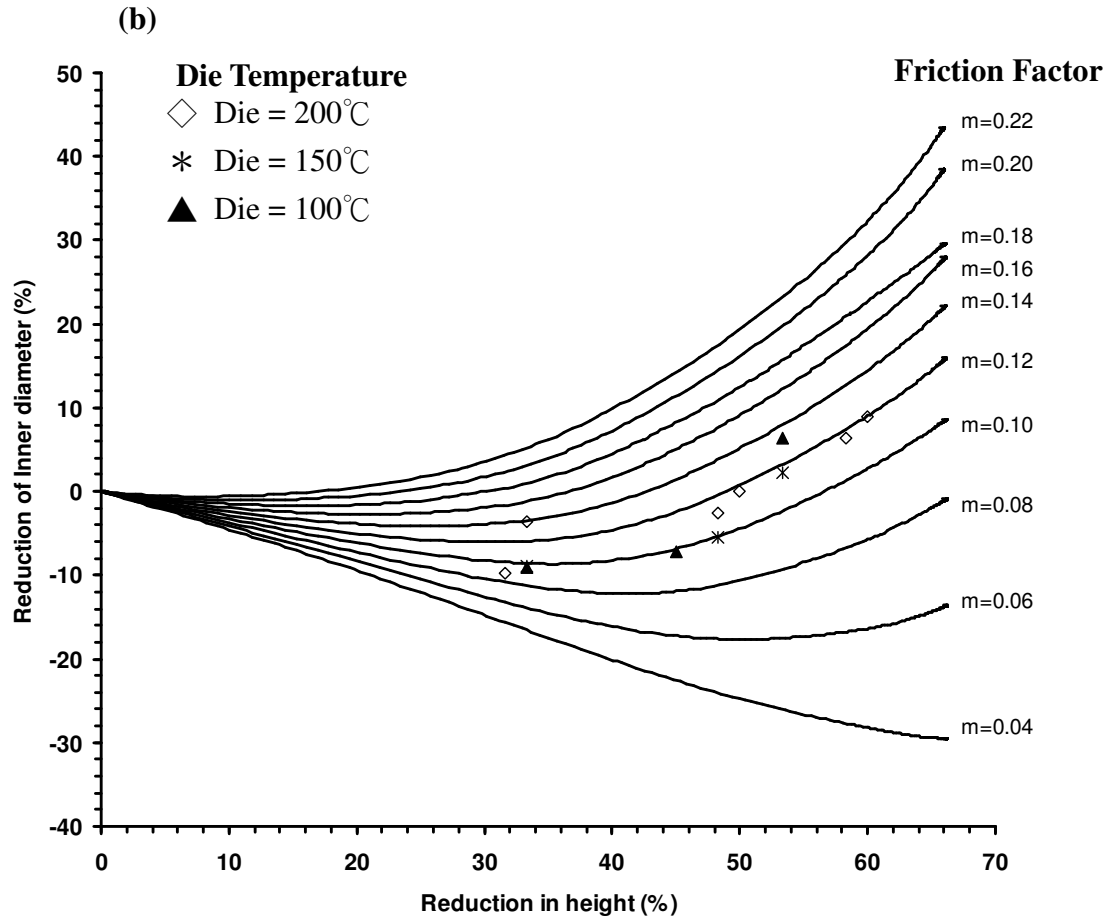
Figure 3.31 Variation of friction under work-piece temperature = 1050℃ and different die temperatures at (a) lubricant = 7.05×10^{-5} **g/mm**^{2} and coating = 40 μm (b) lubricant = 7.05×10^{-5} **g/mm**^{2} and coating = 60 μm.

3.9.4 Load prediction

Figure 3.32, shows a comparison of actual and computed forging forces for a ring test with a die temperature of 200℃ and ring temperature of 1050℃, deformed from 6 mm to 3 mm for lubricant = 2.82×10^{-5} **g/mm**^{2} and coating = 40 μm. In addition, the heat transfer (pressure dependent) and friction conditions (m = 0.16) derived from the experiments were input to the

simulation. The unloading line from the experiment is probably due to press deflection as well as to bearing clearances ignored in the FE analysis. By showing the unloading line for the simulation to be a vertical straight line, it could be seen that the extension is about 0.5 mm. Since the deflection of the press is 200/3 tonne/mm, so for a maximum load of 18 tonne, it could expect an extension of 0.27 mm, which leaves 0.23 mm for the bearing clearance. The difference of the loading shape might be due to the hysteresis in the load cell. However, the maximum load is accurately predicted by simulation, which indicates that the determined process factors were accurate.
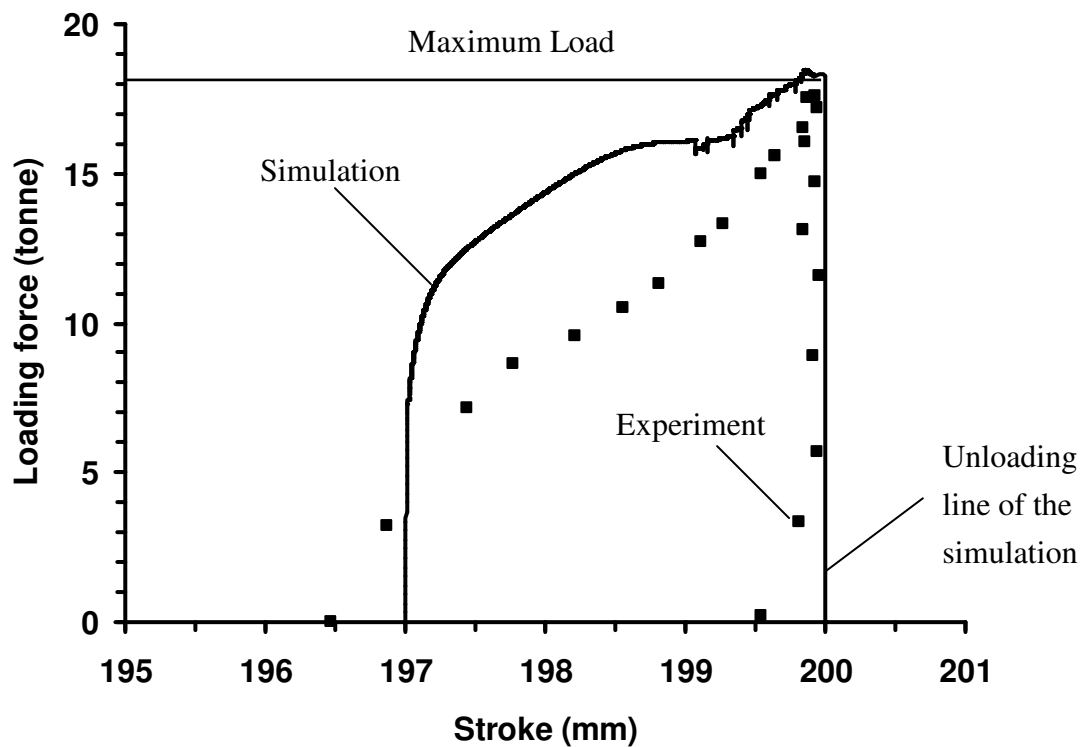
Figure 3.32 A comparison of computed (line) and experimental (symbols) loading forces for deforming a ring from 6 mm to 3 mm at work-piece temperature of 1050℃ and die temperature of 200℃.

CHAPTER 4

WEAR, LUBRICATION AND COATING OF THE DIE IN METAL FORMING

4.1 INTRODUCTION

Dies are the heart of all bulk metal forming processes and they are exposed to extreme process conditions. Service time of dies is ruled by a large variety of fluctuating process parameters, and exhibits significant scatter, which makes die life an unstable factor for the development of profitable manufacturing processes. The reasons for die failure are many, such as wear, fatigue and plastic deformation (Singh *et al.*, 1973). Also, the mechanisms of die failure between cold, warm and hot forming are significantly different (Dean and Sturgess, 1978). For cold forming, mechanical fatigue caused by repeated loads is usually the main reason for tool failure. For hot and warm forming, the situation is more complex, as the dies are exposed to both high thermal and mechanical stresses. These stresses cause die failure through wear, thermo-mechanical fatigue and plastic deformation. In addition, the surface property of a die might be altered at high temperature by chemical reaction with lubricant and/or coating.

In this research, although the various factors affecting die failure are introduced; the focus is placed on wear, especially adhesive and abrasive wear during hot forming, as this is the main failure mechanism found on the studied extrusion die. Below, the nature of wear is discussed and the research of tribology in metal forming is reviewed for the understanding of wear mechanism.

4.2 CLASSIFICATION OF DIE FAILURE

Figure 4.1 shows three stages of forming production related to die failure (Jiang, 1996). The first stage is the running-in stage. At this stage, die failure, if it occurs, is due to faulty design and manufacturing of the die or misuse by shop floor operators. This initial stage is temporary and normally arises only when new products are introduced. Then, in the second stage, the whole process becomes stable, with almost steady-state degradation of the tool, with

occasional die failure caused by inadequate control. Instability arises in the final stage, in which the die has been used for a while and the geometry and properties have been changed due to fatigue, deformation and wear. Since the first stage of running-in is hard to avoid, the main target is to extend the stability to delay fatigue and wear and, thus, prolong die life.
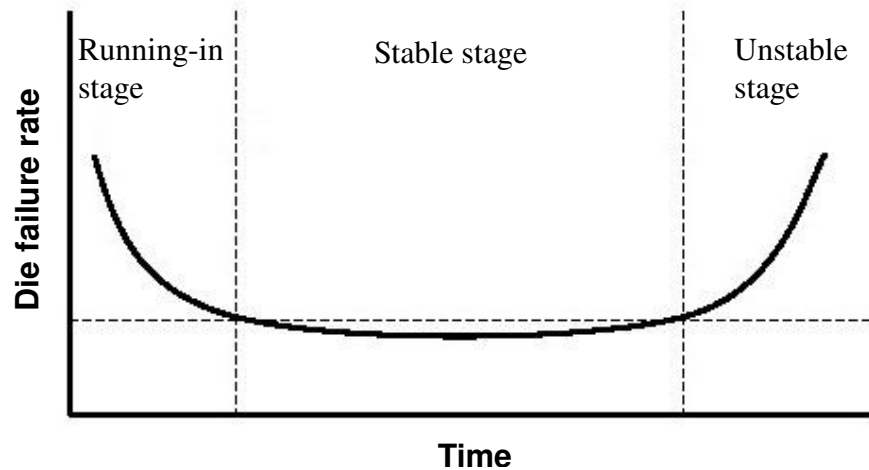
Figure 4.1 Three stages of production leading to die failure (Jiang, 1996).

In hot extrusion, the die undergoes not only high pressure and shear from the deforming material but also significant temperature change, plus oxidation. All these factors constitute a complex and harsh environment for the die.

By examining the extrusion die, factors contributing to failure have been classified into the following three categories:

4.2.1 Surface fatigue

Sometimes called "delamination wear" (Arnell *et al.*, 1991) which is associated with surface cracks penetrating into the sub-surface and lead to the delamination of die material. Two different forms of fatigue occur in die surfaces during hot forming: thermal and mechanical fatigues (Burwell, 1957).

The hot working steels usually used for the extrusion tools are exposed to tempering effects because of high thermal and mechanical loads. These tempering effects increase susceptibility

to wear. Generally, due to the forging temperature being well above 1000℃, the temperature of the surface of the tool temporarily exceeds 500℃ (Andreis *et al.*, 1999; Walter *et al.*, 1999) and so do the tempering temperatures of conventional hot working tool steel. In such a case, the hardness of the tool is reduced and the mechanical loads during forming operations can cause plastic deformation as well as adhesion and abrasion of the tool material (Andreis *et al.*, 1999; Barrau *et al.*, 2003). Also, under thermal and mechanical stresses, the tempered martensitic steels employed in the tools tend to loose their mechanical properties (Doege *et al.*, 1994; Delagnes *et al.*, 1999). Then, the die surface damage is the result of a complex process connected to fatigue (cracking origin), friction (wear origin) and forming ambience (oxidation origin).

Also, elevated temperature brings another issue: After contact with the hot work-piece; the die surface is often quickly cooled by spraying lubricant and transient thermal gradients, reverse to those arising during deformation, are developed inside the tool by thermal conduction. These thermal gradients tend to cause surface cracks. These cracks may result in spalling which will add to loss of metal from the surface by abrasion. Two photographs are shown in Figure 4.2 and Figure 4.3 of the formed cracks on the surface of dies due to mechanical and thermal fatigues, respectively.

Formed crack due
to mechanical
fatigue
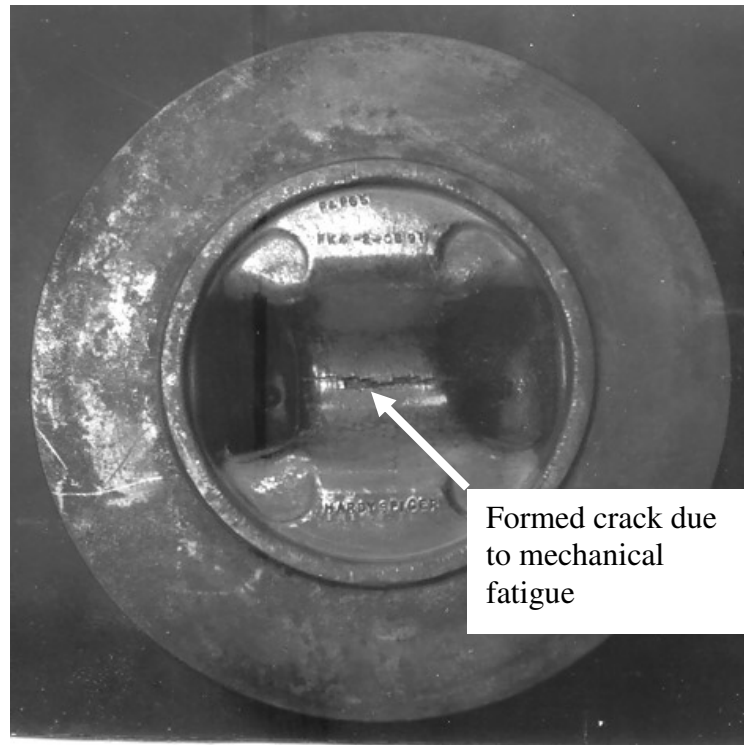
Figure 4.2 The observation of the mechanical fatigue crack on a forging die (Thomas, 1970).
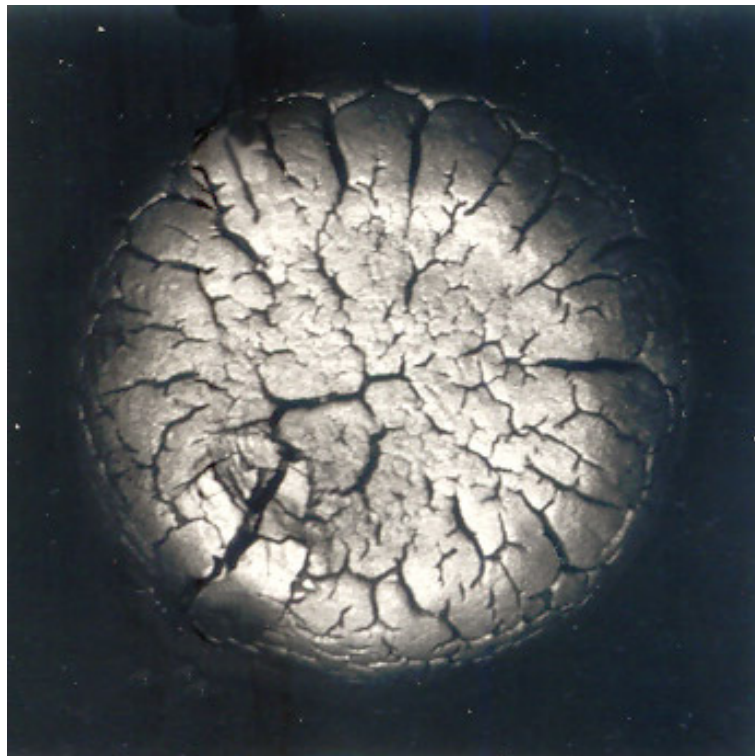
Figure 4.3 The observation of the thermal fatigue cracks on a forging die (Thomas, 1970).

4.2.2 Plastic deformation

Dies not only endure high pressure during hot forming, but also become soft because of the phase change of the material at hot temperature. A corner or peg in a die is likely to be plastically deformed, as they are surrounded by work-piece metal, reach high temperatures and their yield strength is reduced. This causes geometry changes which might make the die unusable. Figure 4.4 is a photograph of the convex radius of a hot forging die (tool steel) after 1000 forging cycles. Due to the forging temperature being above 1000℃, the temperature of the surface of the tool temporarily exceeds 500℃. In such a case, the hardness of the tool is reduced and the mechanical impacts during forging operations can easily cause plastic deformation as well as abrasion of tool material (Barrau *et al.*, 2003). Also, geometry difference between the die and the work-piece could cause plastic deformation on the die. The parts are needed preformed from simple geometry to share the huge forming pressure of the final forging and to avoid the damage of the exposure of pressed lubricant or air at hot temperatures.
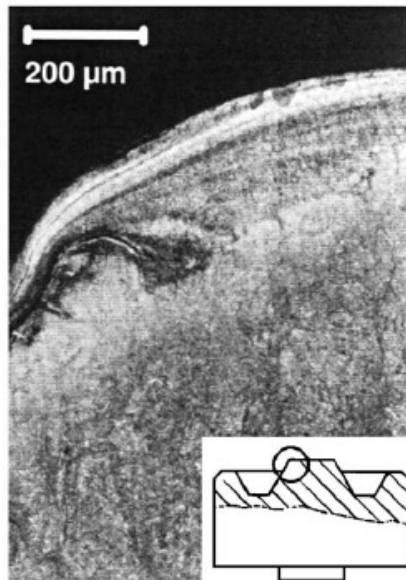
Figure 4.4 The photograph shows the plastic deformation for the convex radius of a hot-worked tool steel after 1000 forging cycles. Tool temperature: 200℃; forging material: C45; forging temperature: 1100℃~1150℃; lubricated contact; cycle time: 13 seconds; hardness of tools: HRC47 (Barrau *et al.*, 2003).

4.2.3 Wear

Wear is not an intrinsic material property, but a characteristic of the engineering system. Any change in load, speed, or environment, for example, can cause a dramatic change in the wear rates of one or both of the contacting surfaces. During extrusion, a die experiences the massive flow of hot metal which readily causes wear (Doege *et al.* 1990). Lange *et al.* (1992) analysed factors affecting die failure for warm and hot forging tools from the statistical data, and found that 70% of die failure is due to wear. Wear can be of several forms such as: corrosion, erosion, scuffing, adhesion (galling) and abrasion (cutting). Figure 4.5 shows the grooves produced by wear at the flash lands of a forging die.
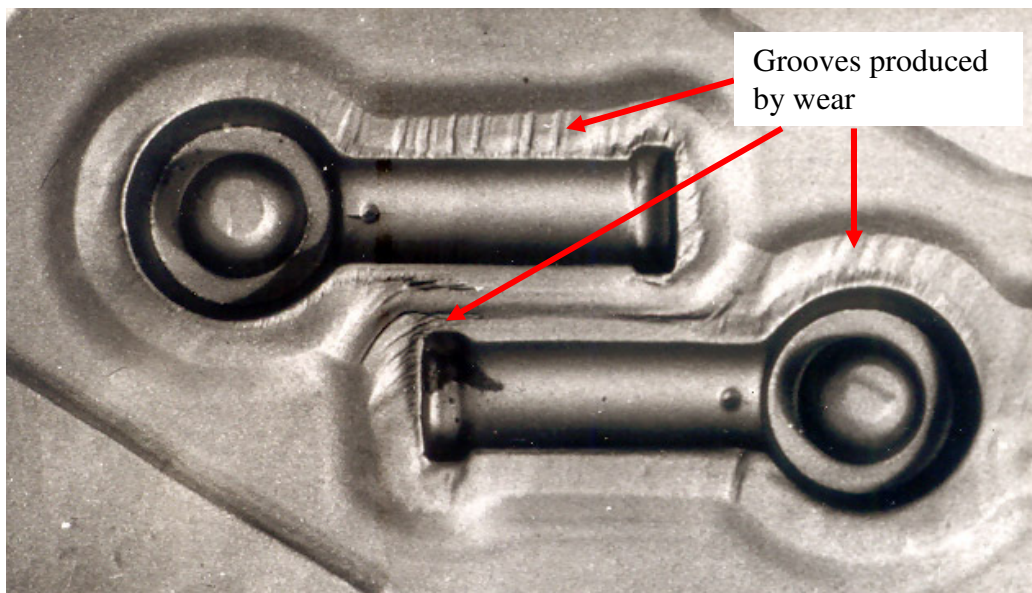
Figure 4.5 A forging die shows the profound grooves at the flash lands (Thomas, 1970).

Corrosive wear may take place when sliding occurs in a corrosive environment. In the absence of sliding, the products of the corrosion will form a film on the surface, which tends to slow down further corrosion. However, sliding action wears the film away, so the corrosive attack continues (Robinowicz, 1995). Erosion is a process in which a particle carried in a fluid medium hits a solid surface and removes material from it, which also leads to the production of abrasives causing abrasive wear (Arnell *et al.*, 1991). Erosion is a physical removal of the material, whereas corrosion is a type of removal by chemical means. Scuffing is usually

identified on cold forging tools, if lubricant breakdown occurs.

Each wear process obeys its own laws, and it is very often on many occasions that one of the modes of wear acts in a way as to affect the others (Czichos, 1974). A complex situation must be disentangled to find the primary cause of wear. Abrasive and adhesive wears are claimed to be the most important factors affecting die life (Burwell, 1957). They exist simultaneously during hot forming, and will be further discussed in sections 4.3 and 4.4.

A popular approach to determining the mechanism of wear is to examine the surfaces of the sliding specimens. This method makes it possible to determine the final stage that must have been reached before wear occurred. For instance, if a clean smooth copper flat surface is slid on a similarly clean smooth steel surface, there is a transfer of particles from each surface to the other, and a scratching of each surface by the other. If the type of wear is judged by inspecting of the surfaces, the decision will be abrasive wear, since the formation of scratches is a sign of abrasive action, but Rabinowicz (1995) argued that this is an example of adhesive wear because the real cause of the particles and scratches is the transfer of particles from one surface to another by adhesive action.

Another approach is to judge the type of wear by its engineering consequence. Thus wear may be termed "light" or "beneficial" if it helps the surfaces to run in properly; "severe" if in the opinion of the observer the wear is too rapid; "galling" if the surfaces become very rough and irregular in appearance. These classifications are not very useful in identifying the mechanism of wear (Ludema, 1996).

A typical forging die profile, with locations of the three categories of die failure, is shown in Figure 4.6. From the figure, it can be observed that wear and deformation usually happen at the corner of the die or at the flash land, due to faster material flow and high pressure. The thermal and mechanical fatigues occur at the larger contact interface as it usually undergoes rapid temperature changes and repeated forming loads.
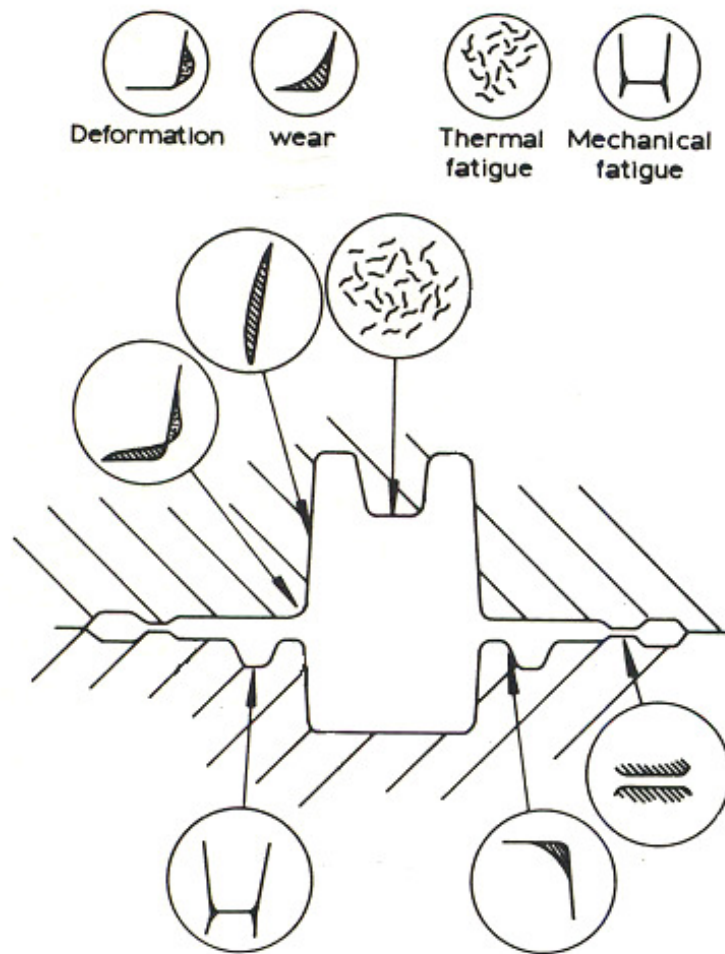
Figure 4.6 Typical locations of damage in a hot forging die (adopted from Schey, 1983).

4.3 ADHESIVE WEAR

Adhesive wear is also called galling wear (Burwell and Strang, 1952; Burwell, 1957; Kuhlmann-Wilsdorf, 2002). When two surfaces are in contact with each other, the load is carried by many high points, or "asperities", that exist on nominally smooth surfaces. Since the die and work-piece surfaces are often contaminated and lubricated. Depending on the material pairing, adhesion may then lead to welding and form a junction from the asperities, as shown in Figure 4.7 and further relative movement affects the junction by one of several mechanisms stated below:

(1) Junction is stronger than or as strong as the die material.

The junction separates either in the work-piece or in the die. Die wear rates become unacceptably high, particularly when high interface temperatures promote diffusion of alloying elements from the die material into the work-piece, thus reducing the strength of the die.

(2) Junction is stronger than the work-piece but weaker than the die.

Separation occurs in the work-piece with incipient pickup on the die.

- The pickup grows and strain-hardens. Once it reaches a critical size, and is subjected to the periodic loading, the pickup will separate from the die due to fatigue and form a wear particle at the die/work-piece contact interface.
- The pickup may be transferred onto the work-piece and back-transferred onto the die repeatedly until the fragment leaves die/work-piece contact interface.
- If the pickup is not removed by any of the above processes, because of work hardening and perhaps also chemical changes, the hard particle becomes a new hard asperity on the die and plows the work-piece surface on a subsequent contact. The pickup may also grow by further metal transfer. In this condition, the working must be terminated because of excessive friction and/or unacceptable work-piece finish.

(3) Junction is weaker than work-piece and die, separation occurs at the interface. Wear, if it occurs at all, is due to other causes.
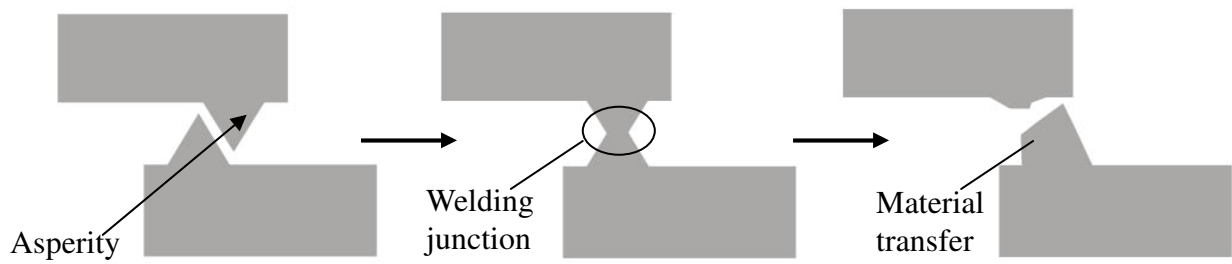
Figure 4.7 A typical adhesive process in a microscopic view as two asperities joined by welding and material transfer from one side to the other as sliding proceed (conical shape is used here to represent the asperity, however, hemispherical shape is also used).

4.3.1 Adhesive wear model

Early research on wear focused on the conditions under which materials wore faster or more slowly, but focused very little on the causes of wear. The adhesion theory based on the concept of asperity contact was first introduced by Holm (1946) and Bowden and Tabor (1950). Real surfaces, being not entirely flat on a microscopic scale, make contact at only a few high points, i.e. asperities. This means that the load is supported on a very small real area during contact. The resulting local contact stress is very high, usually causing plastic deformation when ductile materials are involved. This plastic flow causes the total contact area to grow, both by growth of the individual initial contacts and by initiation of new contacts, until the real area of contact is just sufficient to support the load elastically. Under these conditions, they proposed a relation $W = A \cdot P$, where W is the normal load, A is the contact area and P is the yield pressure or hardness (strength of the material) of the softer material.

Based on this concept, Holm (1946) described that the true area of contact between rubbing surfaces is given by the equation:

$$A = W / P \tag{4-1}$$

Holm next assumed that during sliding, for every encounter of a surface atom in this true contact area with an atom in the other surface, there was a statistically constant probability of

one of the two atoms being pulled out of its parent surface. Then the volume, V, of material removed on sliding a distance L was given by

$$V = k \cdot A \cdot L \tag{4-2}$$

where k is the probability of removing an atom via adhesion. By substituting Equation (4-1) into Equation (4-2):

$$V = k \cdot W \cdot L / P \tag{4-3}$$

The probability k should be characteristic of the composition of the surfaces, condition of lubrication for example. Equation (4-3) can also be written in another form by dividing both sides by the contact area A to give the average depth of material removed, h, as:

$$h = k \cdot \sigma \cdot L / P \tag{4-4}$$

where σ is the average normal stress over the apparent contact area.

Later, Archard (1953) advanced the idea and proposed a similar equation to Equation (4-4) to describe wear according to the adhesive theory, for two bodies sliding under an applied load, W, where hardness of the softer metal is P. Based on the same concept as for Equation (4-1), he assumed that the area of contact comprises a number of circular contact spots each of radius a. The area of each contact spot is πa^2, then the total number of contacts presented as n and the total area of contact, A, is the following:

$$A = n \cdot \pi \cdot a^2 \tag{4-5}$$

then

$$n = A / (\pi \cdot a^2) = W / (\pi \cdot P \cdot a^2) \tag{4-6}$$

Each junction may be assumed to remain in existence during a sliding distance equal to $2a$, after which it is broken and its load-carrying capacity is taken up by a new junction. Thus the total number N, of junctions formed in a sliding distance x is given by:

$$N = n \cdot x / (2 \cdot a) = W \cdot x / (\pi \cdot P \cdot 2 \cdot a^3) \tag{4-7}$$

The probability that any junction leads to the formation of a fragment, that is a wear particle, has been assumed to be equal to k, and, on the assumption that such a fragment is a hemisphere of radius a, the volume Q of wear per distance x of sliding is given by:

$$Q = k \cdot N \cdot 2 \cdot \pi \cdot a^3 / 3 = k \cdot W \cdot x / (3 \cdot P) \tag{4-8}$$

This expression may be considered the fundamental law of adhesive wear, and, k, the coefficient of wear. Similar to the coefficient of friction, k is dimensionless. The number 3 in Equation (4-8) is claimed to be a shape factor. In this case it is applicable to the assumed circular junctions and hemispherical fragments. It is now customary to simplify the wear equation by omitting factor 3. This makes computations slightly easier as unit wear volume is expressed as:

$$Q = k \cdot W \cdot x / P \tag{4-9}$$

k denotes 3 times the probability of forming a wear particle.

This equation denotes the following characteristics of adhesive wear:

- Wear increases in proportion of distance of travel.
- Wear decreases with increasing hardness of the rubbing surfaces.
- Wear is proportional to the load.

Another feature of Equation (4-9) is that the junction radius a is absent in the final expression of the wear volume while Archard (1953) shows that the equation applied for a range of radius of asperities and fragment using pin-on-ring test as shown in Figure 4.8. This fact might explain Thomas's finding (1972). He observed that there was no very strong dependence of wear on die surface roughness for his upsetting forging tests, although the

difference in the wear of "rough" and "smooth" dies is significant at the 10% level, which is an extreme case.
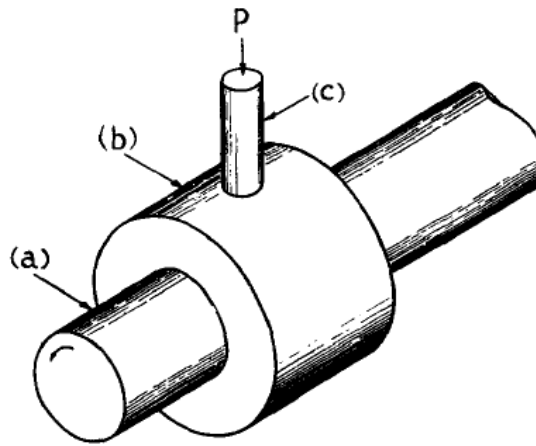
Figure 4.8 Schematic diagram of pin-on-ring wear apparatus (a) shaft rotating at approximately 1500 rpm; (b) the diameter of the ring is 2.38 cm; (c) the diameter of the pin is 0.635 cm, pressed under load P against ring (Archard, 1953).

For the definition of the value of k, Archard used k to represent the probability of the wear particle produced by each asperity encounter. Thus, uncertainty in predicting a wear rate is due to the uncertainty in the value of k, which needs to be found experimentally for different combinations of sliding materials and different conditions of forming processes. Current methods for deriving the value of wear coefficient usually are undertaken in laboratory-scaled experiments, except the mentioned pin-on-ring test, pin-on-disc test and reciprocating rig test are also popular (Kennedy and Hashmi, 1998). It is not possible to perform these tests under the same conditions existing in metal forming processes, as material flow, surface expansion, varying lubrication and the rapidly fluctuating temperature environment experienced in hot forging, for instance, cannot be reproduced. Therefore derived k values are not truly representative of practical situations. Burwell and Strang (1952) stated that *"it is impossible to define any wear coefficient in the sense that Coulomb's first law enables us to define a coefficient of friction"* and the wear data derived from the research may *"have difficulties of obtaining consistent results even under the carefully controlled conditions of the experiments."* Also, *"the wear would change greatly from run to run unless the greatest care was exercised to exactly duplicate conditions."* Unlike the value of friction, the coefficient k is not associated with a particular pair of materials but only to the physical condition of

sliding; the wear coefficient is varied from material to material, and any small change of forming conditions may alter its value. This means that it is very difficult to predict a "real" worn volume in an actual forming condition, by using the equation.

Although the actual wear coefficient is less possible to derive under any circumstance, the equation is still very useful for identifying relative wear and likely regions of major die wear, given that normal pressure and metal flow are known.

4.4 ABRASIVE WEAR

Abrasive wear or cutting wear (Burwell, 1957; Kuhlmann-Wilsdorf, 2002) can be divided into two categories. The first one is two-body wear, which arises when a hard, rough surface slides against a softer surface, digs into it, and plows a series of grooves. The material originally in the grooves is normally removed in the form of loose fragments, or else it forms a pair of mounds along each groove. The material in the mounds is then vulnerable to subsequent complete removal from the surface (Buttery and Archard, 1971).

The second mechanism of abrasive wear is called three-body wear (Burwell, 1957), which takes place when hard abrasive particles are introduced between sliding surfaces and abrade material off each other. It seems that sometimes abrasive particles adhere temporarily to one of the sliding surfaces, or else are embedded on it, and plough out a groove in the other. Figure 4.9 shows two-body abrasive wear and three-body abrasive wear, respectively.

Two-body abrasive wear   **Three-body abrasive wear**
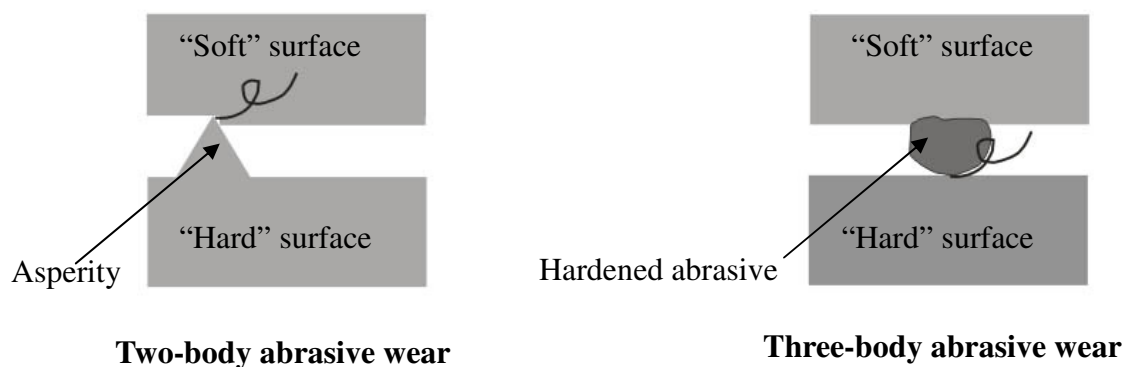
Figure 4.9 Diagrams show two-body abrasive wear and three-body abrasive wear in a microscopic view, respectively.

Two-body abrasive wear does not take place when the hard, sliding surfaces are very smooth. Similarly, three-body abrasive wear does not occur when the particles in the system are very small, or when they are softer than the sliding materials. The most usual situation in the laboratory is that a system is free from abrasive wear initially. Once sliding has commenced, however, abrasive wear may become a problem, since wear debris is often made harder by oxidation or work hardening. In hot forming, these detritus mainly constitute debris, dust and oxidation and start to accumulate in the system as a result of adhesive process. Effective lubricant can sometimes clean the sliding interface by carrying the wear particles away.

Usually, in hot forming, abrasive wear and adhesive wear exist together. In both types, wear is caused by the removal of die material.

4.4.1 Abrasive wear model

To derive a quantitative expression for the abrasive process, a simple model (first suggested by Euler in 1750) may be considered, in which the asperities on the hard surface are conical shape. This is shown in Figure 4.10.
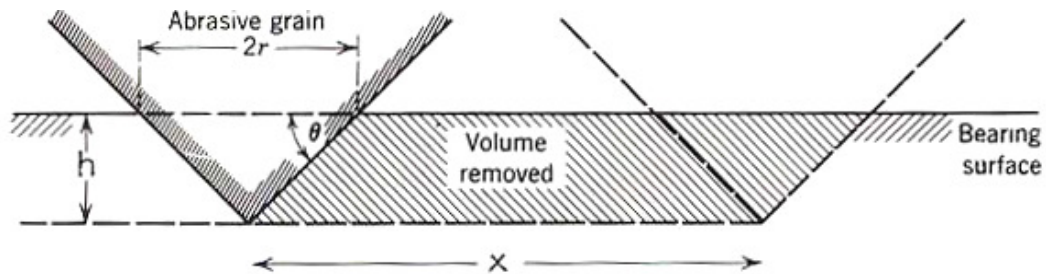
Figure 4.10 A simplified abrasive wear model showing how a cone removes material from a surface (for a distance of x) (Robinowicz, 1995).

Assuming one hard conical asperity carrying a load $\triangle W$ penetrates a softer surface to a depth h, by employing the concept of Equation (4-1), the load could be expressed as:

$$\Delta W = P \cdot \Delta A = P \cdot \pi \cdot r^2 \qquad\qquad (4\text{-}10)$$

where P is the hardness of the softer surface and r is the radius of the asperity, contiguous with the surface.

The projected area of the penetrating cone in the vertical plane is rh. Thus when the cone moves through a distance dx, it will sweep out a volume dV given by:

$$dV = r \cdot h \cdot dx = r^2 \cdot \tan\theta \cdot dx = \Delta W \cdot \tan\theta \cdot dx / (\pi \cdot P) \qquad (4\text{-}11)$$

therefore,

$$dV / dx = \Delta W \cdot \tan\theta / (\pi \cdot P) \qquad (4\text{-}12)$$

Then, considering the contributions of all the asperities, carrying a total load of W, the worn volume V would be

$$V = W \cdot x \cdot \tan\theta / (\pi \cdot P) \qquad (4\text{-}13)$$

This equation has the same form as Equation (4-8), with the term $k/3$ replaced by $\tan\theta / \pi$, denoted as k_{abr}, abrasive wear coefficient.

As same as for adhesive wear, Equation (4-13) can be simplified as:

$$V = k_{abr} \cdot W \cdot x / P \qquad (4\text{-}14)$$

where x is the total sliding distance and the abrasive wear coefficient is designated as k_{abr}.

It is interesting to realise that two principal types of wear have the same form, although some (Shaw, 1977) may argue that this is the consequential combination, since there is no other way the key variables of wear, i.e. load, sliding distance and hardness could be arranged. However, one thing needs to be borne in mind. It is that k and k_{abr} in the two equations symbolises different physical meanings. For adhesive wear, k indicates the possibility of fragment

removal, whereas for abrasive wear, k_{abr} relates to the geometry of the abrasive medium. In addition, since k_{abr} is directly related to the surface roughness, it is usually less than one (Arnell *et al.*, 1991; Robinowicz, 1995; Painter *et al*., 1996).

4.5 LUBRICATION AND COATING

The concept of surface contact involved with lubricant is considered here. To reduce the frictional force and thus allow easier sliding, lubrication and coating are deliberately introduced to separate the asperities either totally or partially.

4.5.1 Fluid-film lubrications

Fluid-film lubrication (Anderson *et al.*, 1992), also known as hydrodynamic lubrication (Ludema, 1996) or thick-film lubrication is most desirable. This type of lubrication refers to the total separation of asperities by a lubricant film thickness many times larger than the size of the lubricant molecules, and is effective only when the load in the contact zone is low. Under these circumstances, the sliding surfaces are separated by a lubricant film that is several times the thickness of the surface roughness.

If this condition exists only partially, that is, if part of the load is carried by the fluid pressure and the rest is borne by contacting asperities separated by a molecularly thin lubricant film, the term thin-film lubrication, or sometimes mixed-film lubrication is used (Schey, 1983; Anderson *et al.*, 1992). In the extreme form of thin-film lubrication, the entire load is carried by asperities lubricated by surface films of molecularly thin liquids, gases, or solids; this condition is known as boundary lubrication (Summers-Smith, 1994). High loads and very slow speeds produce extreme pressures that can lead to the lack of effective lubrication and, hence, promote maximum metal-to-metal contact. If not controlled, the resulting dry metallic friction will cause catastrophic wear and, ultimately, total seizure. Doege *et al.* (1978) have undertaken considerable research to determine the ability of forging lubricants to perform the several tasks required of them in hot forging situations. Essentially these are: physical isolation of work-piece and die; reduction of friction; die cooling and thermal insulation. In their research, the contact condition of the extrusion at hot temperature was assumed to be

boundary lubrication, i.e. the lubricant film was insufficient to prevent surface contact. This results in adhesion/abrasion and is a different mechanism of die failure compared to that arising in cold forming, where thick-film lubrication exists. The three different types of lubrication condition are expressed as diagrams in Figure 4.11.
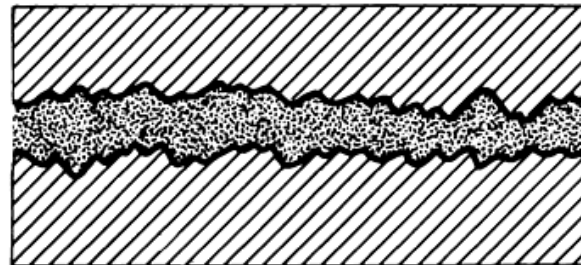
Fluid film lubrication—
surfaces separated by bulk
lubricant film
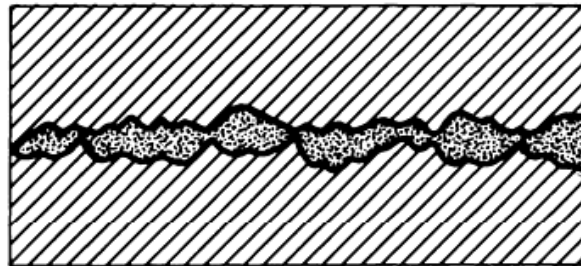
Mixed film lubrication—both the
bulk lubricant and boundary film
play a role
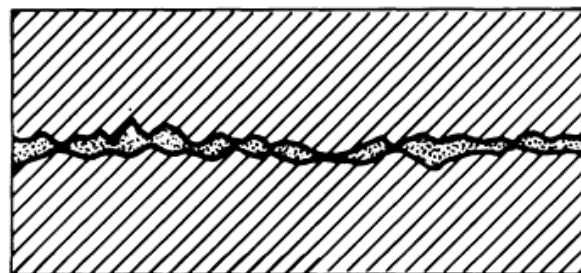
Boundary lubrication—
performance essentially
dependent on boundary film

Boundary film
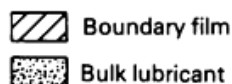
Bulk lubricant

Figure 4.11 Lubricant film thickness and associated lubrication regimes (Schiemann and Schwind, 1984).

The lubrication between two sliding surfaces can shift from one of the three regimes: thick-film, thin-film, or boundary lubrication, to another, depending on the load, speed, lubricant viscosity, contact geometry, and surface roughness of both surfaces. This dependence was first recognised by Stribeck (1902), who observed the variation of the sliding friction with a lubrication parameter $\eta v/p$, where η is the lubricant viscosity, v is the velocity and p is the average contact pressure. Figure 4.12 shows a typical Stribeck curve. At the right hand side, where the friction increases slightly with the lubrication parameter because of increasing viscous drag under lower pressure, lubrication is in the thick-film regime; at the far left, where the friction is nearly constant, lubrication is in the boundary regime. In the middle, lubrication is in the mixed-mode, or thin-film regime. The boundaries of these regimes would move to the right if the surfaces became rougher and to the left if they became smoother.
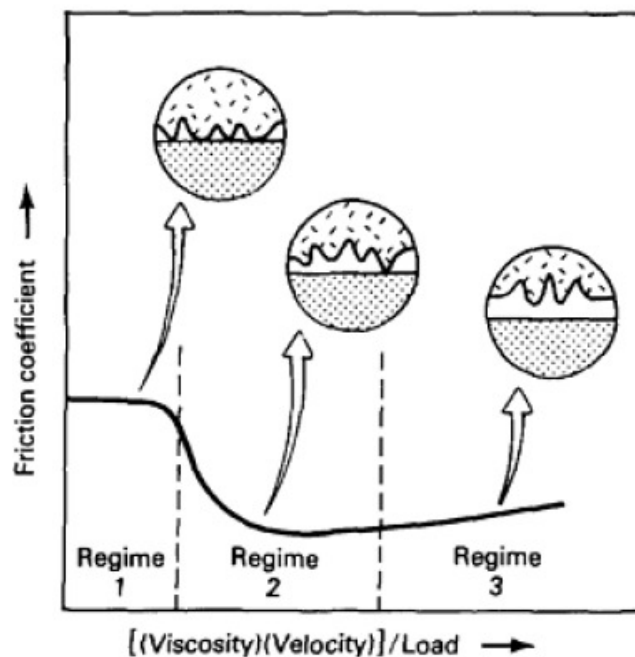
Figure 4.12 Plot of friction coefficient against $\eta v/p$ to show the range of three regimes of lubrication. Regime 1, boundary lubrication; regime 2, thin-film lubrication; regime 3, thick-film lubrication (Anderson *et al.,* 1992).

4.5.2 Solid-film lubrications

Metal surfaces, whether they are lubricated or dry, are covered with native oxides and hydrocarbons which tend to prevent adhesion. Under sliding and rolling contact (light load condition) surface damage is minimal. Increased loads can cause penetration of the hydrocarbon films and fracture of oxide layers. Therefore, adhesion and abrasion result.

Welsh (1958) found that steel resisted wear damage depending on the type of oxide developed. He conducted unlubricated wear experiments by means of a pin-on-ring apparatus with mild steel and cast iron using a wide range of load levels. As the load was increased, a transition point was reached in which friction increased by orders of magnitude and surface damage was severe. However, when the load was increased further, another transition point occurred in which friction dropped and surface damage ceased. Welsh concluded that frictional heating caused a change in oxide chemistry, producing a tougher oxide at the second transition.

Welsh (1965) later, undertook further investigations using pin-on-ring test again on various unlubricated steels, examined the concept of mild wear (oxidative) and severe wear (metallic) and the sharp transitions between these which he refers to as the T1 and T2 transitions as shown in Figure 4.13. In the steel of 0.52% carbon contents, below T1, wear occurs by the removal of oxide debris from an oxidised surface supported on a work hardened substrate. T1 is a transition to severe wear initiated by the breakdown of the protective surface oxide produced at lower loads. Plastic deformation of the substrate occurs, caused by a higher bulk temperature and the wear rate increases considerably with the production of a metallic debris. Between T1 and T2 severe wear occurs. At the T2 transition, the surface temperature is high enough for phase hardening to produce a hard "white layer" structure which prevents deformation and helps to establish an oxidised surface once again. The wear rate is reduced considerably but it is not as low as the wear rate below the T1 transition. Micro-hardness surveys and X-ray analysis of the wear debris confirm these general concepts. He concluded that a low wear rate could be achieved either by use of higher carbon steel or by heat treatment of a low carbon steel.
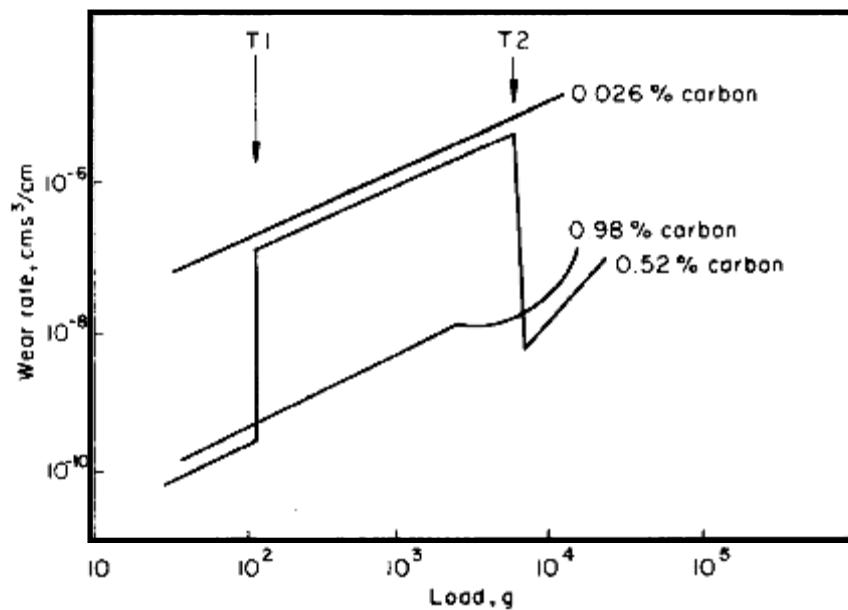
Figure 4.13 Transition wear behaviour of three different steels at constant forming speed from Welsh (adopted from Eyre, 1978).

A similar phenomenon was also found in Thomas's research (1970, 1972). He performed unlubricated real forgings for upsetting mild steel billets from 0.5 in to 0.2 in, to find the effects of work-piece temperature to the die wear. He stated that wear increases steadily with forging temperature from $900℃ \sim 1100℃$ for H13 tool steel and then falls sharply as the forging temperature increases to $1200℃$. The wear at $1200℃ \sim 1250℃$ is only one-third of that at $1100℃$. However, he commented that was ascribed to the transformation of a hard solid oxide to a liquid oxide on the surface of the die, at higher temperatures rather than surface hardening. Figure 4.14 shows his finding.

In order to understand the change of the surface condition of the studied die after forming, energy dispersive X-ray (EDX) spectrographic analyses were carried out to identify chemical composition on the die surface for different regions, and are presented in Appendix G.
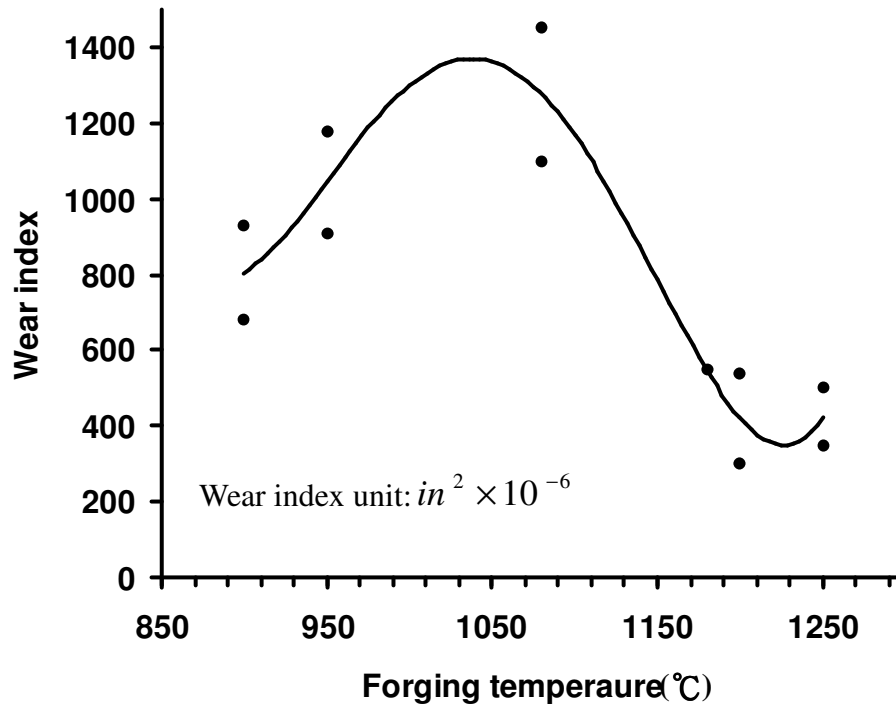
Figure 4.14 Influence of work-piece temperature on die wear (adopted from Thomas, 1970).

4.5.3 Surface coatings

Die coatings and surface treatments also have been found to be effective methods for prolonging die life.

A common surface treatment is nitriding in which hard nitrides are formed in a tool by the absorption of nitrogen, either from a gas or a liquid chemical. Gas nitriding is undertaken using ammonia at $525℃$ to produce a surface hardness of HV1000~1250 for H13 steel (Uddeholm hot work steel manual, 1970). CVD and PVD coatings of various chemical, also have been used widely, especially for cold forging tools (Seidel *et al.*, 1996). The coating procedure stated above could be time consuming and costly (Hudson, 2000), that is why it is still not yet fully implemented in the extrusion die described in this research.

4.6 LIMITATIONS OF ADHESIVE WEAR AND ABRASIVE WEAR MODELS

Three typical contact conditions have been mentioned in section 4.5 for forming processes employing lubricant, i.e. fluid (hydrodynamic), mixed and boundary lubrications. In the case of the hydrodynamic lubrication, a complete separation from the contact surfaces will occur. The applied upsetting load is transmitted predominantly via the lubricant film. The contribution of friction could be assumed to be low enough to be negligible. Therefore, the sliding length of the work-piece on the die reaches its maximum value.

This extreme situation, in which contact surfaces are obviously not affected by wear, represents an example of the insufficiency of the models in which wear is proportional to the sliding distance of the work-piece. Under the hydrodynamic condition, the sliding distance reaches maximum values, therefore, the calculation of the wear must result in maximum values, too. The reason for this is that both models ignore the existence of thick-film lubricant (Sobis, 1992).

As a result, the significance of the real contact area in treating wear problems again must be emphasised. Due to the nature of extrusion studied in this research, the lubricant condition was treated as boundary lubrication, thus the adhesive/abrasive models are valid. However, the model may need to be modified to tailor it for various forming conditions in the future, to account for the effect of lubricant.

Another controversial issue is the derivation of k and k_{abr} values in the models. Holm-Archard assumed that adhesion occurs at the points of asperity contact, or equivalent, whereas adhesion is an unpredictable phenomenon as well as abrasion. They occur between solids often in an environment consisting of contamination and wear particles which is rarely examined, and has not been demonstrated physically as an individual event. The possibility of the values of k and k_{abr} to be represented as a function of temperature, surface roughness or mechanical properties of the surface, remains to be further investigated.

CHAPTER 5

FE MODELLING OF DIE WEAR FOR EXTRUSION

5.1 INTRODUCTION

In industry, usually the frequency at which a die should be changed is judged by experience, or statistical analysis, neither of which are strongly scientific. Recently, numerical computer-aided modelling provides a channel for understanding wear conditions during forming (Vertin and Majlessi, 1993; Tekkaya, 2005).

In the territory of die wear modelling, the majority of research has been carried out by using FE method and adhesive/abrasive wear models. Kim *et al.* (1994) modelled hot closed die forging process. They concluded that material properties such as flow stress play important roles in simulation results. However, the effect of process parameters, such as friction, forging speed and die geometry to the wear, are not included in their research. Painter *et al.* (1996) identified that abrasive and adhesive wear during the valve stem extrusion operation shorten die life markedly under the high pressure and high temperature conditions and tried to predict wear and optimise processes. Their work showed that pressure and velocity distributions during the simulation affect the predicted wear profiles more than temperature, which may not be true since the temperature at the interface for hot forging is very likely to exceed tempering temperature of the die. It will lead to the die softening easily. Later Lee *et al.* (1999) modelled the cold extrusion process to examine the wear and elastic deformation of the die. They found that wear would most likely be the primary cause of die failure in the case of a lower extrusion ratio. On the other hand, it was found that a sudden failure might occur due to fatigue fracture in the case of a higher extrusion ratio, since the stress concentration in the die shoulder was critical. Research revealed that the failure mode in the extrusion dies could be governed by wear or fatigue depending on the die geometry, i.e. the extrusion ratio and the radius of the transition region. Chen *et al.* (2007) modelled the cold extrusion using FE in 3D and also commented that the extrusion force increased with increasing extrusion ratio, which lead to the occurrence of the damage. Recently, some researchers noticed that temperature is an important factor affecting the hardness of the die during hot/warm forming. Kang *et al.* (1999a and 1999b), Lee and Jou (2003) and Behrens and Schaefer (2005) described die

hardness as temperature dependent for modelling die wear. Results showed that temperature is also an affecting factor to die wear.

In this chapter, die wear of extrusion modelled using FE simulation, incorporating the abrasive wear theory, is presented and analysed. The heat transfer variation and friction condition investigated earlier have been implemented in the extrusion model as boundary conditions. By employing the FE method, the degree of wear and critical worn area were predicted and identified from a macroscopic point of view. Results from simulations, die wear and qualitative representations contained in optical and scanning electron micrographs by observing the studied worn die, are presented to provide qualitative comparisons.

5.2 INTEGRATION OF WEAR MODEL

In order to describe the wear condition encountered in this study, the wear model can be modified as:

$$h = k \cdot \sigma \cdot L / P^m (T) \qquad (5-1)$$

where h is the average depth of material removed in mm, σ is the average normal stress over the apparent contact area in MPa, L stands for the sliding distance of the work-piece in mm. The wear coefficient k is dimensionless and the value was suggested to be 0.00001 for the abrasive wear of steel (Schey, 1983; Williams, 1996). For convenience of implementation through FE simulation in this work, P is taken as Rockwell hardness of the die and is temperature dependent. m stands for hardness coefficient, typically equal 2 for steels (Painter *et al.*, 1996).

From the tempering data of H13 steel (derived from Paxton & Vierling Steel manual) the hardness of the die as a function of temperature has been expressed as:

$$P = 5 \times 10^9 \cdot T^{-2.8729} \qquad (5-2)$$

where T is temperature in ℃. In addition, Rockwell hardness measurements were made at

random positions on the non-working surface of a piece of sectioned die, which are assumed to be representative of the original values. The average hardness value of HRC54 was obtained. This value was input as the initial hardness for each element of the die mesh in FE analyses. Then Equation (5-2) was programmed into the subroutine USRUPD in DEFORM to calculate the variation of die hardness according to the temperature reached in different places on the surface during deformation and stored in each node of the die mesh.

In the FE model, Equation (5-1) could also be written as the following with *r* and *t* representing position and time parameters, respectively:

The wear depth can be rewritten in an integral form:

$$h = k \cdot \int_0^t \frac{\sigma(r,t) \cdot V(r,t)}{P^m(T,r,t)} dt \qquad\qquad (5\text{-}3)$$

where *h* is total wear at time t. *V* is sliding velocity of the work-piece and *dt* is time increment.

Equation (5-3) was programmed into WEAR subroutine for calculating the wear amount in the simulation.

The interfacial pressure within the wear model was related to the flow strength of IN718, which is dealt with in Chapter 2, and was programmed using subroutine USRMTR. The corresponding state variables were updated in subroutine USRUPD. Average grain size prediction of the extrudate using the material model is presented in Appendix B as mentioned in Chapter 2, with the metallurgical evidences. Figure 5.1 shows the information passed to and from the routines and models.
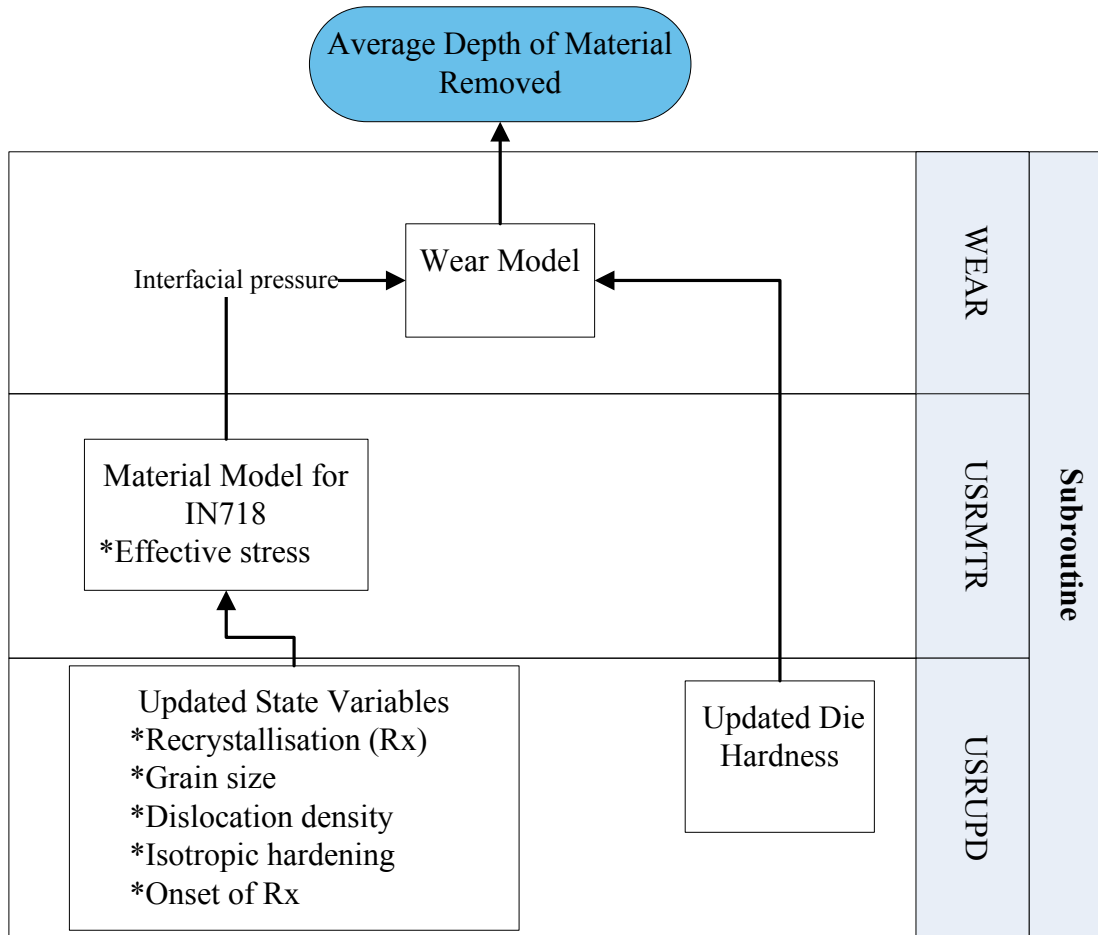
Figure 5.1 Flow chart showing communication paths within the FE software.

5.3 CONSTRUCTION OF EXTRUSION MODELS

Models for the simulations were constructed using two symmetric plane strain conditions, due to non-axisymetric geometry of the die, and the IN718 constitutive equations described previously in Chapter 2 were used in the simulations. Thermal and mechanical properties of H13 die steel, assumed rigid, were taken to be the same as those used in modelling heat transfer compression and ring tests.

Symmetric plane strain models on depth and width sections were employed to examine two regions having different wear amounts. Although 3D simulations could provide complete stress states, temperature and velocity field, the 2D simulations were performed to achieve shorter calculation time and still obtain important wear data.

Friction and heat transfer conditions were set to the values determined in Chapter 3. The dimensions of the work-piece before extruding were 11.5 mm in width and 65 mm in length. In addition, a small radius, 2 mm, was given at the bottom right of the work-piece to facilitate the convergence, and to avoid the overcutting problem during simulations. Dimension of the two sections of the die are presented in Figure 5.2 as semi-infinite models. The punch, also modelled in plane stain, was 12.5 mm in width and 15 mm in length. The extrusion ratio defined by cross-sectional area of the work-piece divided by cross-sectional area of extrusion, is 1.53 for width section and 3.33 for depth section.

The shapes of the die and punch input to DEFORM were meshed for fully coupled thermo-mechanical analyses. Figure 5.3 shows the initial meshes

The conditions and assumptions for the extrusion models were as follows:
- The die was assumed to be homogeneous and possessed isotropic hardness of HRC54 initially before extrusion.
- The surface of the die possessed no surface treatment.
- No heat lost from the work-piece during the transport from furnace to the die.
- Only one single simulation of extrusion for each case was performed.
- Constant friction prevailed at the interface during forming.
- Lubrication, glass coating and surface scale conditions were modelled as for the determined values from heat transfer compression and ring tests described in Chapter 3.
- Abrasive wear was assumed to be the dominated wear mechanism.
- Uniform billet temperature with average grain size (20 μm) before sitting on the die were assumed.

The whole extrusion process was simulated in two stages. First, the billet was transferred to the bottom die and sat for one second. This was followed by extrusion in the second stage. By integrating the subroutines, the extrusion model was completed by adding boundary conditions at the interface. Values of heat transfer and friction were varied within the range derived from the experiments, to examine their effects to wear.

Width section   **Depth section**
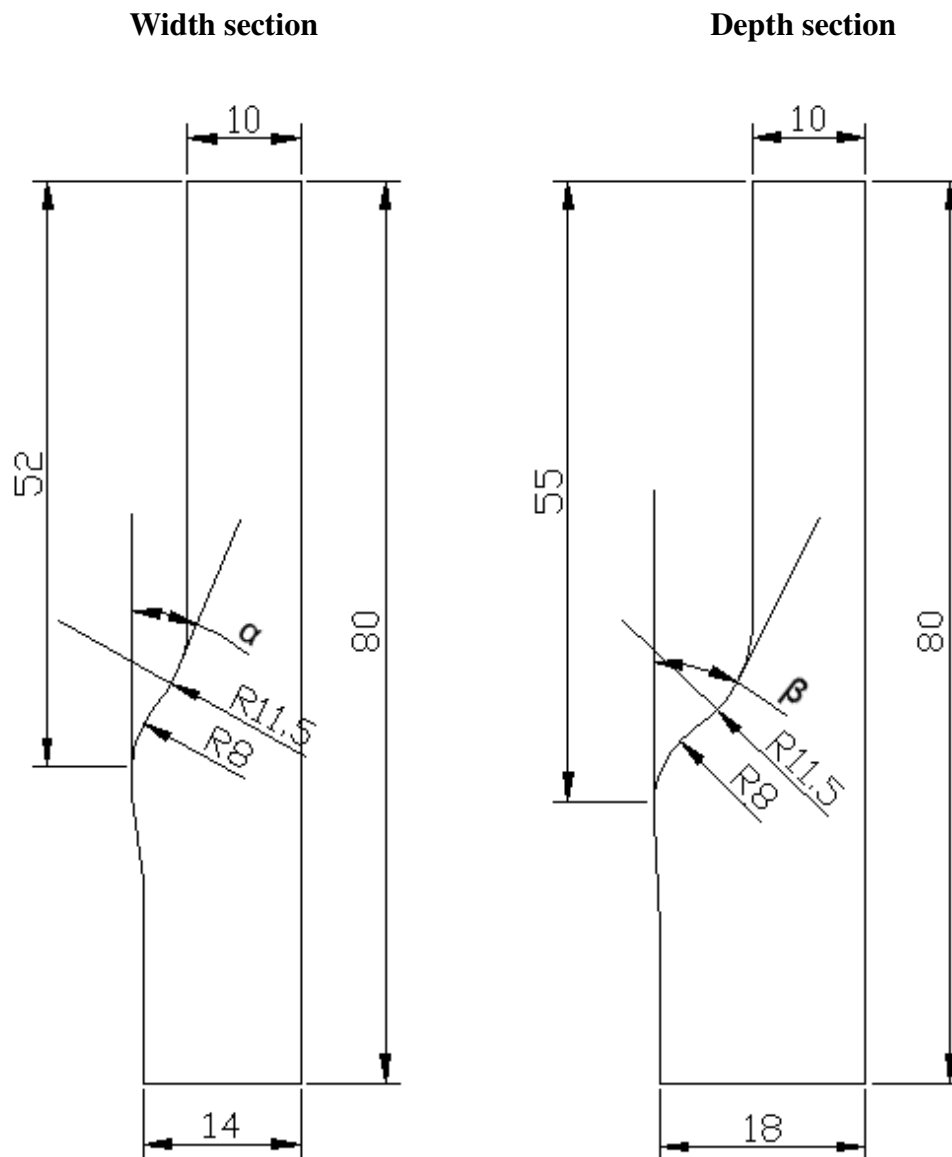
Unit: mm

Figure 5.2 Die dimensions for width and depth sections, where angle α is 25° for width section and β is 35° for depth section.

Width section   **Depth section**

Punch

Work-piece

Punch

Work-piece

Die   Die
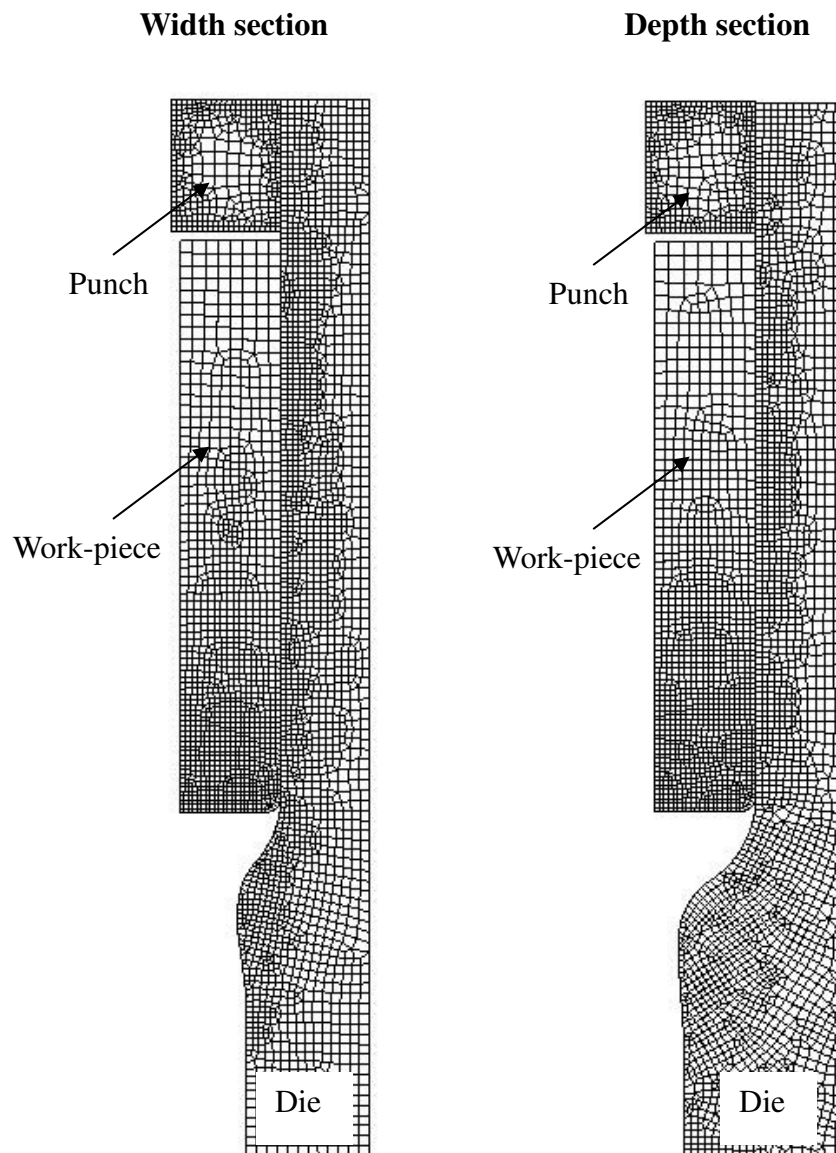
Figure 5.3 FE extrusion models for width and depth sections.

5.3.1 Justification of mesh and step size

Analyses were made for judging appropriate mesh and step sizes for the extrusion model. A quadratic mesh was generated automatically by the DEFORM solver and element number, element size and step size could be amended. It was assumed that the accuracy of results (judged by the maximum wear) would increase with reduction in the mesh size of die. The number of 7000 elements chosen as a standard for high accuracy was 7000, against which the loss in accuracy using coarser meshes could be assessed. The results from the analyses are shown in Table 5.1.

Die Mesh Number	Minimum Element Length (mm)	Error of Predicted Wear (%)	Step Size (s)	Computational Time (min.)
500	0.86	-7.6	4×10^{-6}	68
1000	0.40	1.6	4×10^{-6}	77
2000(used)	0.31	-1.4	4×10^{-6}	90
5000	0.16	0.6	4×10^{-6}	198
7000(standard)	0.12	0	4×10^{-6}	171
7000	0.12	0	4×10^{-7}	1719
2000	0.31	-1	4×10^{-7}	926
2000	0.31	unstable	4×10^{-5}	unstable

Table 5.1 Error analysis for mesh and step size of extrusion model**.**

From the results it was concluded that 2000 elements of length 0.31 mm is a suitable mesh to use, as the accuracy and the calculation time are acceptable. Also, a step size of 4×10^{-6} second was used in the study, considering stability without compromising efficiency.

5.4 RESULTS AND ANALYSES

The results from the FE simulations are presented in this section. The process parameters were altered to examine their effects to the die wear by using the abrasive wear model. The

wear index is introduced as the average depth of material removed in mm for forging distance of 30 mm.

5.4.1 Prediction of abrasive wear

5.4.1.1 Effect of die shoulder angle

The shoulder angles, α and β, shown in Figure 5.2 were altered to examine the effect of the angle to the die wear. Figure 5.4 (a)~(c) show the wear profiles for the width sections and (d)~(f) show the depth sections for different values of die shoulder angle. Among them, angles of 25° (width) and 35° (depth) are adopted by the industry currently.

Considering only wear of the width section, the wear profiles are different for each angle value. In Figure 5.4 (a), maximum wear occurs at the entrance to the extrusion orifice , with a small peak at the transition from cylindrical bore to die cone. In (b), only one peak exists, part way along the bore/orifice transition region. In (c), two peaks of approximately the same value of wear are shown, one at the bore/die transition, the other part way along it. Also, the amount of wear in condition (c) for the die angle of 35°, the maximum amount of wear is 21% higher than that for the other two angles. The results show that as the angle increases, wear increases and different wear profiles are obtained.

The wear profiles for depth sections are similar in disposition but different in magnitude to those in the width sections. Wear of depth sections was approximately 43% higher than that of the width sections, on average. Probably the increase in the amount of wear is due to the higher extrusion ratio in the depth section, which caused higher forming pressure. In addition, the lengths of significant wear for depth sections were greater than those for the width sections and started in the cylindrical bore, before bore/cone transition, as can be seen in figures (d) to (f). Since the forming speed and friction were set the same for both sections, the explanation might be the much bigger normal pressure on the orifice for the depth section before the metal is turned inwards. It is also seen in all wear profiles, that a small unworn length, or length of little wear, exists a short way beyond the minimum cone position.

To further investigate the effect of different shoulder angle to the forming force, the normalised maximum forming load was then defined as F/F_w, where F is the maximum forming force required for different shoulder angles and F_w is the maximum forming force for shoulder angle equals 15° of width section. The comparative results are shown in Figure 5.5. Extruding ratio not only affected die wear which also doubled the forming force for the depth section and is clearly shown in the diagram. The difference of forming load for different shoulder angles is within 18% for width sections and within 4% for depth sections; however, different wear profiles will be produced by different shoulder angles.

(a)

(b)

(c)

(d)

(e)

(f)
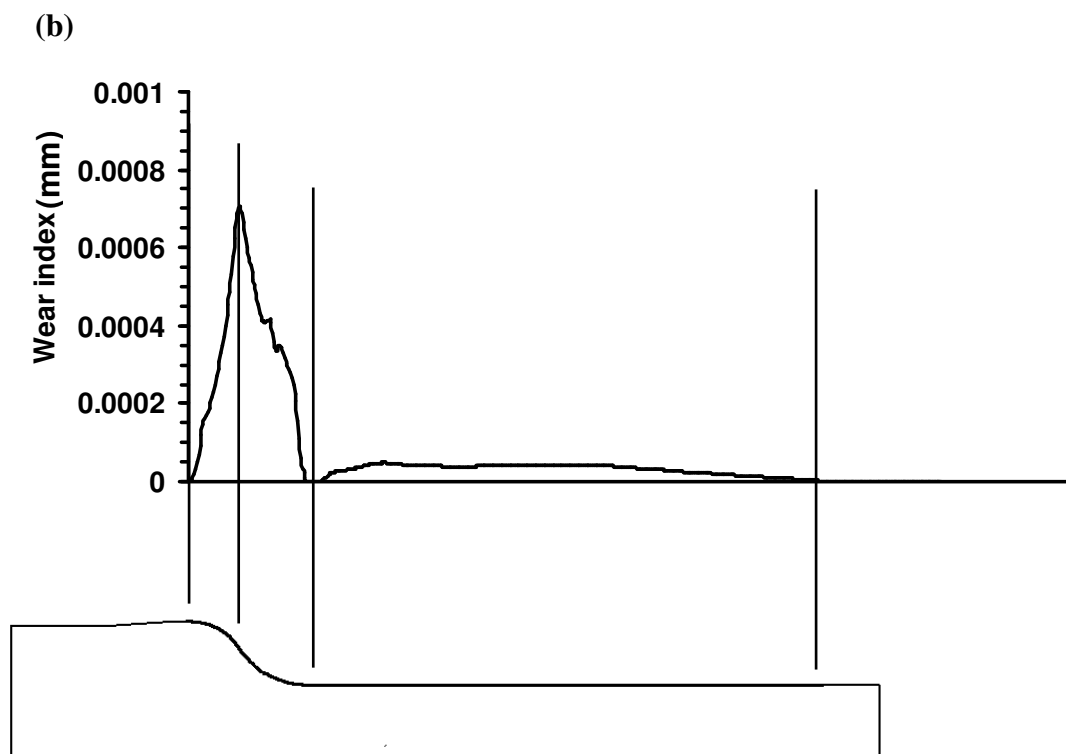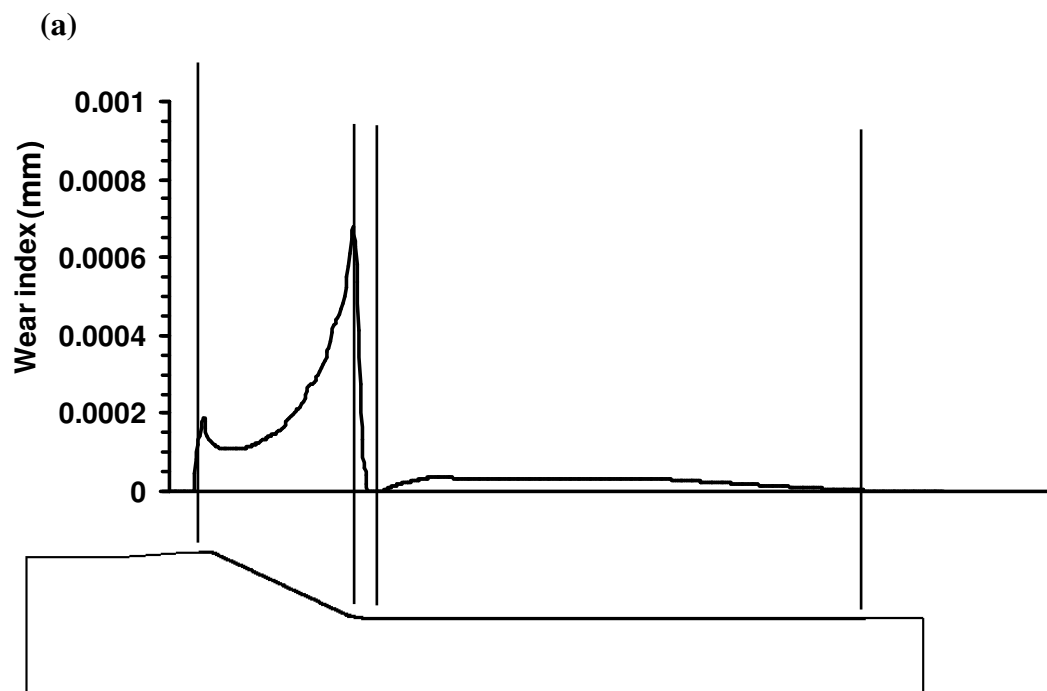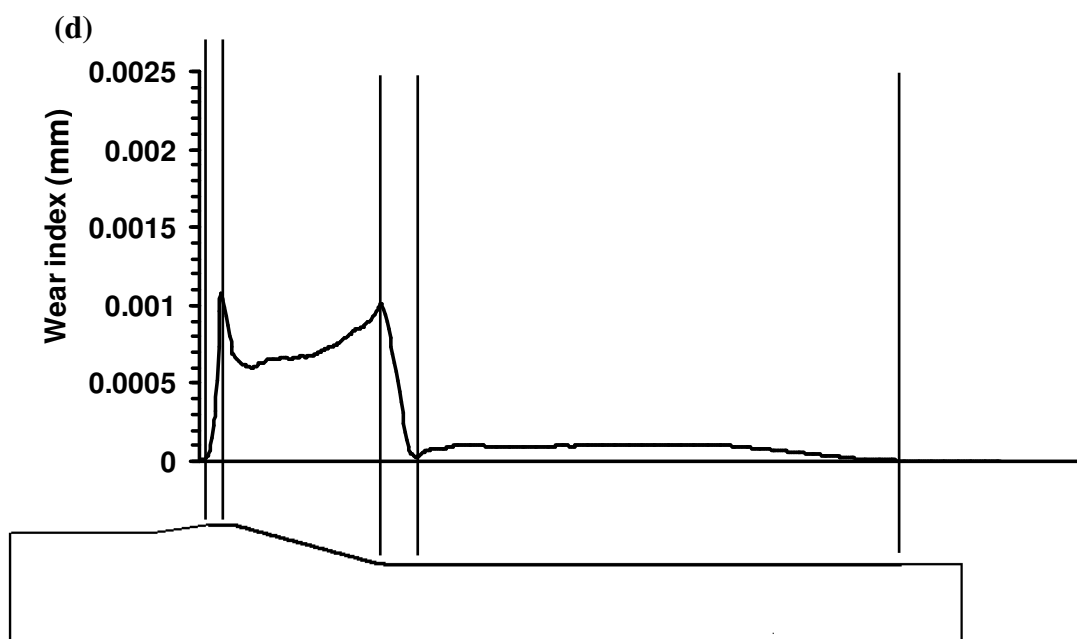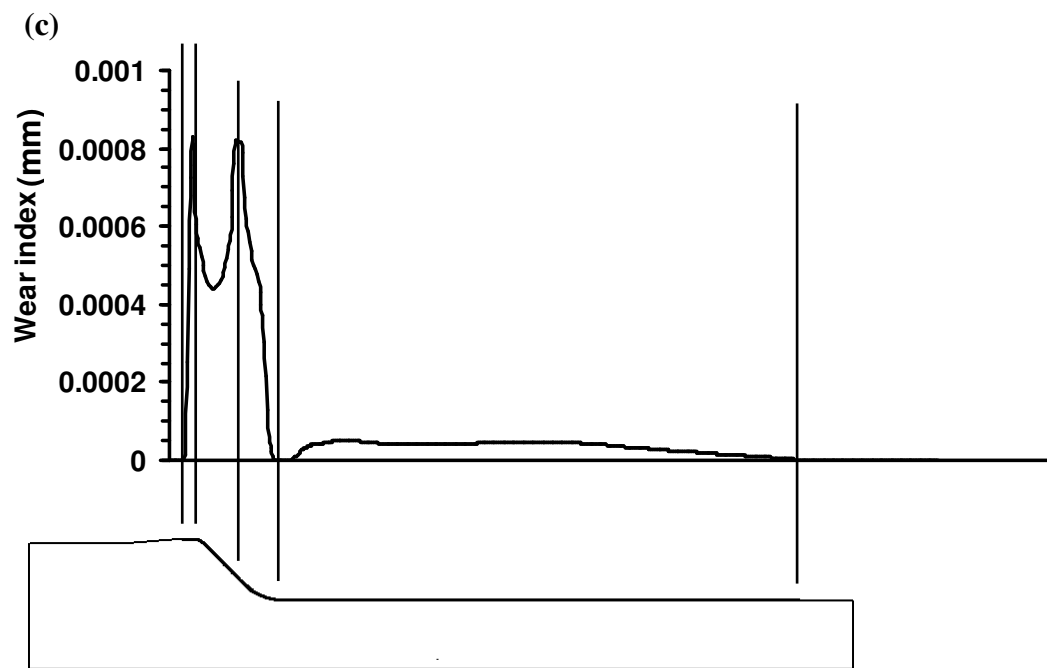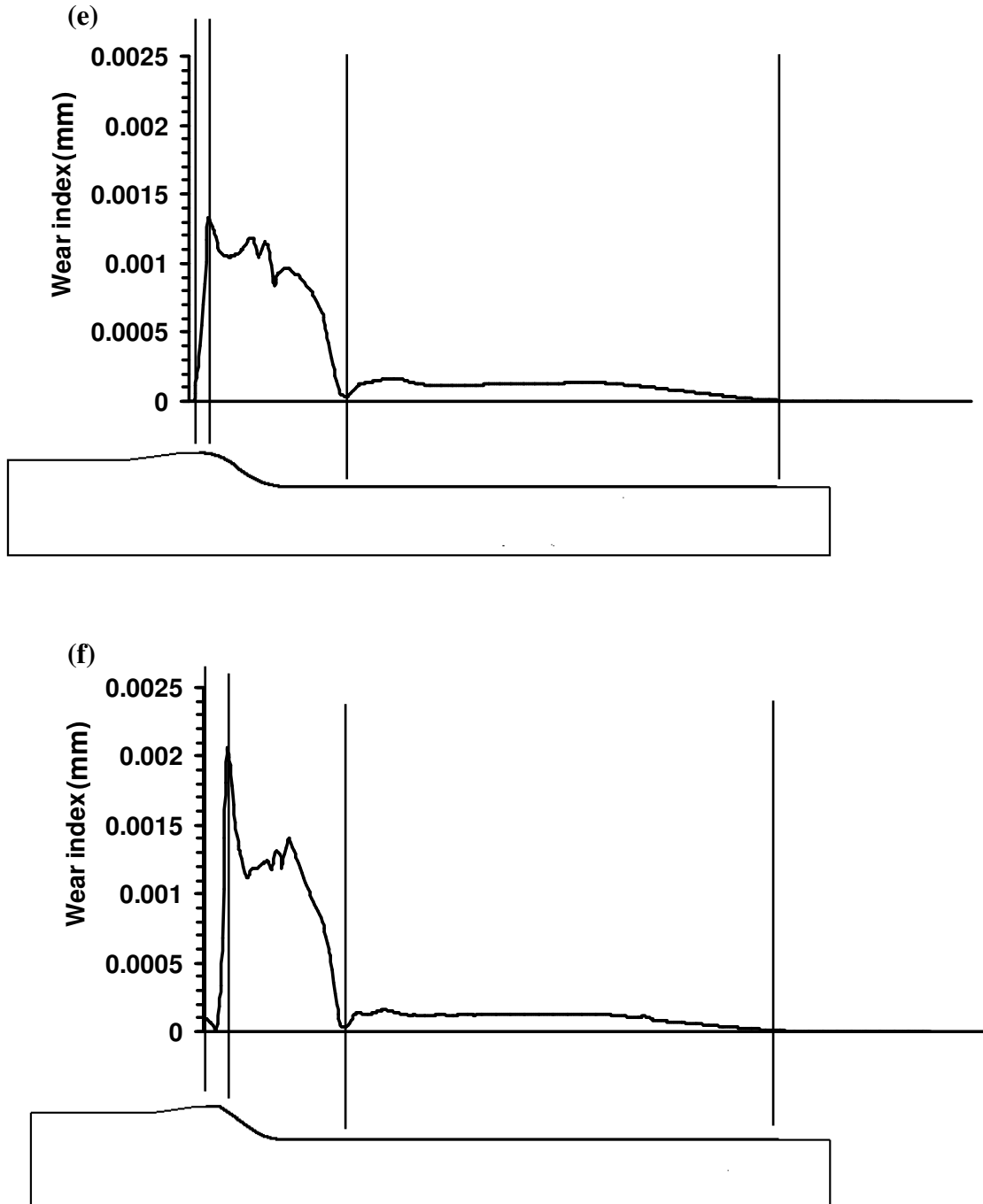
Figure 5.4 Wear profiles after deformation at average forming speed of 186 mm/s (friction factor = 0.18 heat transfer as pressure dependent, ranged from 19kW/m^2 $^\circ$C ~24kW/m^2 $^\circ$C, for a shoulder angle of: width section (a) 15° (b)25° (c)35°; and depth section (d)25° (e)35° (f)45°, respectively.

114
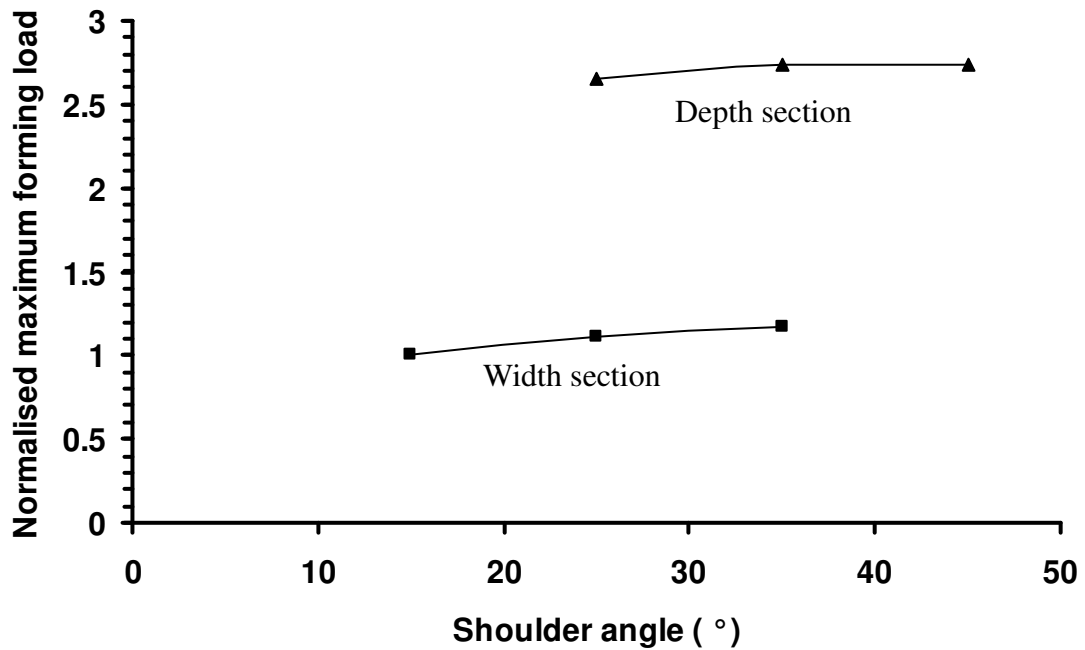
Figure 5.5 The relations between different shoulder angles and forming forces for both sections.

5.4.1.2 No-wear zone analyses

Possible reasons for the no-wear zones, identified in Figure 5.4 above, have either little or no contact between work-piece and die, or sticking of the work-piece to the die. Either of these situations could result in little wear, (no contact, or no sliding), but identifying the existence of either of them has not been possible because metal flow could not be monitored in real extrusions. Another reason for the appearance of a no-wear zone in FE simulations might be due to either too coarse a mesh size for the work-piece or the definition of the geometry of the die for the extrusion.

To investigate these possibilities, simulations were performed using other two mesh number of 5000 and 3000, minimum size of 0.11 and 0.18 mm for the work-piece at zero friction and heat transfer coefficient = 22 kW/$m^2 ℃$ (mesh number = 1200 and minimum mesh size = 0.25 mm for the original one). The relations between mesh number and length of no-wear zone are given in Figure 5.6. The results show that the no-wear zone resulted from the use of

all three mesh numbers with no definite trend exists for the reduction or increase of no-wear zone, as mesh number increases.
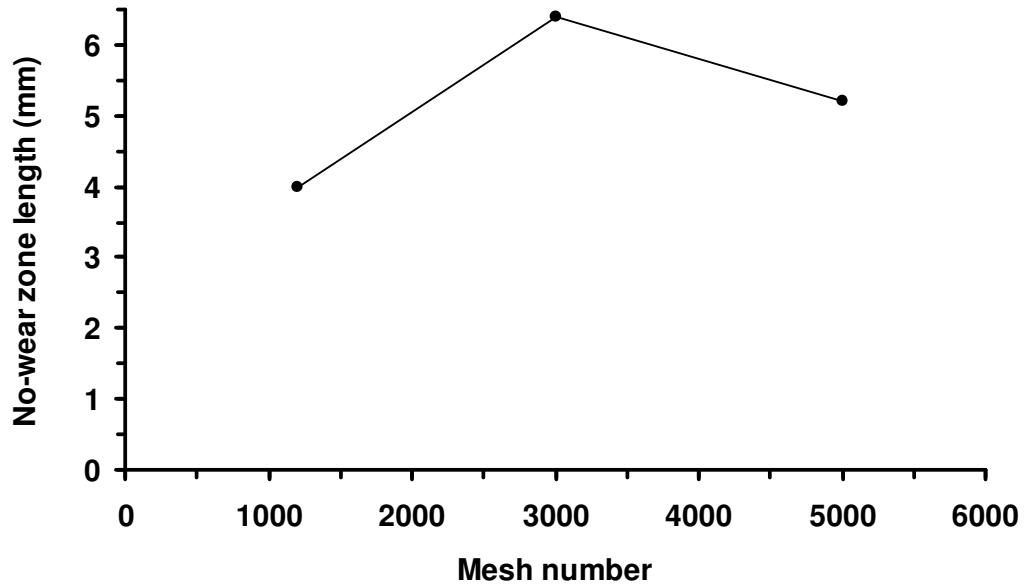
Figure 5.6 Relation between mesh number and no-wear zone.

Analyses were also performed to examine the effects of friction, heat transfer and die shape, on the size of the no-wear zone. In Figure 5.7, the biggest no-wear zone is associated with a heat transfer coefficient as pressure dependent, value ranged from $19kW/m^2\,^{\circ}C \sim 24kW/m^2\,^{\circ}C$, for both friction factors. Also, the average length of no-wear zone is larger for zero friction than that for m = 0.22. Figure 5.8 shows the effect of the shoulder angle at width section on the no-wear zone. The variation is also small with no obvious trend. It is difficult to provide satisfactory explanations for these results because the differences under these conditions were small.

The happening of the no-wear zone from the simulations needs to be contemplated if it appeared on the real extruding processes. The area above the chamfer of the die was assumed to have the least wear among all other area on the die surface from the simulation results. Although no-wear zones exist in the simulation results, no physical explanation for them can be given at this stage. However the worn die under study was carefully examined in an attempt to obtain empirical evidence for them being real. The profile of surface roughness of

the die was measured and is shown in Figure 5.9. Also, in Figure 5.10, photographs from SEM show the different worn surfaces at four positions on the die.
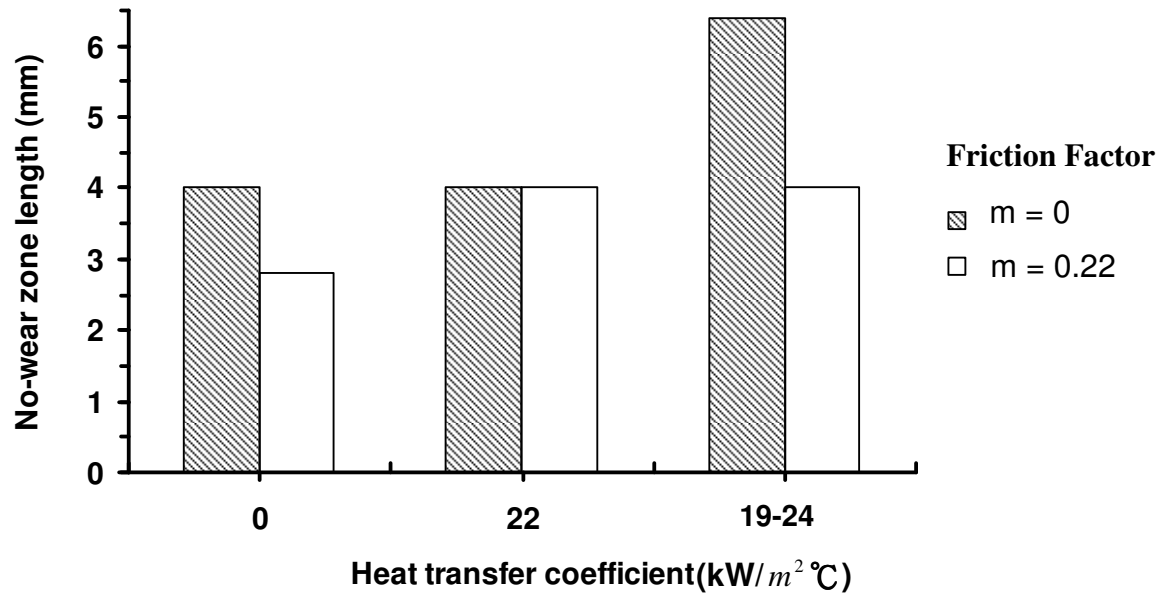
Figure 5.7 No-wear zone length for three heat transfer conditions at friction factor, m, equals 0 and 0.22 respectively.
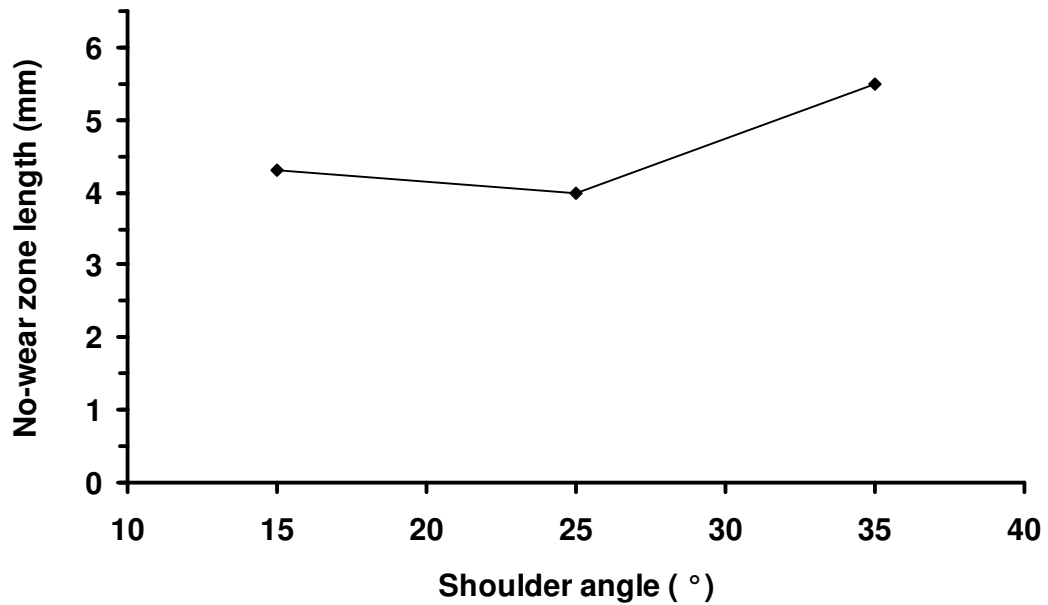
Figure 5.8 Relation between shoulder angle of the die and no-wear zone length for width section.
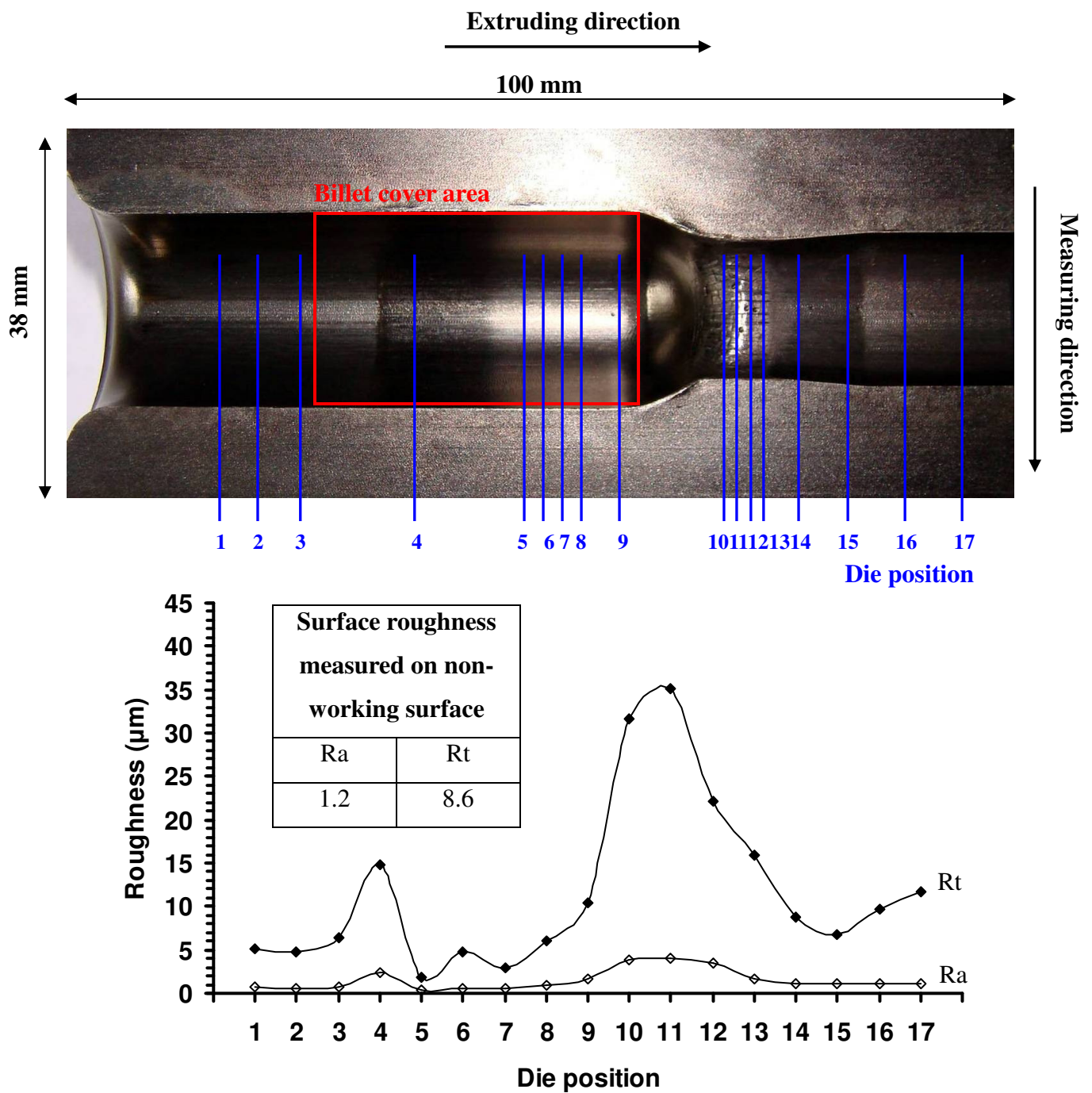
Figure 5.9 The surface roughness of Rt and Ra values at different positions on the die.
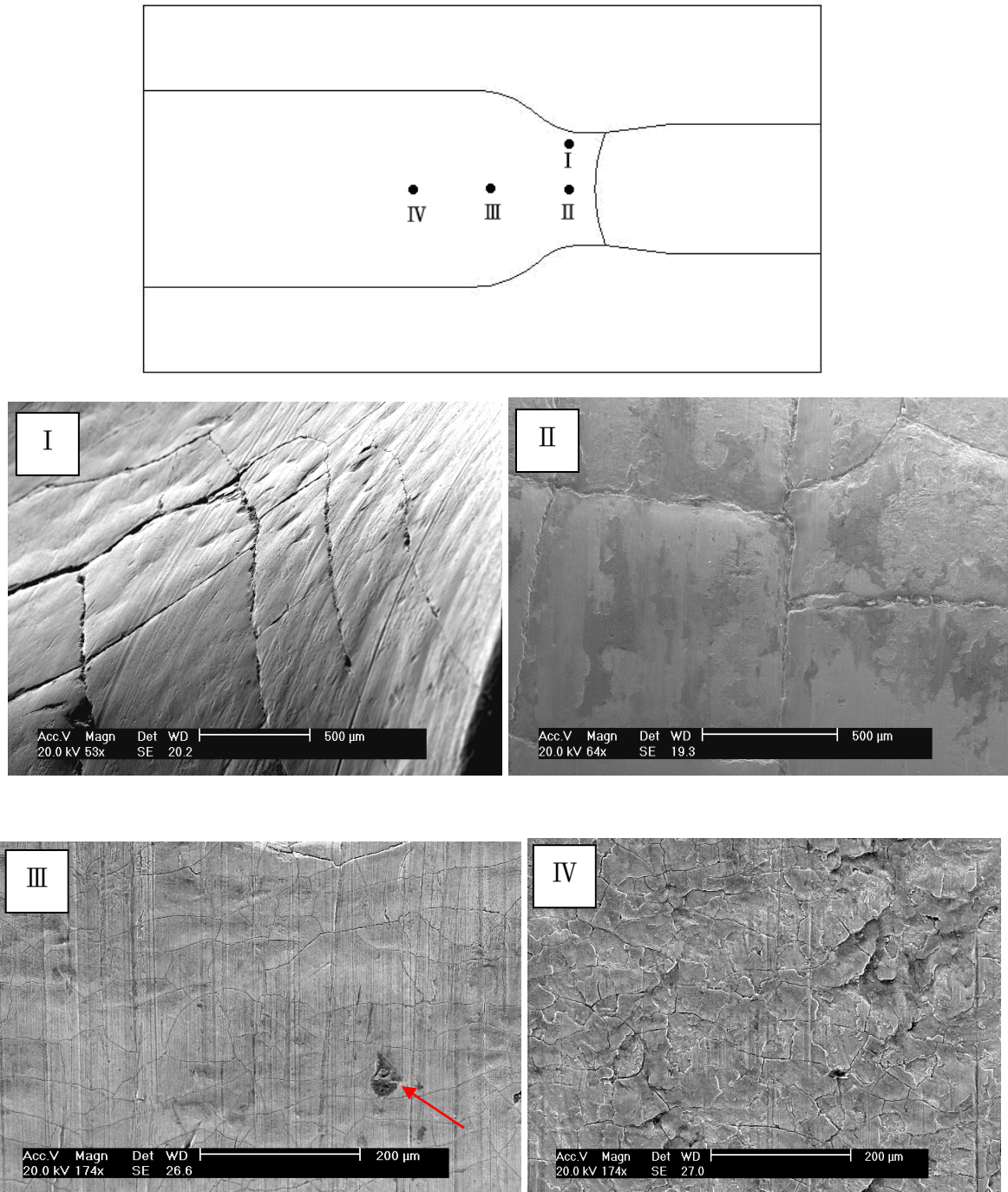
Figure 5.10 The surface topography on the die at four positions. In position Ⅲ, the arrow pointed out a pit which might have been caused either by adhesion or by accidental damage.

Surface roughness was measured using Taylor-Hobson Talysurf-120L equipment. Rt is the value of maximum peak-to-valley height and Ra is the mean height of the surface profile (peaks and inverted valleys). The evaluating length for each value is 1.25 mm. Figure 5.9

shows the change of these two values on the die. Both Rt and Ra values were high between positions 9 to 14, which is the transition of the extrusion orifice, that also matches the position of the maximum wear predicted from the simulations. The reason for this high value of roughness is the presence of the profound fatigue cracks and abrasion trenches. It is also interesting to see that the roughness is low between positions 5 to 8, which corresponds to the no-wear zone described above. Although the mechanics of the no wear phenomenon is not clear, its existence seems to be supported by the roughness measurements.

In addition, SEM inspections using a Philips XL-30 machine have also been carried out on several locations on the worn die as Figure 5.10 shows. Position Ⅰ shows the surface in the transition region. Not only had the presence of the abrasive trenches, but the obvious cracks also observed. In position Ⅱ, the cracks can still be observed accompanied by trenches as shown in the previous photograph. Some dark patches were also found on this area. In position Ⅲ, the abrasive grooves still exist and one pit was found as pointed by the arrow. By observing the shape and the protuberance around the edge of the pit, its forming was considered to have happened after the deformation, which might be due to the accidental damage during the transport of the die. However, it was also possible for the hardened particles transferred back to the die surface due to adhesion. Position Ⅳ presents the surface condition which is close to the "no-wear zone" by observing the wear profile on depth section of the simulation. Compared with other areas, the number of grooves is fewer and less severe, although cracks are numerous.

These photographs exhibit two dominant topographies for the extrusion die:
- Trenches, due to abrasive wear, are distributed all along the extruding distance at the die surface.
- Crack networks, due to significant thermal and mechanical fatigues.

5.4.1.3 Effect of friction under different heat transfer conditions

Material flow is directly affected by friction during forming. In the wear model, the wear amount is proportional to the sliding distance, therefore, the wear amount will be different in terms of different amount material flow at the tool/work-piece interface. Figure 5.11 shows

the effect of the friction factor on the wear under three different heat transfer conditions (the pressure dependent condition is derived from heat transfer tests presented in Chapter 3, ranged from 19170W/m^2 ℃ ~24000W/m^2 ℃). Adiabatic forming simulations were performed to eliminate the effect of die hardness within the wear model without modifying the subroutines.

Under the adiabatic condition, the wear amount decreases with increase in the value of friction, although the change is small. However, when the heat transfer occurs, wear is increased as friction increases. In addition, in the case of heat transfer being a function of pressure, wear is tripled when compared with that arising for constant heat transfer coefficient. In order to further investigate this phenomenon, the relations of nominal sliding distance of the work-piece, maximum die surface temperature, minimum hardness of the die and maximum interfacial pressure to friction factor are plotted and shown from Figure 5.12 to Figure 5.15.

Figure 5.12 shows the nominal material sliding distance for different friction and heat transfer conditions. The sliding distance was derived by tracking a node on the mesh of the work-piece to represent the nominal sliding distance of the work-piece material at the interface. The sliding distance decreased as friction increased but the difference is small. For three heat transfer conditions, the difference is about 1 mm for a forging distance of 30 mm. Sliding distance decreases as the difference between the lower surface and higher sub-surface temperature increases, because sub-surface and interior metal flow becomes relatively greater. Therefore, sliding was most for no heat transfer (adiabatic condition) and least for the pressure dependent heat transfer condition, which resulted in harder surface and sub-surface work-piece metal.

Figure 5.15 shows that values of interfacial pressure have no dramatic difference for various friction factors, in the cases of three heat transfer conditions. In contrast, the die surface temperature is different for different friction factors and heat transfer conditions, which is shown in Figure 5.13. It can be seen that temperature increases for the adiabatic condition, which is ascribed to the retaining of friction heat at the surface nodes. However, this increase does not change the hardness value, since all temperature values are still below the tempering

temperature of H13. For the other two heat transfer conditions, the temperature increased as friction increased, due to frictional heating and heat generated from the deformation. Interfacial temperatures exceed 600℃ for all the friction conditions. Since H13 tempers slightly below 600℃, the surface of the die will soften. Figure 5.14 shows the hardness of the die arising for different friction and heat transfer conditions. It is clear that the die significantly softened, as the die surface temperature reached to 700℃ and 900℃ for heat transfer constant and pressure depending conditions respectively, at friction factor = 0.3. If the cooling rate had been high between forgings, the die surface could have been quenched from the high temperatures and become hard again. This might have resulted in thermal fatigue. Therefore, it can be concluded that, according to the wear model, reduction in die hardness is the dominant factor affecting wear for different friction values. Die hardness does not change for adiabatic situations and, therefore, least wear would arise. In an adiabatic condition, sliding distance, controlled by the value of friction, decides the amount of wear. As the difference in sliding distance for adiabatic forming was under 0.5 mm, friction varying from zero to 0.3, the difference of the amount of wear is small.
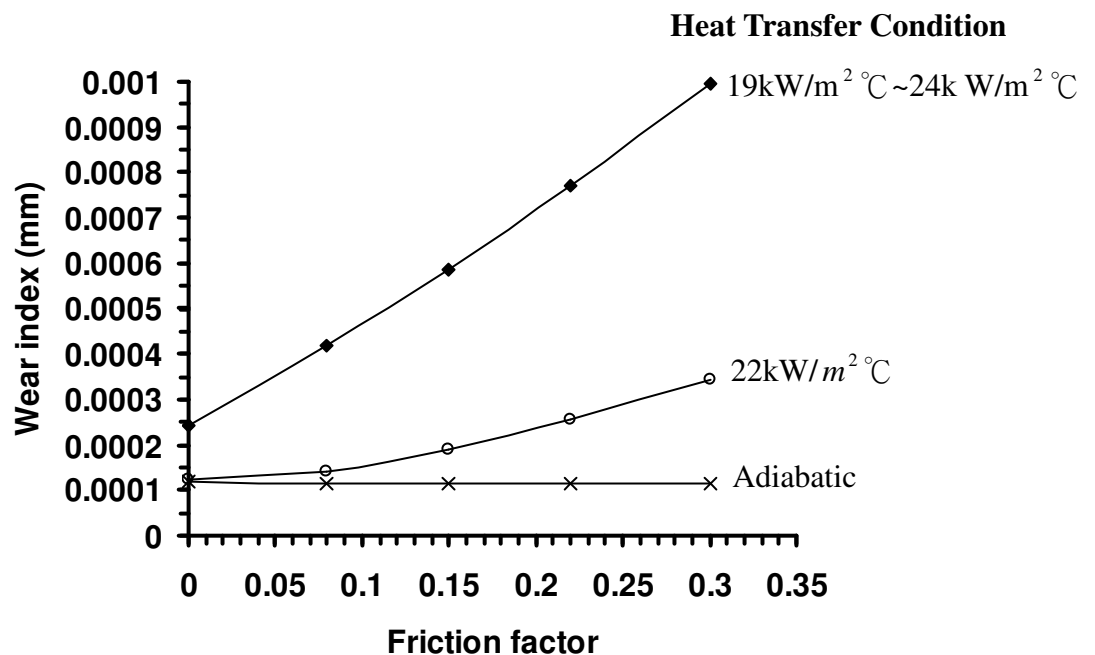
Figure 5.11 Relations between wear and friction under three heat transfer conditions.
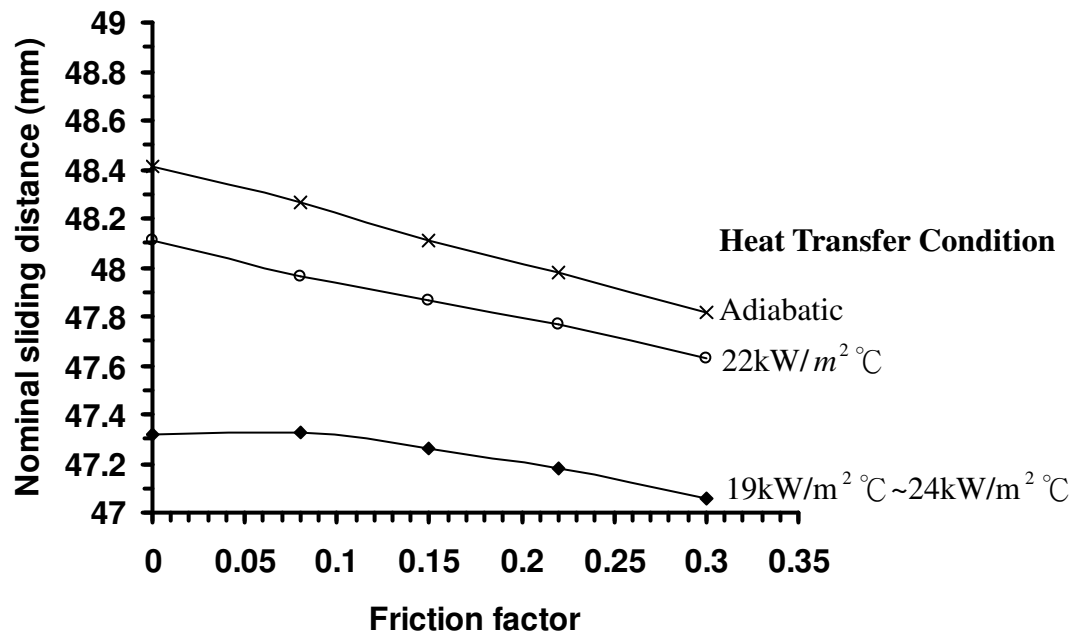
Figure 5.12 Relations between nominal sliding distance and friction under three heat transfer conditions.
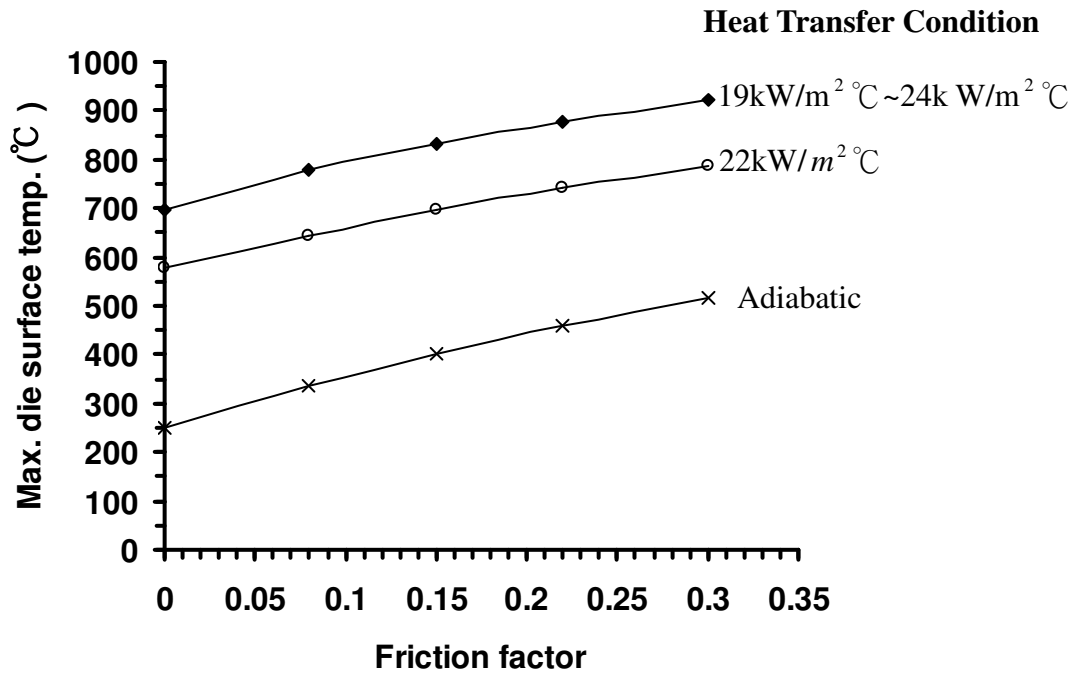
Figure 5.13 Relations between maximum die surface temperature and friction under three heat transfer conditions.
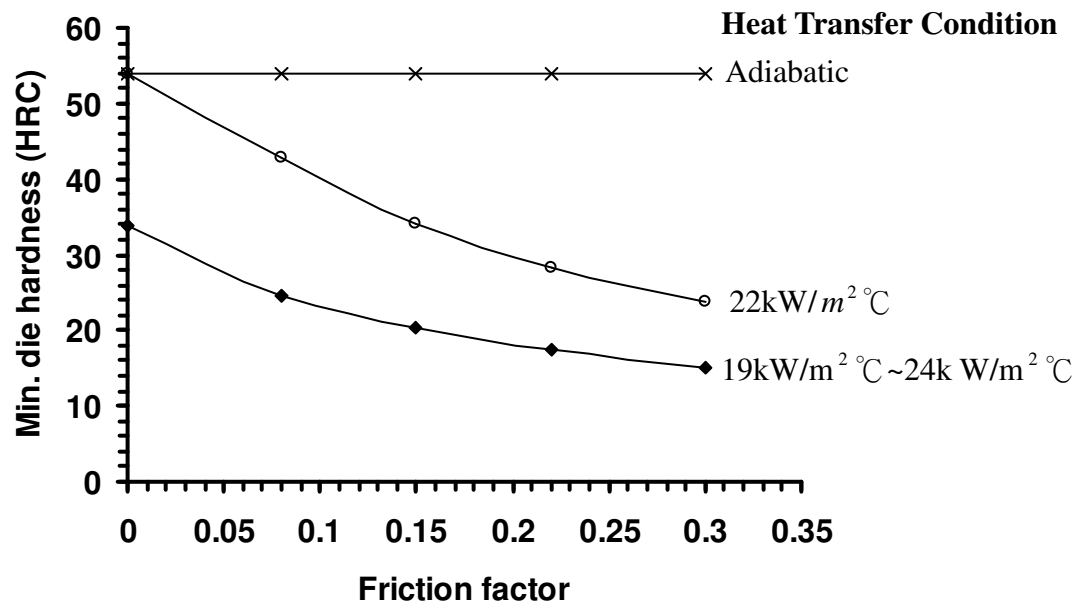
Figure 5.14 Relations between minimum die surface hardness and friction under three heat transfer conditions.
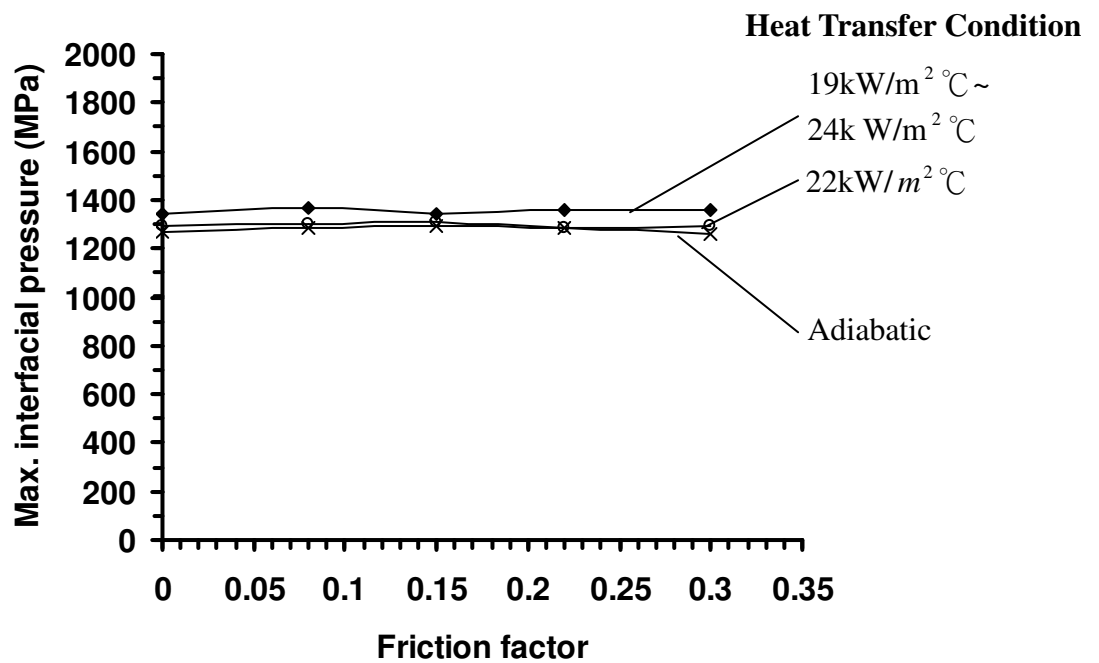
Figure 5.15 Relations between maximum interfacial pressure and friction for three heat transfer conditions.

5.4.1.4 Effect of forming speed

Forming speed is dictated largely by the design of the forming machine and is a forging variable which can be controlled under production forging conditions, and therefore, a knowledge of its influence on die wear will indicate whether improvements in die life are possible by control of the forming speed. The effect of speed on die wear is thus discussed in this section, when other process factors remain constant. Figure 5.16 shows the relation between wear index and average forming speed. Wear on both depth and width sections exhibit a "U" shape, in relation to speed. Three other process surface factors likely to affect wear have been investigated.

In Figure 5.17, die surface temperature increases as forming speed increases, probably due to friction and deformation heat. Higher temperature leads to softening of the die. It is shown in Figure 5.18 that die hardness reduces rapidly as forming speed increases above 79 mm/s. This is probably the reason why the wear amount increases above 79 mm/s in Figure 5.16. The increase in wear as speed below 23 mm/s could be due to the increasing interfacial pressure, as seen in Figure 5.19. This might be due to the work-piece material strengthening in the longer forming duration. With heat lost from the work-piece and less heat generated from plastic deformation, higher pressure would be needed to cause metal flow. Therefore, the lowest wear index occurs at forming speeds between 23 mm/s to 79 mm/s. Thus, the U shaped wear index/speed curve arises from two competing mechanisms (interfacial pressure and die hardness).
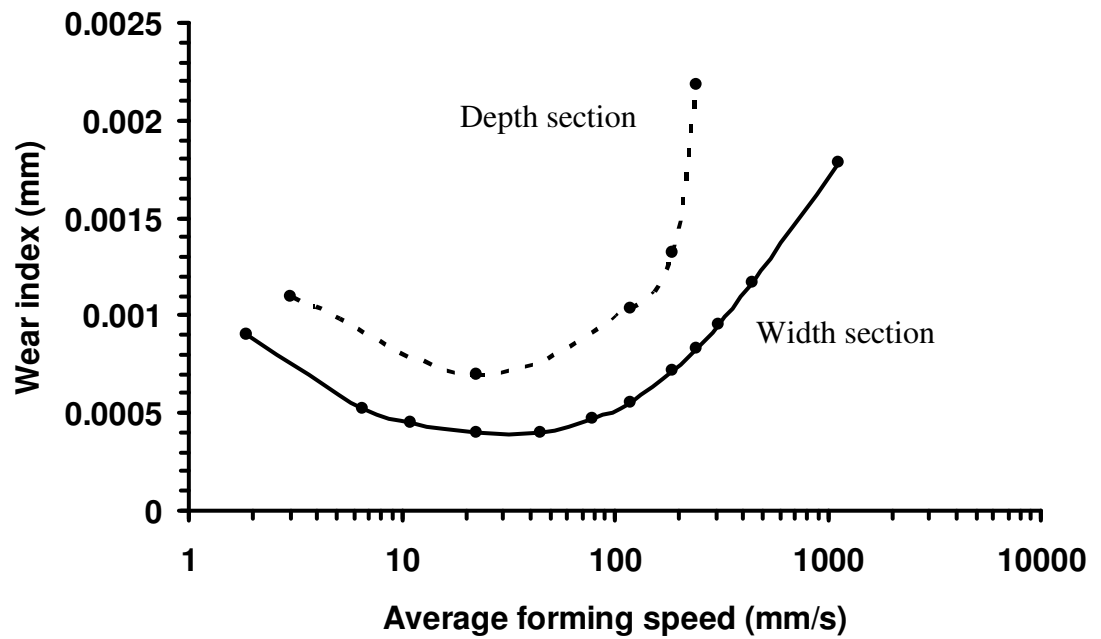
Figure 5.16 The U shape relation between wear and forming speed for depth and width sections.
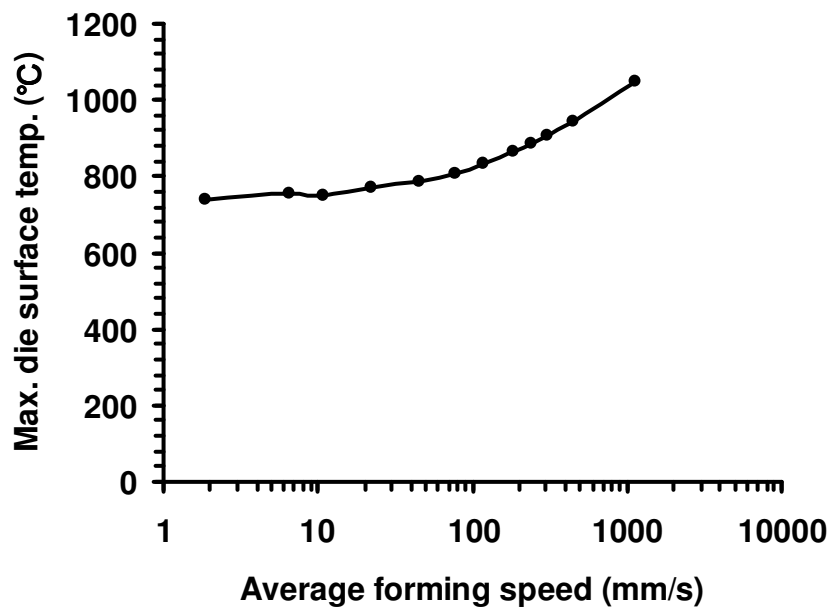
Figure 5.17 Relation of forming speed and die surface temperature for width section.
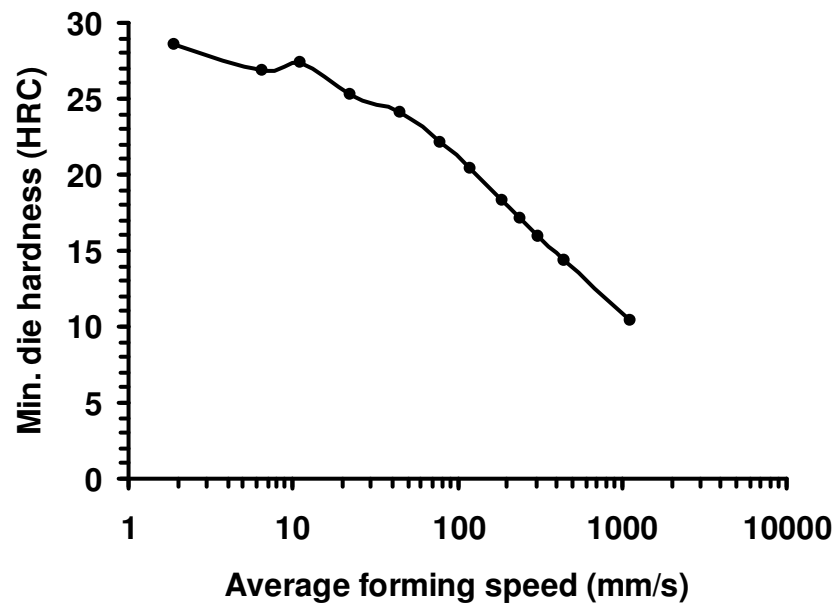
Figure 5.18 Relation of forming speed and die hardness for width section.
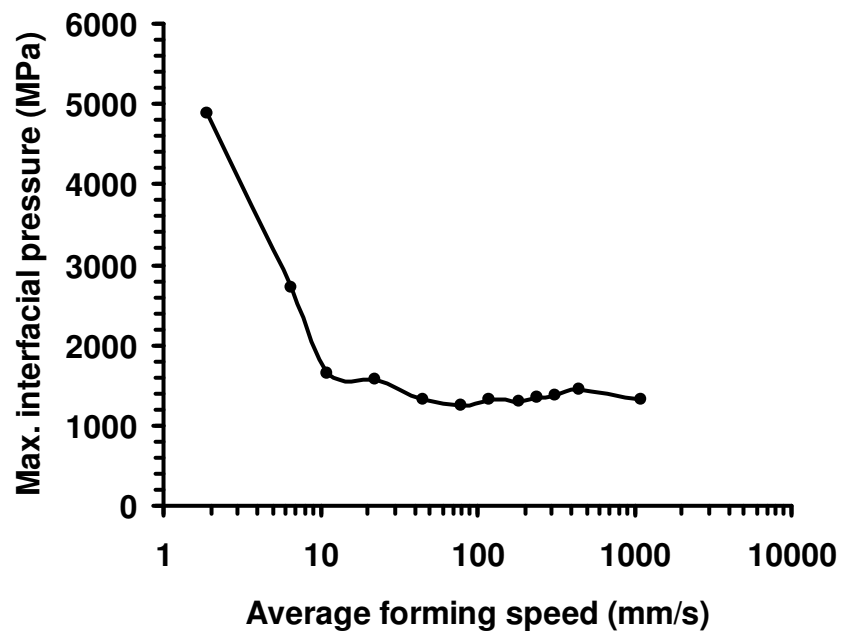
Figure 5.19 Relation of forming speed and interfacial pressure for width section.

5.4.2 Fatigue and deformation in die failure

Apart from abrasive wear, other factors which cause die failure also exist during hot forming, as stated in Chapter 4. In this section, plastic deformation and thermal fatigue frequently encountered in hot extrusion (also presented in the die under study) and which are also detrimental to the die life, will be discussed and the indications of the damage areas derived from the simulations are presented.

The hardness examinations were undertaken on the studied die. The original die hardness, before extrusion was HRC54. Figure 5.20 shows the significantly lower hardness in the encircled neck area. The lower hardness might be due to the change of surface property caused by thermal and mechanical fatigues, the profound cracks found in this area are the evidence. By plotting the 3D topographic image (Figure 5.21) for the area of 1x1 mm at this position (image has been leveled to remove the waviness). It can be seen that the height between the lowest valley to the highest peak (St) is as high as 111 μm. From the simulations, this area was indentified as a critical area for die wear, and the observations support the simulation results really well.
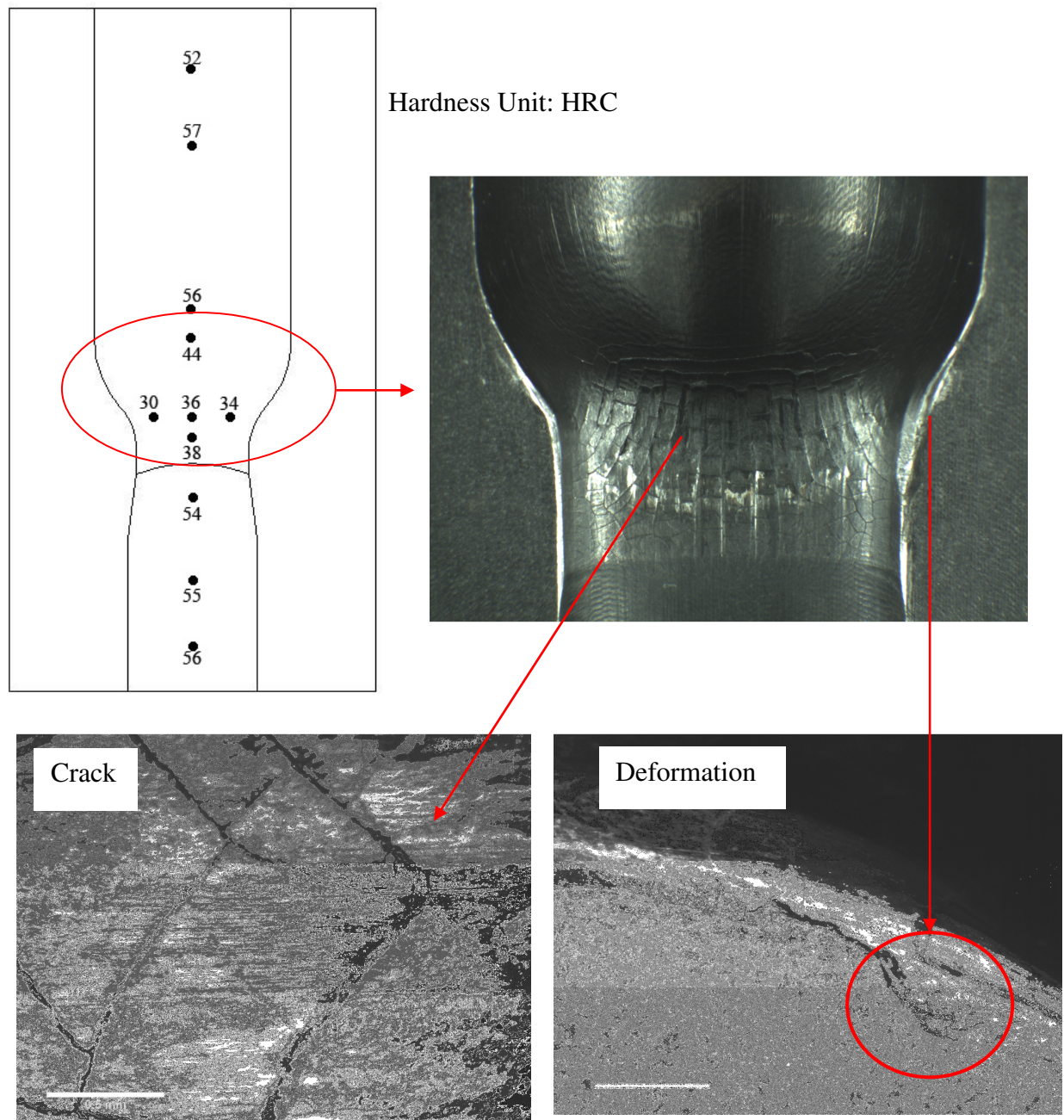
Figure 5.20 Top left hand side: Hardness profile of the bottom worn die. Top right hand side: The photograph shows the shoulder area, in which the cracks and deformation were observed (as shown in the close-up photographs at bottom left and bottom right).
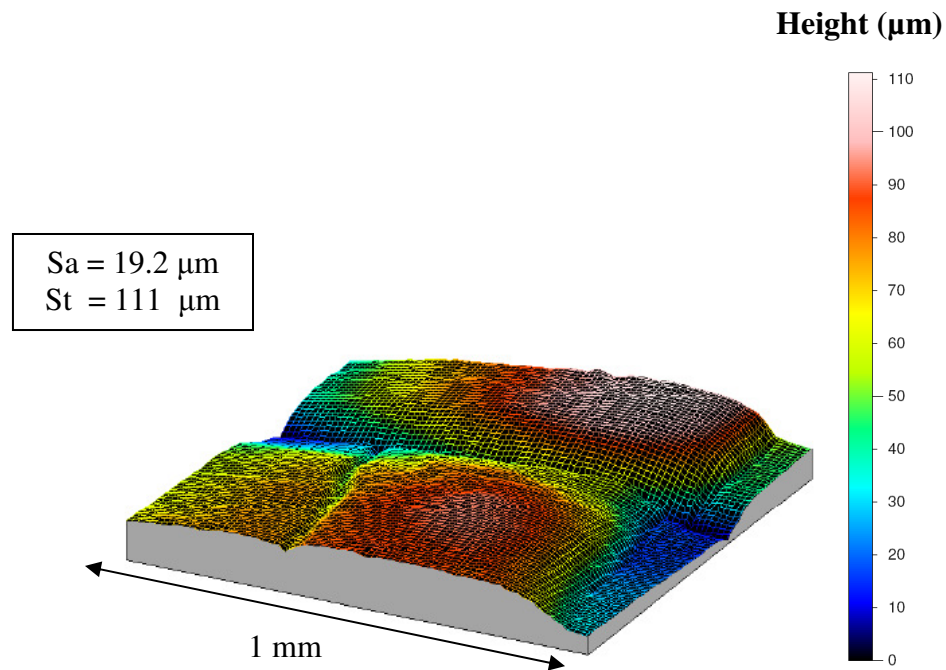
Figure 5.21 3D image showing the surface topography of the critical area.

One of the reasons for the cracks to generate is thermal fatigue, which is due to high temperature gradients within the die during extruding. From the simulation, the temperature curves shown in Figure 5.22 were derived, for five positions within the die. A temperature gradient (up to 600 ℃) can occur with a depth of 2.5 mm. Thermal fatigue will easily take place under this condition. Also, the cracks could be generated by stress gradient within the die from two sources: temperature gradient from the quench between each forging (as mentioned in section 5.4.1.3); or the phase change (accompanied with volume change) of the surface material at hot temperatures.
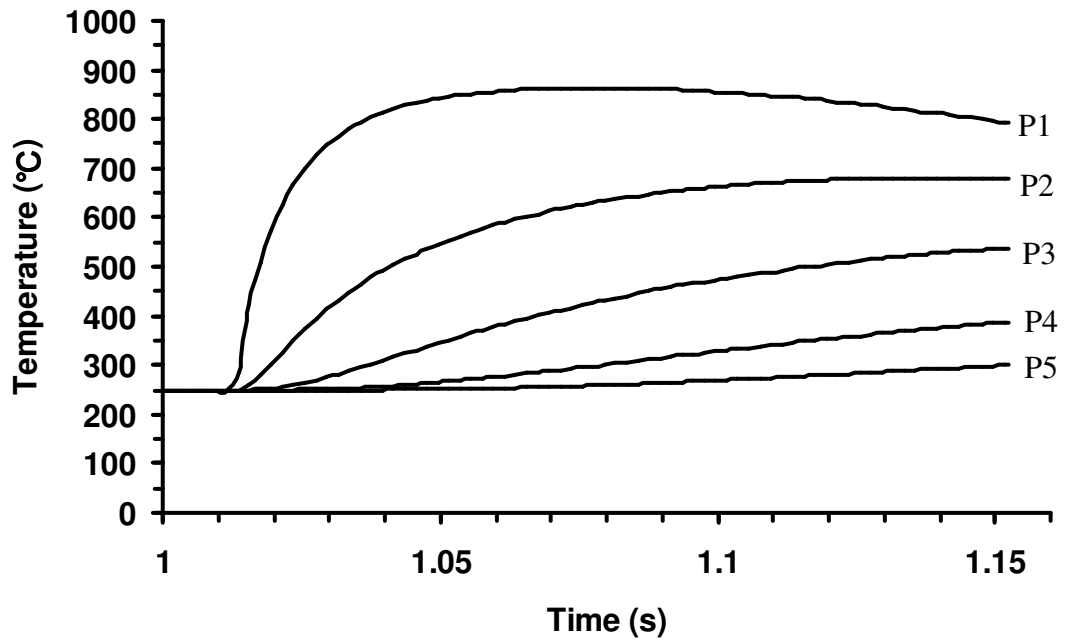
Temperature Measured Positions

P1 at die surface
P2 0.4 mm under the surface
P3 1.0 mm under the surface
P4 1.7 mm under the surface
P5 2.5 mm under the surface

Figure 5.22 Temperature curves of different positions on the die surface and sub-surface.

Figure 5.20 also shows the deformation at the shoulder area on the die as the material has been pushed out (circled on the bottom right-hand picture) and protrudes from the surface. From the simulation, a typical result shown in Figure 5.23 for the interfacial pressure distributions changing with time at the die shoulder is presented. The maximum interfacial pressure in the critical region a~b is approximately 1400 MPa during forming. Data from Shivpuri and Lee (1988) in Figure 5.24 shows the relation between the die hardness and the yield stress for H13. At a hardness of HRC30, which is close to the die hardness during extruding, the yield stress is 800 MPa. Therefore, there is a very high chance for the die to yield and deform. It is also observed that the pressure pattern varied during the forming, which might be due to the alteration of material flow of the work-piece. This variation of pressure history affects wear pattern during forming as well.
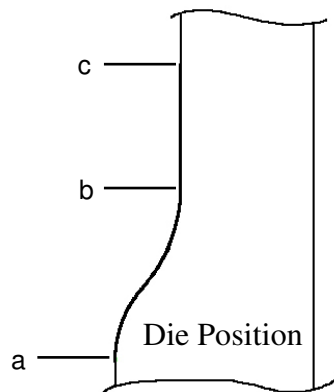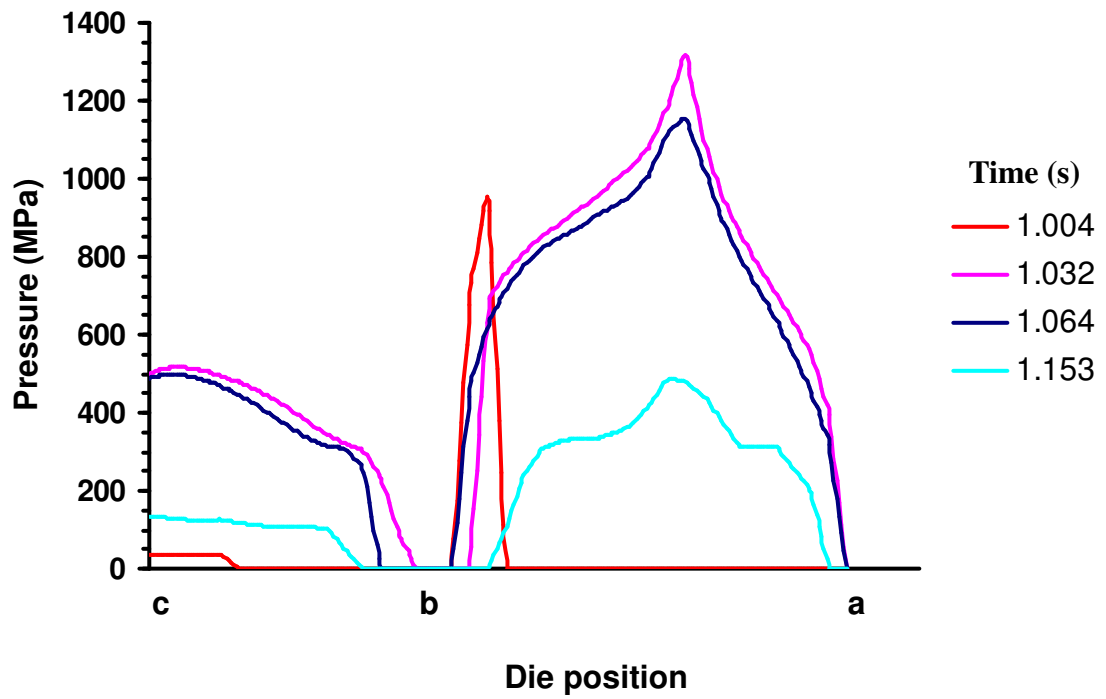
Figure 5.23 A typical simulation result shows the change of interfacial pressure distribution with time at different positions.
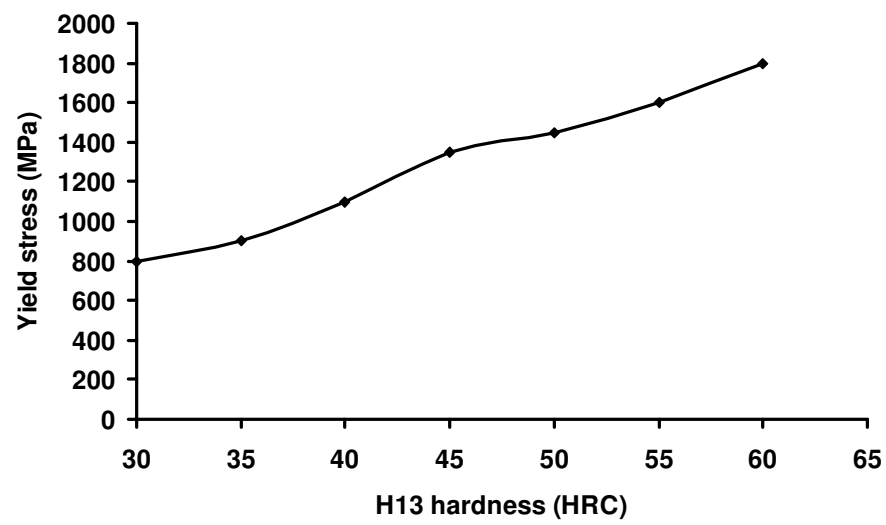
Figure 5.24 The relation of yield stress with variation of H13 hardness (adopted from Shivpuri and Lee, 1988).

CHAPTER 6
CONCLUSIONS AND SUGGESTIONS FOR FUTURE WORK

6.1 CONCLUSIONS

6.1.1 IN718 modelling

- Through the Gleeble experiments, IN718 has been characterised as an elastic-viscoplastic material. In the temperature range of 950℃~1100℃, the stress changes under different temperatures and strain rates. In the case of temperature of 1050℃, the difference for the peak stress is between 5%~52% under four strain rates. For the strain rate of 5/s, the difference for the peak stress is between 6%~18% under four temperatures. In addition, the softening of the material flow is found at the higher strain, especially at higher strain rates 5/s and 10/s for all the temperatures due to the higher energy to initiate the recrystallisation mechanism.

- From the predictions using the mathematical IN718 material model, the critical strain for recrystallisation to occur varies for different temperatures and strain rates. The minimum critical strain is required to initiate recrystallisation when forming at strain rates of 4/s~10/s for all three temperatures (1000℃, 1050℃ and 1100℃). Also, the critical strains for three temperatures are 0.15 (1000℃), 0.1 (1050℃) and 0.08 (1100℃), which decrease according to the increase of the temperature.

- Predictions obtained using the IN718 material model show the effect of grain size on the flow stress is small. In the short duration of a forging operation, changes of flow stress, due to the grain movement, may be ignored for short forming times (say, less than three seconds).

- The predicted distributions of the average grain size were compared with the metallurgical examinations of the microstructure of the extrudate. Both approaches revealed that coarser grains were formed in the head than in the neck of the extrudate.

- Through the theoretical analyses, it can be concluded that without considering recovery, recrystallisation and grain size evolution, the mechanics of elastic-viscoplastic flow behaviour of IN718 and, hence, interfacial pressure during extrusion, cannot be accurately understood.

6.1.2 Heat transfer/ Friction investigations

- In published research, values of heat transfer coefficient and friction factors vary substantially, perhaps due to different experimental methods, material properties, lubricant and forming conditions. Therefore it is essential to derive the values/factors according to a specific forming condition.

- From the heat transfer compression tests, it was found that lubricant and coating were two important factors to affect heat transfer between die and work-piece, before forming. The effective heat transfer coefficient is influenced by lubricant quantity, particularly in the presence of a thin glass coating but, lubricant quantity has little effect on effective heat transfer coefficient, for a glass thickness above 60 μm. The calculated effective heat transfer coefficients before forging varied from 143 W/m^2 ℃ to 200 W/m^2 ℃ for different coating and lubricant thicknesses.

- The reduction of work-piece became the most influential factor affecting heat transfer during forging, as the heat transfer coefficient is increased by about two orders of magnitude by the high forging pressure, comparing those derived before forming. The derived relation of change of effective heat transfer coefficient according to the pressure is (19170 W/m^2 ℃-179 MPa, 20500 W/m^2 ℃-206 MPa and 24000 W/m^2 ℃ -263 MPa, for three reductions, 0.5 mm, 1 mm and 1.5 mm).

- The values of effective heat transfer coefficient after upsetting were approximately the same as those before forging but it was difficult to model the effect of lubricant and coating after deformation because both are dramatically changed during deformation.

- The determined effective heat transfer coefficients could be used for forging simulations

with different die/work-piece temperatures within the practical forging window, with acceptable accuracy, in which the errors were within 16% for before forming stage and within 6% for during forming stage.

- Ring tests were performed to derive friction factors for graphite lubrication amounts of 2.82×10^{-5} **g/mm**^{2} and 7.05×10^{-5} **g/mm**^{2} and glass coatings of 40 µm and 60 µm thick. Measure values of friction factor ranging from 0.08 to 0.20.

- Under the same process conditions, as the amount of lubricant increases, friction decreases; however glass coating thickness has little effect on friction under the experimental forming conditions.

- The ring test results show that die temperature affected friction conditions and ring geometry as the rings deformed at a lower die temperature (100℃) with higher value of friction factor, probably due to changing viscosity of the glaze and also, possibly, to the heat transfer at and close to the interface. However, for a thicker combination of coating and lubricant, a difference in die temperature between 100℃~200℃ had no significant effect on friction. This might be because the coating/lubricant combination is thick enough for no great difference in heat transfer to arise.

- As deformation increases, friction values tend to converge to the same value. This might be because lubricant thinning caused by the increasing pressure and by surface expansion, change conditions from thick film to boundary contact with a similar characteristic, regardless of the different starting conditions.

- The derived heat transfer/friction conditions were used to predict the load for a ring test from FE simulation. A good correlation was obtained between the simulation and the practical experiment, which indicates that the determined IN718 material property and interfacial heat transfer/ frictional conditions during hot forming were accurate.

- Both isothermal and adiabatic rings deformed as though they were a solid body without

barrelling for zero friction but the barrelling appear for heat transfer rings, and, as friction increases, barrelling starts to take place for all three conditions, therefore it is apparent that both interfacial heat transfer and interfacial friction contribute to barrelling.

- For the simulations of ring tests, the small ring with greater temperature gradient and lower temperature within the ring has the same effect as friction in causing barrelling.

6.1.3 Calibration curves for the ring tests

- The difference in results using two methods, (measuring average ring bore diameter and mid-height ring bore diameter), to generate the calibration curves, using FE simulation is small enough to be ignored and the simpler approach of measuring the mid-height (smallest) inner diameter provides sufficiently accurate data and was adopted for the work of developing calibration curves.

- The results show that different material constitutive relations do produce different calibration curves at high friction but the effect at low friction could be ignored.

- The calibration curves were affected greatly by ring size, heat transfer conditions, and forming speed and cannot be used generally, i.e. a set of calibration curves should be generated for a specific forming condition.

6.1.4 Die wear modelling and examinations

- The results show that as the angle increases, wear increases and different wear profiles are obtained. In the simulations of width section for the die angle of 35°, the difference for maximum amount of wear is 13% higher than that for the angle of 15°. In the case of depth section, the difference is 91 % between angle of 25° and 45°.

- Simulated wear profiles were different for each angle value of the shoulder of the extrusion die. The wear profiles for depth sections were similar in disposition, but different in magnitude, to those in the width sections. Wear of depth sections was

approximately 110% higher than that of the width sections, on average. In addition, the lengths of significant wear, for depth sections were greater than those for the width sections and originated in the cylindrical bore, before bore/cone transition. It might be due to the much bigger normal pressure on the orifice for the depth section before the metal is turned inwards.

- The normalised maximum forming load was then defined as F/F_w, where F is the maximum forming force required for different shoulder angles and F_w is the maximum forming force for shoulder angle equals 15° of width section. The simulated normalised forming force for the depth section is double than that for the width section. The difference of forming load for different shoulder angles is within 18% for width sections and within 4% for depth sections; however, different wear profiles will be produced by different shoulder angles.

- Zones of 'no-wear' were found from simulations. Although no physical explanation for them can be given at this stage the results show their existence to be supported by roughness measurements and by SEM observations.

- SEM examinations show two dominant topographies for the extrusion die: trenches, due to abrasive wear, are distributed all along the extruding distance at the die surface; crack networks, due to significant thermal and mechanical fatigues.

- According to the wear model, reduction in die hardness is the dominant factor affecting wear for different friction values in the simulations. Die hardness does not change for ideal adiabatic situations and, therefore, least wear would arise. In the adiabatic condition, sliding distance, controlled by the value of friction, decides the amount of wear.

- In the simulations, the sliding distance was derived by tracking a node on the mesh of the work-piece to represent the nominal sliding distance of the work-piece material at the interface. The sliding distance decreased as friction increased but the difference is small. For three heat transfer conditions, the difference is about 1 mm for a forging distance of 30 mm. Sliding distance decreases as the difference between the lower surface and

higher sub-surface temperature increases, because sub-surface and interior metal flow becomes relatively greater. Therefore, sliding was most for no heat transfer (adiabatic condition) and least for the pressure dependent heat transfer condition, which resulted in harder surface and sub-surface work-piece metal.

- Under the heat transfer conditions, the interfacial temperature increased as friction increased in the simulations, due to frictional heating and heat generated from the deformation. Interfacial temperatures exceed 600℃ under all friction values. Since H13 tempers slightly below 600℃, the surface of the die will soften. Also, it is found that the die significantly softened, as the die surface temperature reached to 700℃ and 900℃ in simulations for heat transfer constant and pressure depending conditions respectively, at friction factor = 0.3.

- Wear on both depth and width sections exhibits a minimum in relation to speeds derived from the simulations, and the lowest wear occurs at average forming speeds between 23 mm/s to 79 mm/s due to the effects of two competing mechanisms (interfacial pressure and die hardness).

- From the hardness tests, the significantly lower hardness is presented in the transition area. The lower hardness might be due to the change of surface property caused by thermal and mechanical fatigues, the profound cracks found in this area are the evidence. By plotting the 3D topographic image for the area of 1x1 mm at this position, it is found that the height between the lowest valley to the highest peak (St) is 111 μm.

- A typical simulation result for the interfacial pressure distributions changing with time at the die shoulder shows the maximum interfacial pressure in this area is approximately 1400 MPa during forming, which is highly to deform the die as the yield stress of the die is 800 MPa for HRC30 during forming.

- Trenches, cracks and deformations were found on the studied worn die by observations. From the simulations, the indications of the reasons for causing these damages on the die were derived and possible happening positions were predicted particularly at bore/cone

transition with good correlations of the observations.

- By examining the transition area on the worn die using EDX, both high amounts of oxygen and carbon are found. The existence of the oxygen might be caused by air within the EDX chamber since the complete vacuum is difficult to achieve in the machine. However, it might be also due to the oxidation of the die, whereas, the high portion of carbon is considered to result from the diffusion of the graphite lubricant at high temperatures and remaining lubricant on the surface/sub-surface.

6.2 SUGGESTIONS FOR FUTURE WORK

- Although 2D simulations posses the advantages of shorter computational time and also predicted the reliable results for die wear, the 3D process modelling is recommended for the future to derive a comprehensive temperature distribution of the die, velocity field and stress states of the forming processes.

- Heat transfer/ friction conditions could be described as a function of contact condition, incorporating the effect of changes in lubricant and coating, such as thinning, during forming, which is affected by temperature, pressure, sliding distance and time, for obtaining more realistic variation of the interfacial conditions in forming.

- The wear model should be modified to include a more realistic description of lubrication, as the assumption of thick-film lubrication is not true.

- The detections of the wear particles from the SEM examinations have not been investigated yet. Generation and circulation of wear particles (three-body abrasion) in the system jeopardize the efficiency of the forming processes and also affect die wear. The presence of particles could be assumed as a function of time to be integrated to the abrasive wear model to find its effect.

- Holm-Archard assumed that adhesion occurs at the points of asperity contact, or equivalent, whereas adhesion is an unpredictable phenomenon as well as abrasion. They

occur between solids often in an environment consisting of contamination and wear particles which is rarely examined, and has not been demonstrated physically as an individual event. Therefore, in the wear models, the possibility of the values of k and k_{abr} to be represented as a function of temperature, surface roughness or mechanical properties of the surface, remains to be further investigated.

- The wear pattern will be changed according to the increased number of forgings significantly; therefore, several extrusions need to be performed to examine their history. Worn dies under different forming conditions are also necessary to be studied. In addition, temperature variation during the forging cycles is needed to be examined to have a further understanding of the temperature gradient within the die.

- The changes of the material property/treatment of the die surface might affect the die wear and investigations of the effect on wear, of lubrication and oxidation/surface scale on the die surface might be necessary to be carried out. The EDX examinations reveal a high amount of carbon on the die surface, which is possibly due to the diffusion of the graphite lubricant. Different temperatures and forming time will lead to different diffusional conditions of the lubricant; these need looking into. The future work might be useful to model the changes of material property of surface/sub-surface for the die to reflect its effect on the die wear.

- Dies modelled as elastic, to examine the stress distribution could reveal its contribution to damage and wear, but the staggering increase of the computational time might be a problem.

REFERENCES

Anderson *et al.* Friction, Lubrication, and Wear Technology (1992) ASM Handbook, Volume 18.

Andreis, G., Fuchs, K.D., Schruff, I. (1999) The wear behaviour of hot-work tool steels used in forging processes, in: Proceedings of the Fifth International Conference on Tooling, Loeben, pp.593–600.

Archard, J. F. (1953) Contact and rubbing of flat surfaces, Journal of applied physics,Vol.24, No.8, 1953, pp.981-988.

Arnell, R. D., Davies, P. B., Halling, J., Whomes, T. L. (1991) Tribology: Principles and design applications, New York, Springer-Verlag.

Avitzur, B. (1964) Forging in hollow discs, Israel Journal of Tech., 2, pp.102-127.

Avitzur, B. (1968) Metal Forming: Processes and analysis, New York, London, McGrawhill.

Azadian, S., Wei, L.Y., Warren, R. (2004) Delta phase precipitation in Inconel 718, Materials Characterization, 53, pp.7-16.

Bariani, P. F., Bruschi, S., Negro, T. D. (2004) Prediction of nickel-base superalloys' rheological behaviour under hot forging conditions using artificial neural networks, Journal of Materials Processing Technology, 152, pp.395–400.

Barrau, O., Boher, C., Gras, R., Rezai-Aria, F. (2003) Analysis of the friction and wear behaviour of hot work tool steel for forging, Wear 255, pp.1444–1454.

Bay, N., Hansen, B. G. (1985) Simulation of friction and lubrication in cold forging, 7th International Congress, Cold Forging, Birmingham, England, pp.55-62.

Beck, G. (1958) Thermal conditions in tool steels in hot upsetting and forging between dies, Stahl und Eisen, Vol. 78, pp.1556-1563.

Behrens, B. A., Schaefer, F. (2005) Prediction of wear in hot forging tools by means of finite-element-analysis, Journal of Materials Processing Technology 167, pp.309–315.

Bowden, F.P. and Tabor, D., (1950) <u>The friction and lubrications of solids</u>, Clarendon Press.

Burte, P. R., Im, Y. T., Altan, T., Semiatin, S. L. (1990) Measurement and Analysis of Heat Transfer and Friction During Hot Forging, Transactions of the ASME, Vol. 112, pp.332-339.

Burwell, J. T. and Strang, C. D. (1952) On the empirical law of adhesive wear, Journal of applied physics, Vol.23,no.1, pp.18-28.

Burwell, J. T., Jr, (1957) Survey of possible wear mechanisms, Wear, Vol.1, pp.119-141.

Buttery, T. C., Archard, J. F. (1971) Grinding and abrasive wear, Proceedings of the Institution of Mechanical Engineers 185 43, pp.537–551.

Cao, J., Lin, J. (2008) A study on formulation of objective functions for determining material models International Journal of Mechanical Sciences, 50, pp.193-204.

Cervenka, M. Online document, Rolls-Royce, 2000, www.materials.ac.uk/resources/FE/trent.ppt. Accessed 2007.

Chang, C. C., Bramley, A. N. (2002) Determination of the heat transfer coefficient at the Workpiece-die interface for the forging process, Proc Instn Mech Engrs, J. Engineering Manufacture, Vol. 216 Part B, pp.1179-1186.

Chen, Dyi-Cheng, Syu, Sheng-Kai, Wu, Cing-Hong, Lin, Sin-Kai (2007) Investigation into cold extrusion of aluminum billets using three-dimensional finite element method, Journal of Materials Processing Technology ,Volumes 192-193, pp.188-193.

Cheong, B. H., Lin, J. and Ball, A. A. (2000) Modelling of the hardening characteristics for superplastic materials, Journal of Strain Analysis, 35, pp.149-157.

Czichos, H. (1974) Failure criteria in thin film lubrication: the concept of a failure surface, Tribology 8, pp.14-20.

Dean, T. A. and Sturgess, C. E. N. (1978) Warm-forming practice, Journal of Mechanical Working Technology, 2, pp.255-265.

Delagnes, D., Rezai-Aria, F., Levaillant, C., Grellier, A. (1999) Influence of temperature and initial hardness on fatigue behaviour and life of a 5% Cr hot work tool steel, in: Proceedings of the Fifth International Conference on Tooling, Loeben, pp.195-204.

DePierre, V., Gurney F. (1974) A method for the determination of constant and varying friction factors during ring compression test, J. Lubric. Technol. ASME, 96, pp.482-488.

Dieter, G. E. and Bacon, D. (1989) Mechanical metallurgy, McGraw-Hill Education.

Djaic, R. A. P., Jonas, J. J. (1972) Static recrystallization of austenite between intervals of hot working, Journal of the Iron and Steel Institute, 210, pp.256-261.

Doege, E., Groche, P. and Bobke, Th. (1990) Application of Adhesion Theory to Friction and Wear Processes in Hot Die Forging, Advance Technology of Plasticity, Vol.1, pp.27-32.

Doege, E., Melching, R., Kowallick, G. (1978) Investigations into the behaviour of lubricants and the wear resistance of die materials in hot and warm forging, Journal of Mechanical Working Technology, 2, pp.129-143.

Doege, E., Nägele, H., Schliephake, U. (1994) Aspect of wear prediction in precision forging, Proc. Inst. Mech. Eng. B: J. Eng. Manuf., 208, pp.111-119.

Estrin, Y. (1998) Dislocation theory based constitutive modelling: foundations and applications, Journal of Materials Processing Technology, 80, pp.33-39.

Eyre, T.S. (1978) The mechanisms of wear, Tribology International.

Feng, J. P., Luo, Z. J. (2000) A method for the optimal control of forging process variables using the finite element method and control theory, Journal of Materials Processing Technology, 108, pp.40-44.

Fereshteh-Saniee, F., Pillinger, I., P. Hartley (2004) Friction modelling for the physical simulation of the bulk metal forming processes, Journal of Materials Processing Technology, 153-154, pp.151-156.

Frederiksen, N., Wanheim, T. (1985) Development of friction tests for lubrication in model-material experiments, Journal of Mechanical Working Technology, 12, pp.261-268.

Ghobrial, M. I., Lee, J. Y., Altan, T., Bay, N., Hansen, B. G. (1993) Factors affecting the double cup extrusion test for evaluation of friction in cold and warm forging, Annals of CIRP, 42, pp.347-351.

Grass, H., Krempaszky, C., Reip, T., Werner, E. (2003) 3-D Simulation of hot forming and microstructure evolution, Computational Materials Science, 28, pp.469-477.

Hawkyard, J. B., Johnson, W. (1967) An analysis of the changes in geometry of a short hollow cylinder during axial compression, Int. J. Mech. Sci., 9, pp.163-182.

Hill, R. (1950) On the inhomogeneous deformation of a plastic lamina in a compression test, Philosophical Magazine, 41, pp.733-744.

Hironaka, Tomohisa, Ito, Shigekazu, Yoshida, Hiroaki, Isogawa, Sachihiro (2009) Development of new tribo-meter for forging, Proceeding of the 5th JSTP international seminar on precision forging, Japan, pp193-196.

Holm, R. (1946) Electric contacts, Almqvist and Wiksells, Stockholm.

Honeycombe, R. W. K., Pethen, R. W. (1972) Dynamic recrystallization , Journal of the Less Common Metals, 28, pp.201-212.

Hu, Z. M., Brooks, J. W., Dean, T. A. (1998) The interfacial heat transfer coefficient in hot die forging of titanium alloy, Proc Instn Mech Engrs, Vol. 212 Part C, pp.485-496.

Huang, Y. (2001) Mechanical property, microstructural development and constitutive analysis associated with the high temperature deformation of Inconel 718, Thesis (Ph.D), University of Birmingham, UK.

Hudson, R. (2000) Coating for the protection of structural steelwork, NPL document.

Humphreys, F. J. (1999) A new analysis of recovery, recrystallisation, and grain growth, Materials Science and Technology, 15, pp.37-44.

Humphreys, F.J. and Hatherly, M. (1994) <u>Recrystallization and related annealing phenomena</u>, Elsevier Science.

Im, Y. T. (1989) Investigation of heat transfer and simulation of metal flow in hot upsetting, J. of Engineering for Industry, Vol. 111, pp.337-344.

INCONEL alloy 718 material property report, Special metals, 2004.

Isogawa, S., Kimura, A., Tozawa, Y. (1992) Proposal of an evaluating method on lubrication, Annals of the CIRP, 41, pp.263-266.

Jain, V. (1990) Dermination of heat transfer coefficient for forging applications, J. Mater. Shaping Technol, 8, pp.193-202.

Jeswiet, J., Zou, S. (1992) Temperature, heat flux and conductivity in bar rolling, Annals of the CIRP, Vol. 41 (1), pp.299-302.

Jiang, C. Y (1996) The analysis for the die failure (in Chinese), Die Industry, No.12, pp.8-11.

Jo, C. Y., Kim, H. M. (2003) Effect of recrystallisation on microstructural evolution and mechanical properties of single crystal nickel based superalloy CMSX-2 Part 2 - Creep behaviour of surface recrystallised single crystal, Materials Science and Technology, Vol.19 (12), pp.1671-1676.

Kalpakjian, Serope (1997) <u>Manufacturing processes for engineering materials</u>, 3rd edition, Addison-Wesley Publishing Company.

Kang, J.H., Park, I.W., Jae, J.S., Kang, S.S. (1999) A study on a die wear model considering thermal softening: (2) Application of the suggested wear model, Journal of Materials Processing Technology 94, pp.183-188.

Kang, J.H., Park, I.W., Jae, J.S., Kang, S.S. (1999) A study on a die wear model considering thermal softening: (1) Construction of the wear model, Journal of Materials Processing Technology 96, pp.53-58.

Kellow, M. A., Bramley, A. N., Bannister, F. K. (1969) The measurement of temperatures in forging dies, International Journal of Machine Tool Design and Research, Vol. 9, Issue 3, pp.239-260.

Kennedy, D. M., Hashmi, M. S. J. (1998) Methods of wear testing for advanced surface coatings and bulk materials, Journal Of Materials Processing Technology, 77, pp.246-253.

Kim, Heon-Young, Kim, Joong-Jae, Kim, Naksoo, (1994) Physical and numerical modeling of hot closed-die forging to reduce forging load and die wear, J. Mater. Process. Technol, 42, pp.401-420.

Kluge, A, Langguth, K, Öchsner, R, Kobs, K, Ryssel, H (1989) Examination of wear, hardness and friction of nitrogen-, boron-, carbon-, silver-, lead- and tin-implanted steels with different chromium contents, Materials Science and Engineering: A, Volume 115, pp.261-265.

Kuhlmann-Wilsdorf, D. (2002) The nature of interfacial processes in friction and wear, Science & Technology of Interfaces, TMS, pp.207-218.

Kunogi, M. (1954) On the plastic deformation of the hollow cylinder under axial load, J. Sci. Res. Inst. 30, pp.63-92.

Lancaster, P. R. and Rowe, G. W. (1958) A comparison of boundary lubricants under light and heavy loads, Wear, 2, pp.428-437.

Lange, K. (1976) Handbook of Metal Forming, New York, McGraw-Hill.

Lange, K., Cser, L., Geiger, J. A., Kals, J. A. G (1992) Tool Life and Tool Quality in Bulk Metal Forming,   Annals of the CIRP, Vol.41, No.2, pp.667-675.

Lee, C. H., Altan, T. (1972) Influence of flow stress and friction upon metal flow in upset forging of rings and cylinders, J. Engineering for Industry ASME, 94, pp.775-782.

Lee, Geun-An, Im, Yong-Taek (1999) Finite-element investigation of the wear and elastic deformation of dies in metal forming, Journal of Materials Processing Technology, 89-90, pp.123-127.

Lee, R. S., Jou, J. L. (2003) Application of numerical simulation for wear analysis of warm forging die, Journal of Materials Processing Technology, 140, pp.43-48.

Li, B., Lin, J., Yao, X. (2002) A novel evolutionary algorithm for determining unified creep damage constitutive equations, International Journal of Mechanical Sciences, 44, pp.987-1002.

Li, L. X., Peng, D. S., Liu, J. A., Liu, Z. Q., Jiang, Y. (2000) An experimental study of the lubrication behavior of glass lubricant by means of the ring compression test, Journal of Materials Processing Technology, 102, pp.138-142.

Li, Q., Xu, Y., Lai, Z., Shen, L., Bai, Y. (1999) A model of dynamic recrystallization in alloys during high strain plastic deformation, Journal of Materials Science & Technology, 15, pp.435-438.

Li, Y. H., Sellars, C. M. (1998) Comparative investigations of interfacial heat transfer behaviour during hot forging and rolling of steel with oxide scale formation, Journal of Materials Processing Technology, 80–81, pp.282–286.

Lin, J., Yang, J. (1999) GA-based multiple objective optimization for determining viscoplastic constitutive equations for superplastic alloys International Journal of Plasticity, 15, pp.1181-1196.

Lin, J., Liu, Y., Farrugia, D. C. J., Zhou, M. (2005) Development of dislocation-based unified material model for simulation microstructure evolution in multipass hot rolling, Philosophical Magazine, 85, pp.1967-1987.

Lin, Y. C., Chen, Ming-Song, Zhong, Jue (2008) Study of static recrystallization kinetics in a low alloy steel, Computational Materials Science, 44, pp.316-321.

Lissel, L., Online document, Royal Institute of Technology, Sweden, 2006,
www.diva-portal.org/diva/getDocument?urn_nbn_se_kth_diva-4118-2__fulltext.pdf.
Accessed 2007.

Liu, J. Y. (1972) An analysis of deformation characteristics and interfacial friction conditions in simple upsetting of rings, J. Engineering for Industry, ASME, 94, pp.1149-1156.

Liu, W. C., Xiao, F. R., Yao, M., Chen, Z. L., Jiang, Z. Q., Wang, S. G. (1997) Relationship between the lattice constant of γ phase and the content of δ phase, γ"and γ' phases in inconel 718, Scripta Materialia, 37, pp.59-64.

Liu, Y., Lin, J., Farrugia, D. C. J. and Dean, T. A. (2005) A numerical and experimental study of cavitation in a hot tensile axisymmetric testpiece, Journal of Strain Analysis, 40, pp.571-586.

Luce, R., Wolske, M., Kopp, R., Roters, F. and Gottstein, G. (2001) Application of a dislocation model for FE-process simulation, Computational Materials Science, 21, pp.1-8.

Ludema, K. C. (1996) Friction, wear,lubrication,a textbook in tribology, CRC-Press.

Luo, Z. J., Tang, H., Zeng, F. C., Guo, N. C., Xu, H. Y., Zhang, H. B., Qi, L. F. (1991) An effective technique for producing high performance IN718 forgings using hammers, Journal of Materials Processing Technology, 28, pp.383-390.

Male, A. T. (1962) The friction of metals undergoing plastic deformation at elevated temperatures, Thesis (PhD), University of Birmingham.

Male, A. T. (1964) The effect of temperature on the frictional behaviour of various metals during mechanical working, J. Institute of Metals, 93, pp.489-494.

Male, A. T., Cockcroft, M. G. (1964) A Method for the determination of the coefficient of friction of metals under condition of bulk plastic deformation, J. Institute of metals, 93, pp.38-46.

Male, A. T., DePierre, V. (1970) The validity of mathematical solutions for determining friction from the ring compression test, J. Lubric. Technol. ASME, 92, pp.389-397.

Male, A. T., Gurney, F., Depierre, V. (1972) Mathematical calibration of the ring test with bulge formation, Tech. Rep. AFML-TR-72-37.

Malinowski, Z., Lenard, J. G., Davies, M. E. (1994) A study of the heat-transfer coefficient as a function of temperature and pressure, Journal of Materials Processing Technology, Vol. 41, Issue 2, pp.125-142.

Matsumoto, K., Izawa, M., Nakanishi, T., Tsubouchi, K. (2009) Tribological properties of water glass lubricant for hot metalworking, Tribology Transactions, pp.553-559.

Medeiros, S. C., Prasad, Y. V. R. K., Frazier, W. G., Srinivasan, R. (2000) Microstructural modeling of metadynamic recrystallization in hot working of IN 718 superalloy, Materials Science and Engineering , A 293, pp.198-207.

Na, Y. S., Yeom, J. T., Park, N. K., Lee, J. Y. (2003) Simulation of microstructures for Alloy 718 blade forging using 3D FEM simulator, Journal of Materials Processing Technology, 141, pp.337-342.

Painter, B., Shivpuri, R., Altan, T. (1996) Prediction of die wear during hot-extrusion of engine valves ,Journal of Materials Processing Technology 59, pp.132-143.

Park, N. K., Kim, I. S., Na, Y. S., Yeom, J. T. (2001) Hot forging of a nickel-base superalloy, Journal of Materials Processing Technology, 111, pp.98-102.

Paxton & Vierling Steel manual.

Rao, K. P., Sivaram, K. (1993) A review of ring compression testing and applicability of calibration curves, J. Mater. Process Technol., 37, pp.295-318.

Robinowicz, E. (1995) Friction and wear of materials, Wiley-Interscience.

Roebuck, B., Lord, J. D., Brooks., M, Loveday, M. S. Sellars, C. M., Evans, R. W. (2002) Measurement good practice guide-Measuring flow stress in hot axisymmetric compression tests, National Physical Laboratory.

Rosochowska, M., Balendra, R., Chodnikiewicz, K. (2003) Measurements of thermal contact conductance, Journal of Materials Processing Technology, 135, pp.204–210.

Sakai, T., Jonas, J. J. (1984) Dynamic recrystallization: Mechanical and microstructural considerations, Acta Metallurgica, 32, pp.189-209.

Sandstrom, R., Lagneborg, R. (1975) A model for static recrystallization after hot deformation, Acta Metallurgica, 23, pp.481-488.

Sandstrom, R., Lagneborg, R. (1975) Interpretation of thermodynamic data of Fe-Ni-C and Fe-Ni-N alloys, Scripta Metallurgica, 23, pp.387-390.

Schey, J. A. (1983) <u>Tribology in Metalworking</u>, American society for metals.

Schey, J. A., Wallace, P. W. (1968) Press speed and lubricants affect forging quality, The Tool and Manufacturing Engineering, pp.36-39.

Schiemann, L. F., Schwind, J. J. (1984) Fundamentals of Automotive Gear Lubrication, Fuels and Lubricants Technology: An Overview, SP.603, Society of Automotive Engineers, pp.107-115.

Seidel, F., Stock, H. R., Mayr, P. (1996) Development of ion-implanted hard coatings for industrial applications in low lubricated cold forging processes Surface and Coatings Technology 84, pp.506-511.

Semiatin, S. L., Collings, E. W., Wood, V. E., Altan, T. (1987) Determination of the interface heat transfer coefficient for non-isothermal bulk-forming processes, J. of Engineering for Industry, Vol. 109, pp.49-57.

Shaw, M. C. Ber, A., Mamin, P. A. (1960) Friction characteristics of sliding surfaces undergoing sub-surface plastic flow, Trans. ASMS, Journal of Basic Engineering, 82, pp.342-346.

Shaw, M. C. (1977) Dimensionless analysis for wear systems, Wear, 43, pp.263-266.

Shivpuri, R., Semiatin, S. L. (1988) Wear of Dies and Molds in Net Shape Manufacturing, Report ERCNSM-88-05, Ohio State University.

Sims, C. T., Stoloff, N. S., Hagel, W. C. (1987) <u>Superalloys II,</u> Wiley-Interscience, ISBN: 0471011479

Singh, A. K., Rooks, B. W., Tobias, S. A. (1973) Factors affecting die wear, Wear, 25, pp.271-279.

Sobis, T., Engel, U., Geiger, M. (1992) A theoretical study on wear simulation in metal forming processes,Journal of Materials Processing Technology, 34, pp.233-240.

Sofuoglu, H., Rasty J. (1999) On the measurement of friction coefficient utilizing the ring compression test, Tribology International, 32, pp.327-335.

Stribeck, R. (1902) The Principal Properties of Sliding and Rolling Bearings (in German), VDI Zeitschrift, Vol 46, pp.1341, 1432, 1463.

Summers-smith, J. D. (1994) An introductory guide to industrial tribology, Wiley.

Tan, Xincai (2002) Comparisons of friction models in bulk metal forming, Tribology International, 35, pp.385-393.

Tekkaya, A. E. (2005) A guide for validation of fe-simulations in bulk metal forming, The Arabian Journal for Science and Engineering, Volume 30, Number 1C, pp.113-136.

Thomas, A., El-Wahabi, M., Cabrera, J. M., Prado, J. M. (2006) High temperature deformation of Inconel 718, Journal of Materials Processing Technology, 177, pp.469-472.

Thomas, A. (1970) Investigations on die materials, National academic awards, Thesis (PhD).

Thomas, A. (1972) Wear of forging dies, Report, The drop forging research association.

Tien, J. K., Vignoui, G. E., Kopp, M. W. (1991) Materials for elevated-temperature applications, Materials Science and Engineering, A143, pp.43-49.

Tuncer C., Dean, T. A. (1987) A new pin design for pressure measurement in metal forming processes, Int. J. Mach. Tools Manufact., Vol. 27. No. 3. pp.325-331.

Uddeholm hot work steel manual, 1970.

Van Rooyen, G. T., Backofen, W. A. (1960) A study of interface friction in plastic compression, Int. J. Mech. Sci., 1, pp.1-27.

Vertin, K. D., Majlessi, S. A. (1993) Finite Element Analysis of the Axisymmetric Upsetting Process Using the Deformation Theory of Plasticity, Journal of Engineering for Industry, Trans. ASME, pp.450-458.

Vigor, C. W., Hornaday, J. W. (1961) A thermalcouple for measurements of temperature transients in forging dies, Temperature, Its Measurements and Control in Science and Industry, Vol. 3, Part 2, Rheinhold, New York, pp.625-630.

Walter, S., Haferkamp, H., Niemeyer, M., Bach, Fr. W., Henze, A. (1999) Material failure mechanisms of forging dies, Proceedings of the Fifth International Conference on Tooling, Loeben, pp.215-224.

Wanheim, T. (1973) Friction at high normal pressures, Wear, Vol. 25, Issue 2, pp.225-244.

Welsh, N. C. (1958) Philos. Trans. R. Soc. A, Vol 257, pp.1077.

Welsh, N. C. (1965) The dry wear of steels: I. The general pattern of behavior, Philos. Trans. R. Soc., Ser. A 257, pp.31-50.

Williams, J. A. (1996) Engineering Tribology, Cambridge University Press.

Won, H. C. (2001) A constrained thin-wall ring method to investigate friction in metal forming, Thesis (PhD), University of Birmingham, UK, School of Manufacturing and Mechanical Engineering, Faculty of Engineering.

Yi, H. (2001) Mechanical property, microstructural development and constitutive analysis associated with the high temperature deformation of Inconel 718, Thesis (PhD), University of Birmingham, UK, School of Metallurgy and Materials, Faculty of Engineering.

Yuan, H., Liu, W.C. (2005) Effect of the δ phase on the hot deformation behavior of Inconel 718, Materials Science and Engineering, A 408, pp.281-289.

Zhang, J. M., Gao, Z. Y., Zhuang, J. Y., Zhong, Z. Y. (2000) Grain growth model of IN718 during holding period after hot deformation, Journal of Materials Processing Technology, 101, pp.25-30.

Zhao, X., Guest, R. P., Tin, S., Cole, D., Brooks, J. W., Peers, M. (2004) Modelling hot deformation of Inconel 718 using state variables, Materials Science and Technology, 20, pp.1414-1421.

APPENDIX A

FLOW STRESS PLOTS FOR GLEEBLE COMPRESSION TESTS

The matrix shows the flow stress for four different strain rates and temperatures. Different colours symbolise the number of the test has been repeated.
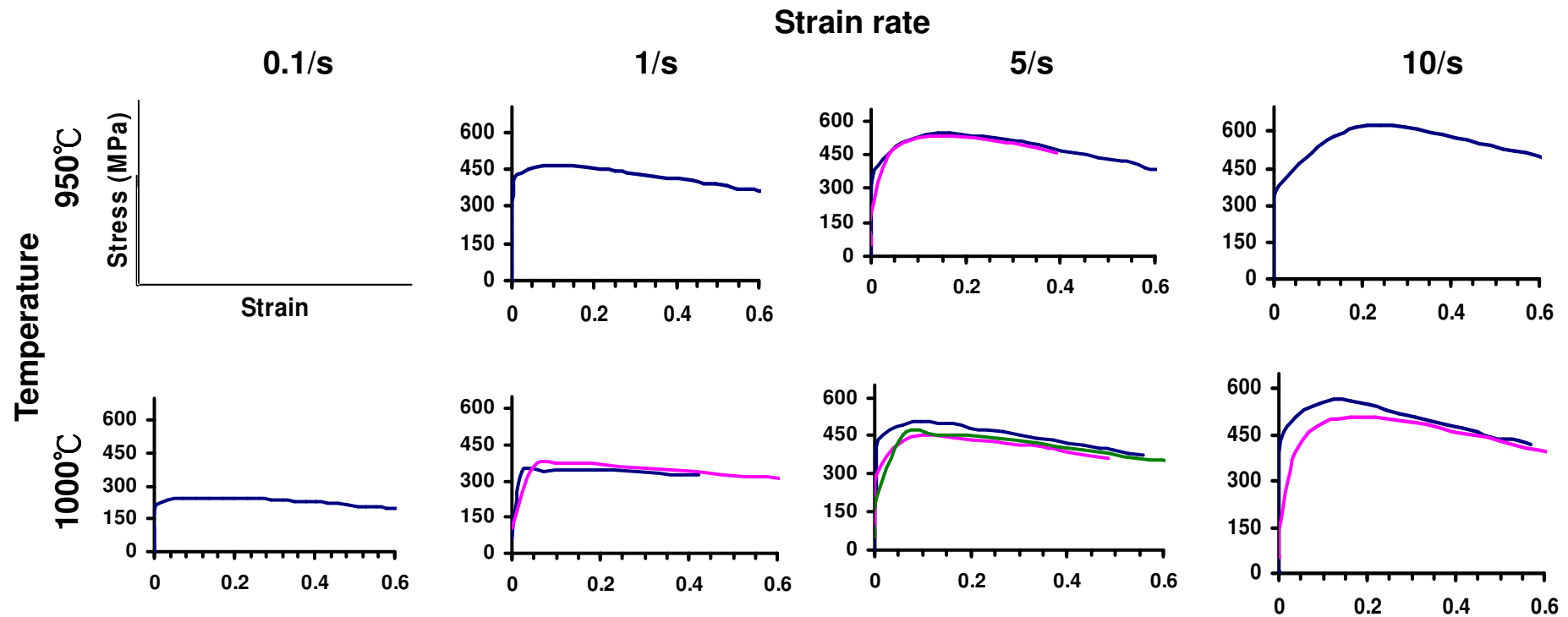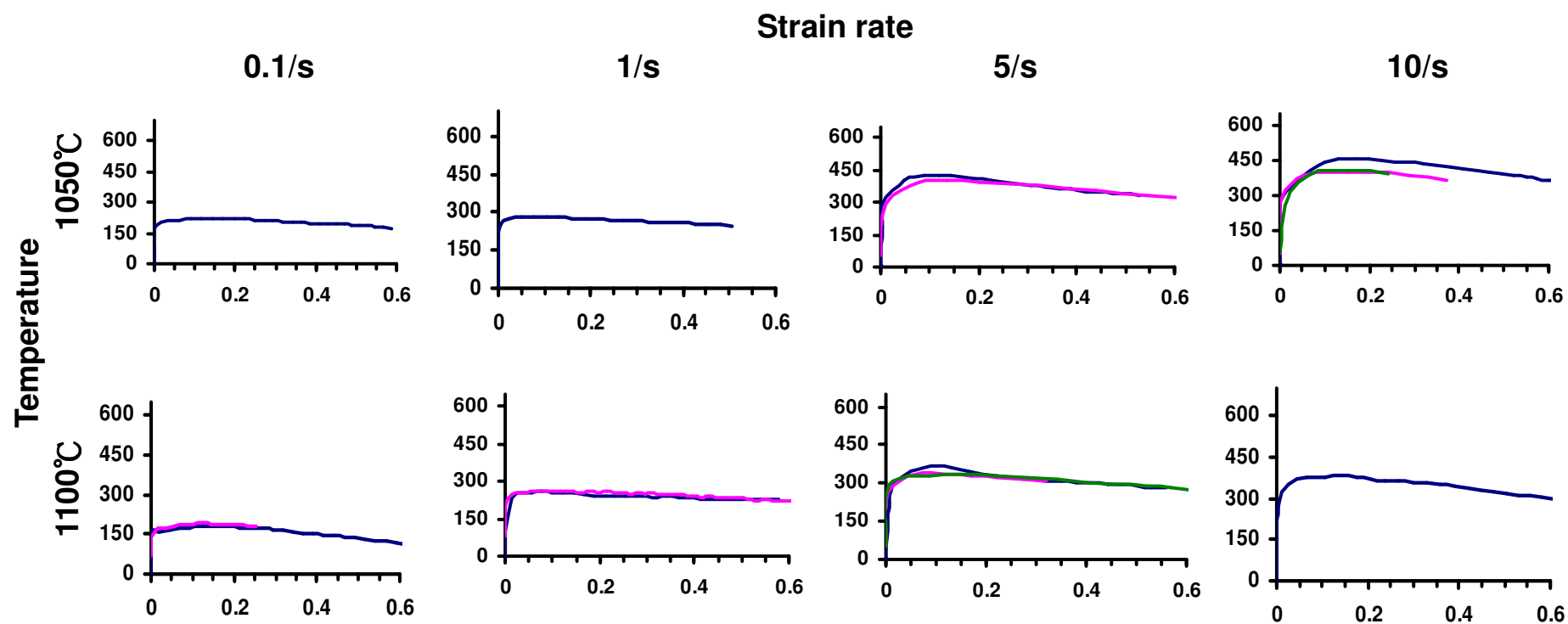
APPENDIX B
MICROSTRUCTURAL INVESTIGATION OF THE EXTRUDATE

Figures B1 (width section) and B2 (depth section), show comparisons of computational results with those from the metallurgical examination for average grain size distribution within the extrudate. For both sections, good correlations are observed. The initial average grain size was 20 μm for IN718 before extruding. The diagram shows that average grain size was big on the head of the extrudate, due to grain growth at the high temperature. At the neck part, the grain size is small because of the refinement caused by recrytallisation under large deformation. Grain growth occurs in material that has passed the neck.

These evidences show that the material model can predict the average grain size a fact which is considered to be relevant to the microstructural structure of the blade.
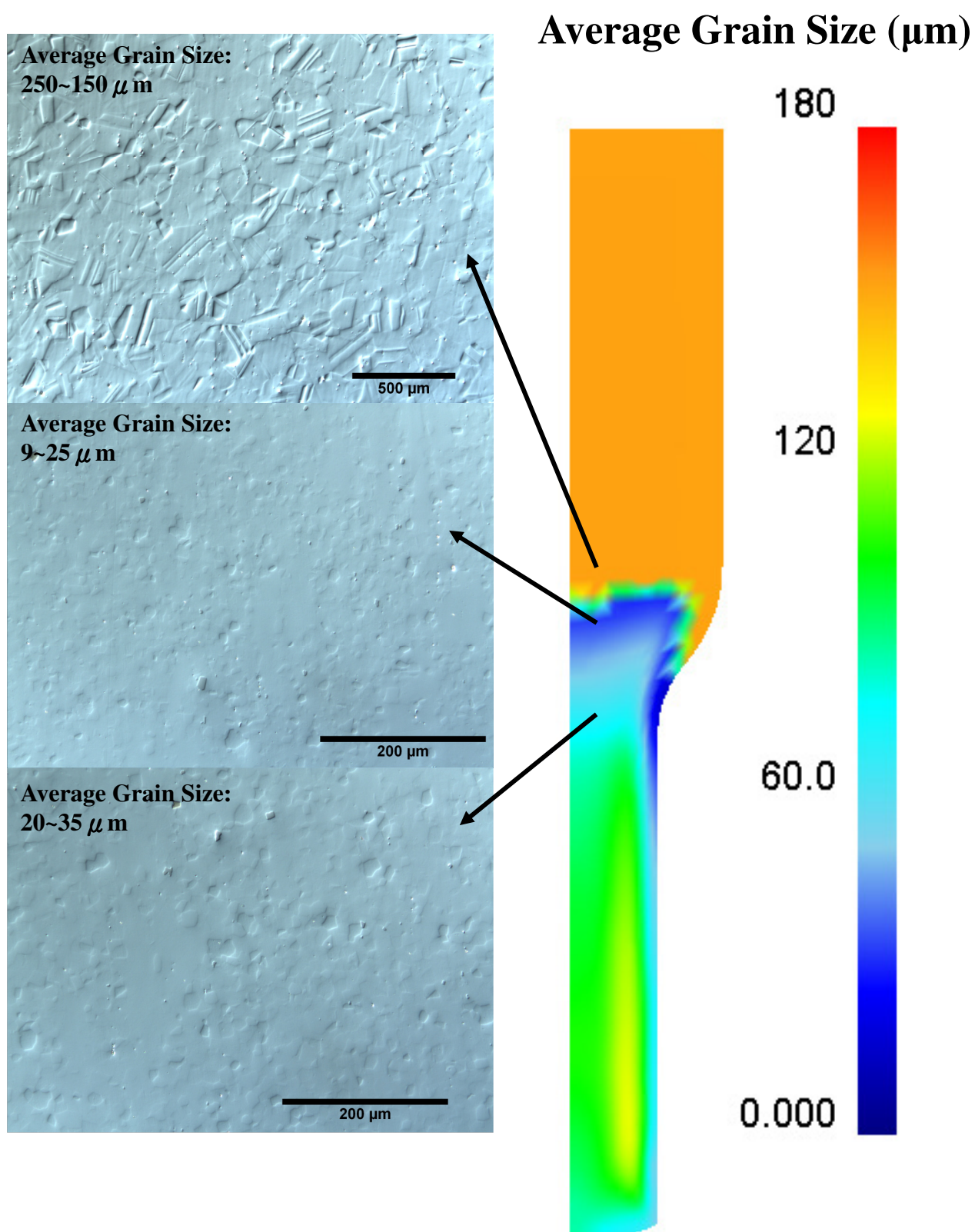
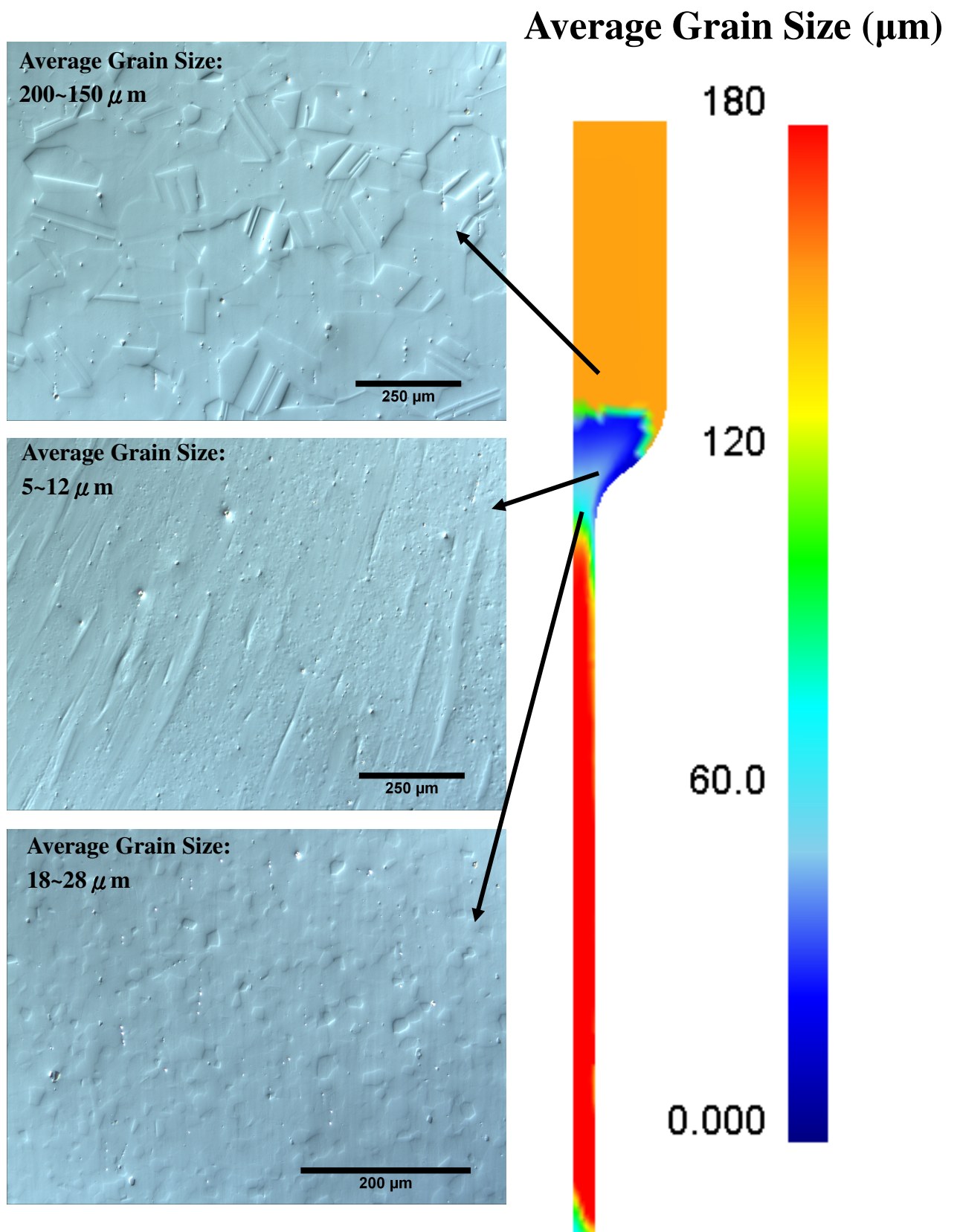**Figure B1** Grain size comparison of the computational width section and just deformed extrudate.

Figure B2 Grain size comparison of the computational depth section and just

deformed extrudate.

APPENDIX C
TESTS FOR EXAMINING FRICTION IN FORMING
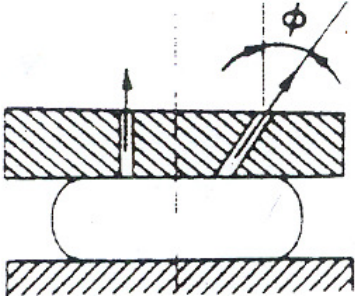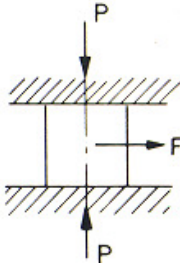
Test	Description
Upsetting of slab test (Cigar test)	**Frederiksen and Wanheim (1985)** The dimensional change of a slab along the longer dimension is treated as an indication of friction. The method is that when a rectangular slab is compressed between flat dies, material flows along both the longer (**b**) and shorter (**a**) dimensions. The material flows more along the shorter dimension as **b** is at least ten times greater than **a**, therefore the sliding resistance in the length direction will be greater than in the width direction. The test is sensitive for low coefficients of friction.
Extrusion forging (Spike forging test)	**Frederiksen and Wanheim (1985)** Cylindrical billet was forged with a platen into a conical impression die containing a central tapered cavity. The spike height is the height of the work-piece extruded into the central cavity used as an indication of the function of friction. A large amount of surface expansion could be obtained using this test.
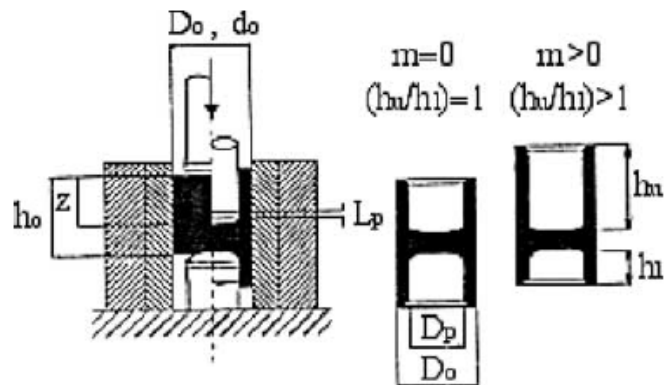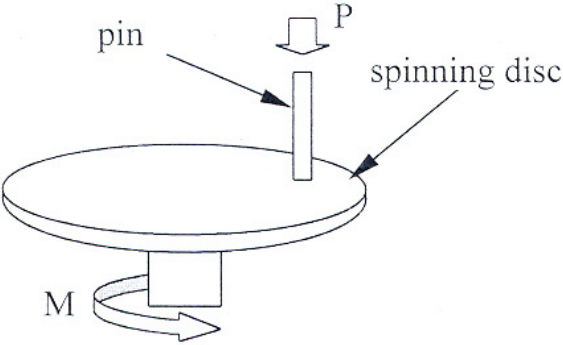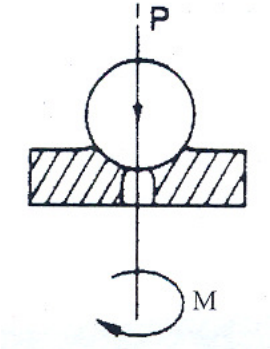
Combined-forward-backward cup extrusion (Double-cup test)	**Adopted from Fereshteh-Saniee *et al.* (2004)** In this test, a cylindrical specimen was located in a die with the same nominal diameter. Then it was deformed between two punches with the same diameter which smaller than that of specimen. Two cups with a single base were produced when the upper punch moves downwards. The upper height to lower height ratio of cups, h_u / h_l, is very sensitive to the friction conditions and by calculating the ratio, the coefficient of friction could be determined.

Surface stress measurement using pins	**Van Rooyen and Backofen (1960)** In order to measure the local friction stress in a simple upsetting process. Two pins were inserted into the upper punch, one normal to the interface and the other one at an angle. The coefficient of friction is obtained from the pressures measured on the pins. The problem of this design is that the lubricant and work-piece may extrude into the space between the pins and the die and friction over the pin face which causes a force between the pin and its bore which leads to a resistance of movement of the pin.
Total force measurement in upsetting	**Schey (1983)** *Sliding* The total force or energy in upsetting depends on friction, material property and geometry of the work-pieces. With the aid of simple theory, the friction stress or the coefficient of friction and the friction factor can be calculated from the measurement of the average pressure of dies. The problem of this test is that the total force or energy are not sensitive enough to show the effect of friction.

Total force measurement in upsetting	**Bay and Hansen (1985)** *Twist* The principal of the test is that a cylindrical specimen is pressed and rotated over on the tool surface. The test requires the resultant torque and the normal force to be measured in order to evaluate the coefficient of friction, which is calculated by the expression, $\mu = T/rP$, where T is the torque, r is the radius of the cylindrical specimen and P is the normal force.
Strip drawing test	**Schey (1983)** The test is performed where a strip is drawn between inclined die surfaces to produce a specific reduction in thickness. The test involves bulk plastic deformation as it can be seen in the figure. However, it is not easy to perform for work-pieces at high temperatures.

Pin-on-disk test	 **Won (2001)** The level of friction is evaluated by measuring the normal and lateral forces and the test can be classed as a low pressure test, i.e. small deformation, with its usefulness highly dependent on the performance of the experiments. The test is also quite complex and highly sensitive instruments are required to execute the tests.
Hard ball on ring test	 **Schey (1983)** The test is similar to the Brinell hardness test. A hard ball is used to compress the ring shaped specimen. After compression, the specimen is rotated The friction force was calculated by measuring torque. In this test, only a small area under the ball is plastically deformed.

Ridge plough test
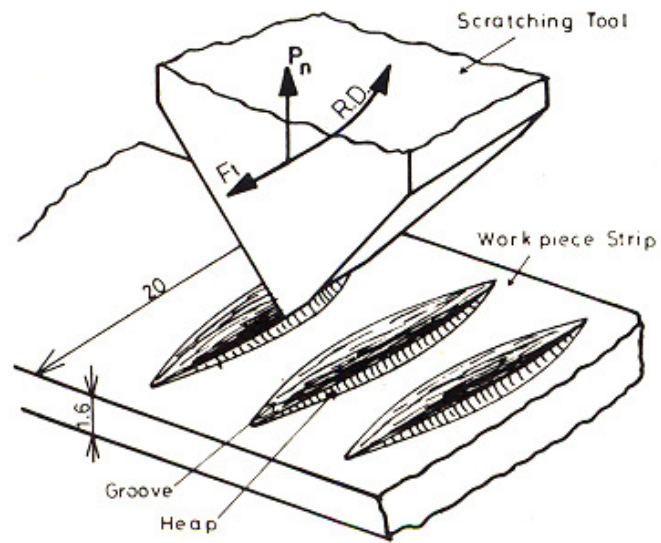
Schey (1983)

Local plastic deformation of a smooth specimen surface is obtained by a wedge tool. The tool geometry is designed to plough the work-piece which will produce normal pressures to about twice the flow stress, but the surface expansion is small, hence limiting its application in metal forming. |

Table C1 Tests developed for examining the friction.

	Test	Forming Condition	Characteristic	Execution/ Analysis
Intuitive test	Ring test	Hot/Cold forming	Bulk deformation	Easy
	Upsetting of slab test (Cigar test)	Hot/Cold forming	Small deformation	Easy
	Extrusion forging (Spike forging test)	Hot/Cold forming	Bulk deformation	Difficult
	Combined-forward-backward cup extrusion (Double-cup test)	Cold forming	Medium deformation	Difficult
Quantitative test	Surface stress measurement using pins	Cold forming	Small deformation	Difficult
	Total force measurement in upsetting	Hot/Cold forming	Bulk deformation (sliding test)	Simple
			Medium deformation (twist test)	Difficult
	Strip drawing test	Hot/Cold forming	Bulk deformation	Difficult
	Pin-on-disk test	Cold forming	Very/ Small deformation	Difficult
	Hard ball on ring test	Cold forming	Very/ Small deformation	Easy/ Difficult
	Ridge plough test	Cold forming	Very/ Small deformation	Easy/ Difficult

Table C2 Comparison of friction tests.

APPENDIX D

JUSTIFICATION OF MESH AND STEP SIZE FOR SIMULATIONS OF HEAT TRANSFER COMPRESSION AND RING TESTS

In order to find a balance between efficiency and accuracy of FE simulations, analyses for different mesh and deformation step size were made for the bottom die. A quadratic mesh was generated automatically by the DEFORM solver and element number, element size and step size could be amended. The concept of the analysis is to assume that a very accurate result (judged by maximum temperature during forming) would be obtained by using a very fine mesh of die. A number of 5000 elements is adopted as a standard for accuracy and, thus, the error for larger element and step size can be identified. The results from the analyses are shown in Table D1.

Mesh Number of the Die	Minimum Element Length (mm)	Error of Predicted Temp. (%)	Step Size (s)	Computational Time (s)
100	1.33	89.5	0.001	69
500	0.55	15.2	0.001	69
1000	0.35	5.8	0.001	70
1500	0.22	-0.5	0.001	71
5000 (standard)	0.08	0	0.001	75
5000	0.08	-30.7	0.1	64
5000	0.08	0	0.00001	1097

Table D1 Analysis for mesh and step size for simulations of heat transfer compression tests**.**

From the results it is concluded that 1500 elements of length 0.22 mm and a step size 0.001 second is sufficient for the FE modelling without reducing accuracy significantly and thus are used in the simulations of heat transfer compression tests.

Mesh Number of the Work-piece	Minimum Element Length (mm)	Error of Predicted Load (%)	Step Size (s)	Computational Time (min.)
100	0.59	-0.9	5×10^{-6}	18
500	0.24	-0.9	5×10^{-6}	32
1000	0.17	0	5×10^{-6}	39
5000 (standard)	0.07	0	5×10^{-6}	4:51
5000	0.07	0	5×10^{-7}	6:22
5000	0.07	unstable	5×10^{-5}	unstable

Table D2 Analysis for mesh and step size for simulations of ring tests**.**

In the simulations of ring test, it is assumed that a very accurate result (judged by the maximum load of forming of a ring from 6 mm to 2 mm) will be obtained by using a very fine mesh for the work-piece. A number of 5000 elements is adopted as a standard for accuracy and, the error for larger element and step size can be identified. The results from the analyses are shown in Table D2.

From the results it was concluded that 1000 elements of length 0.17 mm was the suitable mesh to use. Compared with heat transfer simulations, the choice of the step size was quite critical simulations of ring tests, due to the large deformation. A step size of 5×10^{-6} second

is sufficient as without reducing accuracy significantly and faster to converge in this case, thus, was used in the study.

APPENDIX E

THERMAL MATERIAL PROPERTIES OF H13 AND IN718 FOR FE SIMULATIONS

Thermal material properties for H13 and IN718 are listed in Table E1 and E2. They are used in the simulations of heat transfer compression tests, ring tests and extrusions, respectively.

Temp. (℃)	Thermal Conductivity (N/Sec/℃)	Temp. (℃)	Heat Capacity (N/mm^2/℃)
148.88889	24.574927	93.333333	2.78136
215.55556	24.574927	204.44444	3.01314
348.88889	24.40297	315.55556	3.24492
476.66667	24.231012	426.66667	3.82437
604.44444	24.746884	537.77778	4.51971
648.88889	24.746884	648.88889	5.7945
713.77778	24.746884	760	6.25806

Table E1 Thermal material properties for H13.

Temp. (℃)	Thermal Conductivity (N/Sec/℃)	Heat Capacity (N/mm^2/℃)
20	10.3174	3.62156
23	10.3174	3.62156
100	11.8875	3.77801
200	13.607	3.91013
300	15.1771	4.00052
400	16.6724	4.11641
500	18.4667	4.28098
600	20.9339	4.60199
700	24.1488	5.02151
800	26.0926	5.44104
900	25.7188	5.35064
1000	26.3169	5.53143
1100	29.0084	5.68788
1200	30.9523	5.83622
1371	30.9523	5.83622

Table E2 Thermal material properties for IN718.

APPENDIX F

DETERMINED FRICTION FACTORS FROM RING TESTS

The friction factors determined from ring tests under different forming conditions are listed in Table F1.

Work-piece Temperature (℃)	Die Temperature (℃)	Thickness of Coating (μm)	Lubricant Quantity (g/mm^2)	Friction Factor (m)
1050	100	40	2.82×10^{-5}	0.14~0.16
		40	7.05×10^{-5}	0.12~0.14
		60	2.82×10^{-5}	0.10~0.16
		60	7.05×10^{-5}	0.10~0.16
	150	40	7.05×10^{-5}	0.10
		60	7.05×10^{-5}	0.10
	200	40	7.05×10^{-5}	0.12~0.10
		60	2.82×10^{-5}	0.16~0.18
		60	7.05×10^{-5}	0.12~0.14
1080	200	60	7.05×10^{-5}	0.08
1100	100	40	7.05×10^{-5}	0.15
		60	2.82×10^{-5}	0.20
		60	7.05×10^{-5}	0.18
	200	40	2.82×10^{-5}	0.14
		60	2.82×10^{-5}	0.18

Table F1 The friction factors determined from the ring tests under different forming conditions.

APPENDIX G

EDX EXAMINATIONS FOR IDENTIFYING CHEMICAL COMPOSITION ON THE DIE SURFACE

Energy dispersive X-ray (EDX) spectrographic analyses were carried out to identify chemical composition on the worn surface. Several positions at serious worn regions (transition area on the die), have been chosen to derive an average quantitative chemical composition for the specific area and the noise elements have been eliminated. All the EDX data were normalised and are presented with the regions for EDX examinations. The chemical compositions of IN718 derived from the literature are shown in Figure G1 while H13 are shown in Figure G2 for comparisons of change of chemical compositions of the worn die.
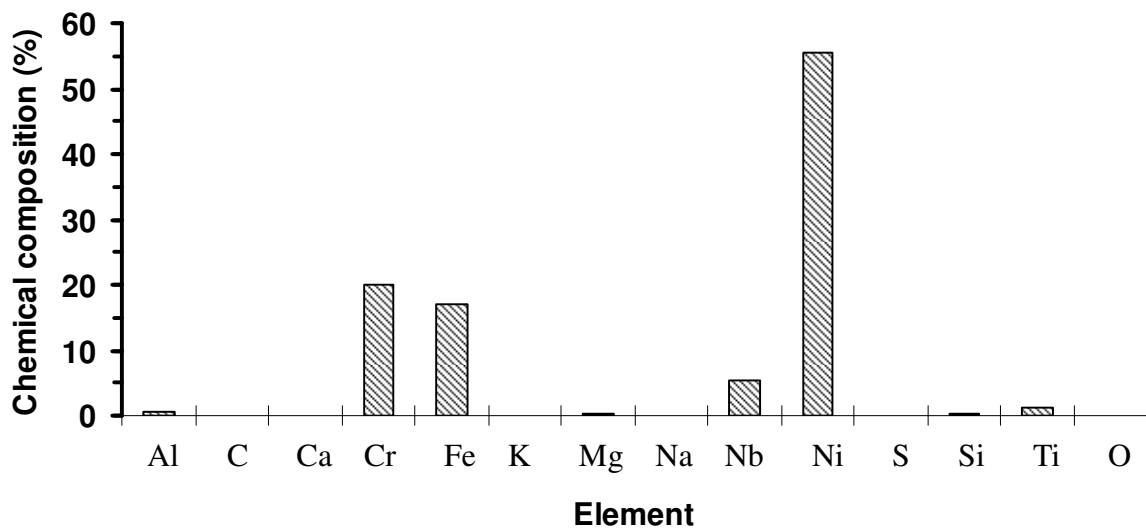

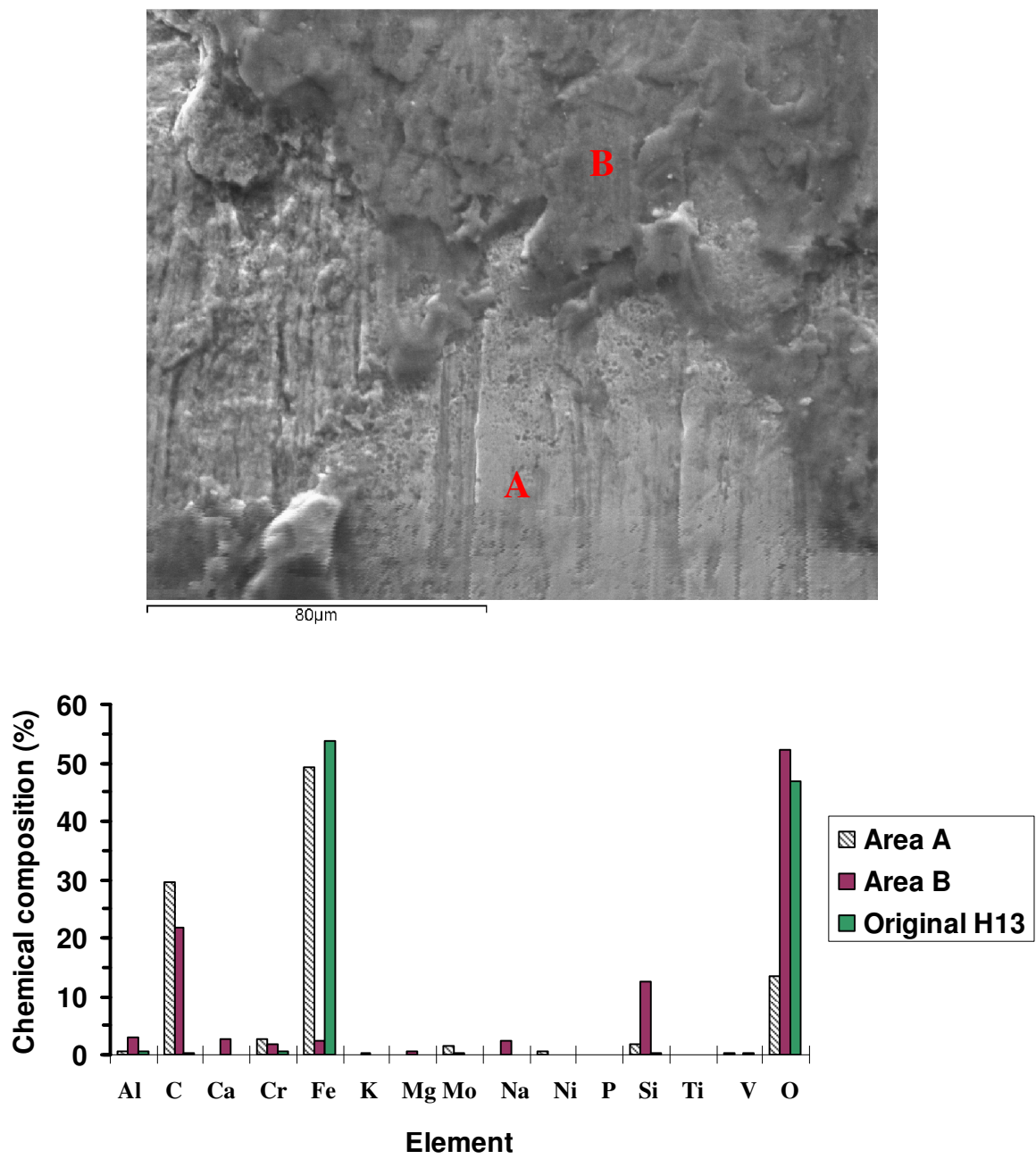**Figure G1** Chemical compositions of IN718 (data provided by Special Metals, 2004).

Figure G2 EDX examinations at serious worn region in two areas shown as a photograph above.
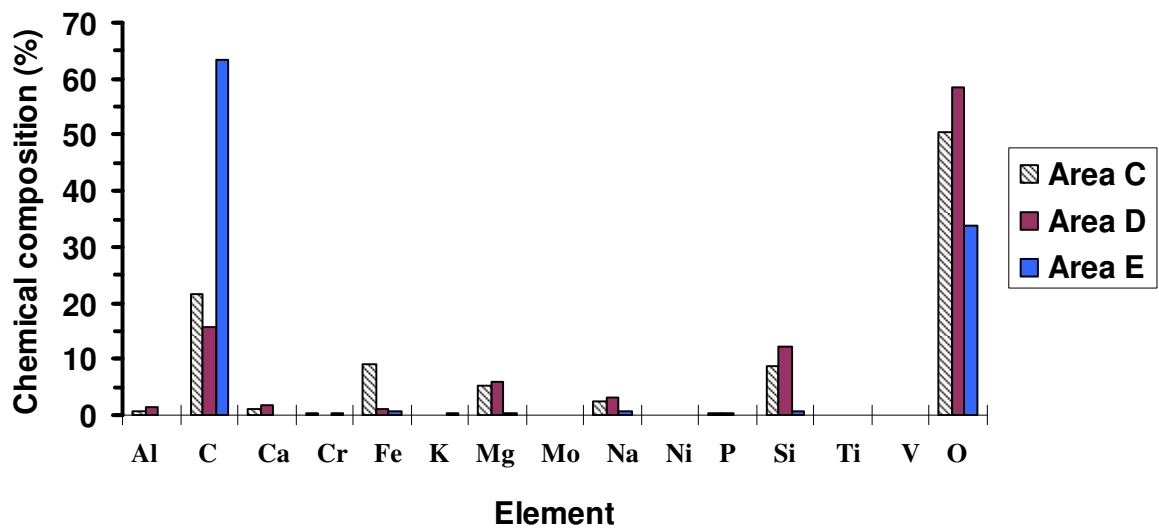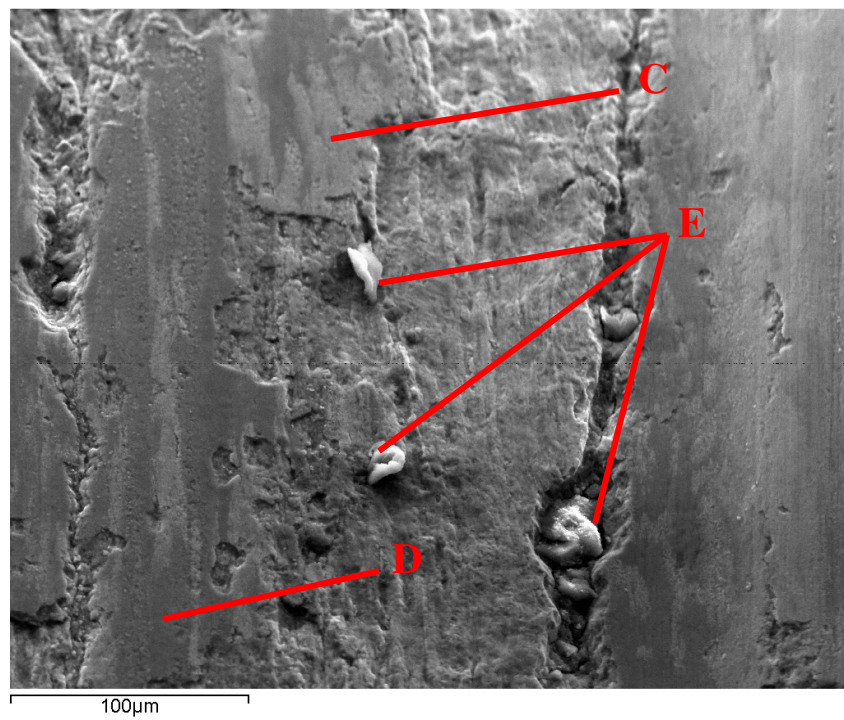
Figure G3 EDX examinations at serious worn region in three areas shown as a photograph above.

By examining the two photographs, the regions are observed to be covered with patches consisting of white and dark areas. Cracks and particles are also found in Figure G3. In the chemical spectra, both Figures G2 and G3 show a large amount of carbon at the die surface/sub-surface This is considered to result from the diffusion of the graphite lubricant at high temperatures and remaining lubricant on the surface.

The high proportion of oxygen in both regions might be caused by air within the EDX chamber since the complete vacuum is difficult to achieve in the machine. However, it might be also due to the oxidation of the die. The presence of oxygen is evident in all EDX results.

It is found that in addition to carbon and oxygen, silicon, calcium, aluminum and sodium were also identified. Since graphite lubricant and glass coating were used on the die and billet respectively during extrusion, the possibility for them to stick on the die after extrusion is high. From the literature (Li *et al*., 2000; Matsumoto *et al.*, 2009), it is a known fact that the most common elements existing in glass coatings are, silicon, calcium, magnesium and sodium, all of which might also be combined with oxygen. Therefore, silicon, calcium, and sodium could be assumed to be from the glass coating. The increase of aluminum might be that within IN718 stuck to the die, but it is difficult to judge since both IN718 and H13 contain aluminum.

A small amount of nickel is only identified in the white area in Figure G2 but none is observed in either dark or white areas in Figure G3, which indicates that the dark patch might be only adhered coating. The small amount of iron recorded in Figure G3, indicates that only the coating was examined. However, the amount of iron shown in Figure G2 is high and nickel is recorded. The presence of IN718 adhered to the die surface could not be confirmed since the chemical compositions are complex for both IN718 and H13. The larger amount of iron detected in white area of Figure G2, indicates that little coating was present compared with the dark patch in Figure G2 and white/dark areas in Figure G3. The particles found in region E (Figure G3) contain carbon and oxygen and might have been detached from the die/work-piece surface to act abrasively during forming.

Complex chemical compositions for H13 and IN718, coating/lubricant at the interface and the

material changed due to the high temperatures, all these factors weave a very complex interface structure on the surface of the die. This also affects the result of the chemical composition identified on the surface/sub-surface. Although a very precise interpretation could not be given, the data presented here could provide an overall picture of possible interfacial conditions arising during extrusion.